Semi-Dirac Dispersion, and its Various Aspects

By

SWAPNONIL BANERJEE

DISSERTATION

Submitted in partial satisfaction of the requirements for the degree of

DOCTOR OF PHILOSOPHY

in

PHYSICS

in the

OFFICE OF GRADUATE STUDIES

of the

UNIVERSITY OF CALIFORNIA

DAVIS

Approved:

_____

_____

_____

Committee in Charge

2012

1

CONTENTS

1. INTRODUCTION

The isolation of single layers of graphite (graphene) with its unique linear ("Dirac-Weyl") low energy band structure has become, within only a few years, a heavily studied phenomenon.[12, 13] The appearance of unanticipated new features in band structures, which generally have far-reaching implications, have in the past included half metallic ferromagnets and compensated half metals ("half metallic antiferromagnets"), and more recently topological insulators. Each of these provide the promise of not only new physical phenomena but also new applications of these properties.

Another key feature of graphene is the point Fermi surface aspect. The touching (or crossing) of bands is accompanied by a gap throughout the rest of the Brillouin zone that pins the Fermi level (E_F) in the intrinsic material to lie precisely at the point of crossing – the point Fermi surface (two of them in graphene). This point Fermi surface aspect has been well studied[17] in conventional zero gap semiconductors where a touching of the valence band maximum and conduction band minimum is symmetry determined and occurs at a high symmetry point. The dielectric susceptibility of such a system is anomalous[3] – not metallic and not semiconducting in character – and unusual consequences of the touching bands and residual Coulomb interaction promise unusual phases, such as excitonic condensates or even excitonic superconductors.

The linear dispersion at the zone boundary in graphene has been known for many decades; it took the ability to prepare the delicate material and perform a variety of experiments to ignite interest. There are quasilinear (and potentially truly linear) band structure features in certain materials, viz. skutterudites,[4] that have been known for some time and with recent developements[5] may attract new attention. To actually discover a feature in a band structure that provides the quasiparticle dispersion of a new

and unexpected type is rare, and the discovery of a "semi-Dirac" dispersion pinned to the Fermi energy is a very recent example.

Pardo *et al.*[33, 34] reported such a finding in ultrathin (001) VO_2 layers embedded in TiO_2. This new point Fermi surface system, dubbed 'semi-Dirac,' is a hybrid of conventional and unconventional: dispersion is linear ("massless", Dirac-Weyl) in one of the directions of the two-dimensional (2D) layer, and is conventional quadratic ("massive" Dirac) in the perpendicular direction. At directions between the axes the dispersion is intermediate and highly direction-dependent. Interest in this unique, maximally anisotropic, dispersion arises for several reasons. The (topologically determined pinning at the) point Fermi surface is itself of interest. The highly anisotropic dispersion (from massive to massless depending on angle) is unique to this system. The fact that it arises in an oxide nanostructure of the general type that is grown and studied regularly these days also strengthens the promise of applications. Another layered superstructure, a double cell layer of Ti_3SiC_2 embedded in SiC, has displayed a point Fermi surface, but the dispersion is of the convention type.[6]

Such a spectrum had been noted earlier in different contexts. Volovik obtained such a spectrum at the point node in the A-phase of superfluid He^3 [7] and studied its topological robustness.[8] More relevant to solids was the discovery by Montambaux's group of this spectrum in a graphene-like model.[50] The model has a broken symmetry such that hopping to two nearest neighbors is t but to the third neighbor is t'. When t' differs from t, the graphene "Dirac points" wander away from the K and K' points, and at $t' = 2t$ they merge, resulting in the semi-Dirac spectrum. This group began a study of low energy properties of such a system[51], which was continued by Banerjee *et al.*[42] and was extended in [66].

2. MATHEMATICAL INTRODUCTION TO THE SEMI-DIRAC DISPERSION

2.1   Semi-Dirac Dispersion

In condensed matter physics properties of a material depends on how an electron moves
in a material. An electron is a quantum mechanical object and hence its dynamics is
described not by Newton's equation, but Schrodinger's equation. None the less, when
the positively charged ions are arranged in a periodic structure inside material, the final
expression for the energy of an electron is dispersive, i,e varies with the momentum and
in simple cases looks formally very similar to the that of an object moving in the free
space under Newton's law of motion. As Feynman said, in his lecture on 'Propagation in
a Crystal Lattice' [26], "...it is a ubiquitous phenomenon of nature that if the lattice is
perfect, the electrons are able to travel through the crystal smoothly and easily–almost as
if they were in vacuum. this strange fact...has also permitted the development of many
practical devices. It is, for instance, what makes it possible for a transistor to imitate the
radio tube. In a radio tube electrons move freely through a vacuum, while in the transistor
they move freely through a crystal lattice." The reason for this apparent similarity can
be explained by a simple but insightful model called the tight-binding model. In spite of
this remarkable analogy between the energy momentum dispersion in free-space and that
in a periodic lattice, one must remember that it comes out so as a consequence of solving
quantum mechanical equations. There can be materials for which the quantum mechanical
calculation gives a very different energy momentum dispersion. For example, in case of
graphene the dispersion is linear instead of being quadratic. The semiDirac dispersion is
quadratic along one symmetry direction in the Brillouin zone and linear along the direction
perpendicular to it. Choosing k_x and k_y to be the momentum variables along the quadratic

direction and the direction perpendicular to it respectively, the semi-Dirac dispersion is given by:

$$\varepsilon_{\mathbf{k}} = \pm\sqrt{\left[\frac{\hbar^2 k_x^2}{2m}\right]^2 + \left[\hbar v k_y\right]^2} \tag{2.1}$$

where the effective mass m applies along k_x and v is the velocity along k_y. Two natural scales are introduced, one for the momentum and the other for the energy: $p = 2mv$ (momentum scale) and $\varepsilon_0 = 2mv^2 = 2pv$. (Untidy factors of 2 appear because of the differences in the natural classical $\frac{1}{2}pv$ and relativistic pv units for energy.) One can then define the dimensionless momenta $K_x = \frac{\hbar k_x}{p}$ and $K_y = \frac{\hbar k_y}{p}$ in terms which the semi-Dirac dispersion given by Eq. 2.1 becomes

$$\varepsilon_{\mathbf{k}} = \pm\varepsilon_0\sqrt{K_x^4 + K_y^2}. \tag{2.2}$$

Thus all possible semiDirac points (all possible m and v combinations) scale to a *single unique semiDirac point*, with the materials parameters determining only the overall energy scale. There is no limiting case in which the semiDirac point becomes either a Dirac point or a conventional effective mass zero-gap semiconductor.

2.2   Density of states

The density of states for a system with a two dimensional dispersion is given as

$$D(\varepsilon) = \int \frac{d^2\mathbf{k}}{(2\pi)^2}\delta(\varepsilon - \varepsilon_{\mathbf{k}}). \tag{2.3}$$

Using Eq. 2.2 in Eq. 2.3, one obtains the following expression for the density of states for the semi-Dirac dispersion.

$$D(\varepsilon) = \frac{\sqrt{2m\varepsilon}}{\pi^2\hbar^2 v}I_1, \tag{2.4}$$

where I_1 is a dimensionless number given by

$$I_1 = \int_0^1 dk_x'(1 - k_x'^{\,4})^{-\frac{1}{2}} \approx 1.3110. \tag{2.5}$$

To arrive at Eq. 2.4, the following trick was used: instead of directly computing $D(\varepsilon)$, a quantity $g(\varepsilon) = \int \frac{d^2\mathbf{k}}{(2\pi)^2}\delta(\varepsilon^2 - \varepsilon_\mathbf{k}^2)$ was first computed. Since it involves $\varepsilon_\mathbf{k}^2$ instead of $\varepsilon_\mathbf{k}$, $g(\varepsilon)$ is easier to compute. Finally, using the relationship between $D(\varepsilon)$ and $g(\varepsilon)$, which is given by $D(\varepsilon) = 2\varepsilon g(\varepsilon)$ Eq. 2.4 was obtained. For the semi-Dirac dispersion the density of states $\sim \varepsilon^{\frac{1}{2}}$. For comparison, the density of states $D(\varepsilon)$ is constant (i,e $\sim \varepsilon^0$) for effective mass systems and goes as $|\varepsilon|$ for Graphene. Now $\frac{1}{2}$ (the power of the energy that appears in the density of states expression for the semi-Dirac dispersion), is in between 0 and 1, which appear in the density of states for the other two dispersions. Hence the the semi-Dirac dispersion is intermediate so far as the energy dependence of the density of states is concerned.

2.3 Velocity:k-space Distribution and Fermi Surface Averages

Since a semi-Dirac dispersion is Dirac like in one direction and massive in the direction orthogonal to it, its velocity distribution in the momentum space is of particular interest. For the Dirac dispersion the velocity is everywhere constant in magnitude. In case of the parabolic dispersion, the magnitude of the velocity vector increases linearly with the magnitude of $\mathbf{k}$. Given an energy momentum dispersion $\varepsilon_\mathbf{k}$, the velocity is given by $\mathbf{v_k} = \hbar^{-1}\nabla_\mathbf{k}\varepsilon_\mathbf{k}$. For the semi-Dirac dispersion, the velocity can be scaled to a dimensionless form $\mathbf{V_K}$ defined as

$$\mathbf{v_k} = \frac{\varepsilon_0}{p}\nabla_\mathbf{K}\xi_\mathbf{K} = v\mathbf{V_K}, \tag{2.6}$$

where $\vec{V}_K$ is $\nabla_K\xi_K$. Writing explicitly in terms of components,

$$\mathbf{V_K} \quad = \quad \frac{2K_x^3}{\sqrt{K_x^4 + K_y^2}}\hat{K}_x + \frac{K_y}{\sqrt{K_x^4 + K_y^2}}\hat{K}_y \tag{2.7}$$
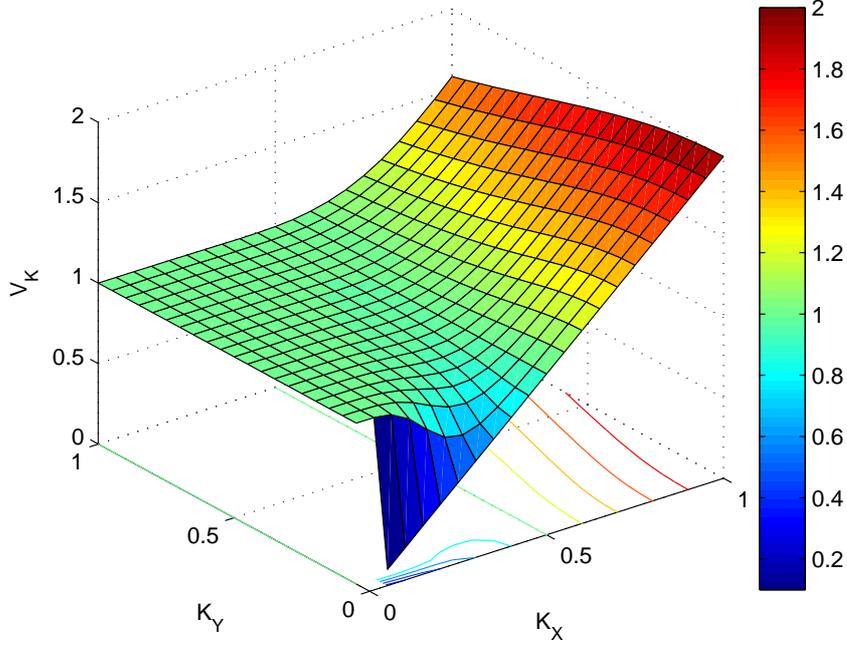
Fig. 2.1: Surface and contour plots of the dimensionless semi-Dirac velocity. The velocity has a singularity at $(K_X = 0, K_Y = 0)$. The velocity changes monotonically from a constant value to a linear dispersion as one goes from the K_Y(relativistic) direction to K_X(non-relativistic) direction.

From Eq. 2.7, the magnitude of the dimensionless velocity vector of the semi-Dirac dispersion is obtained as follows.

$$|\mathbf{V_K}| = \sqrt{(V_K)_x^2 + (V_K)_y^2} = \sqrt{\frac{4K_x^6 + K_y^2}{K_x^4 + K_y^2}} \tag{2.8}$$

10
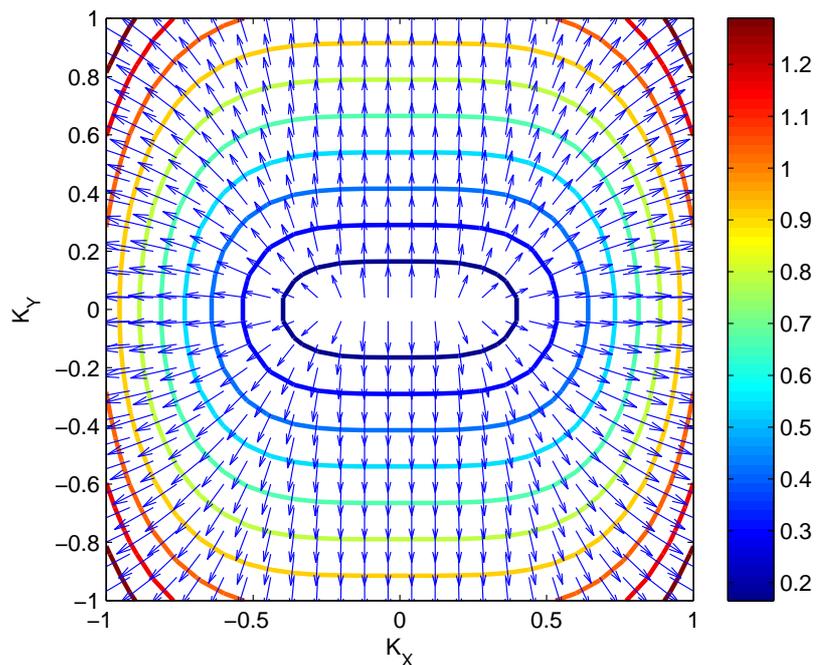
Fig. 2.2: Contours of the Fermi surfaces change from being elongated along the non-relativistic direction to those elongated in the relativistic direction with the increase of the total energy. The arrows indicate the vector $V_{\mathbf{K}}$. The length of an arrow is proportional to the magnitude of $V_{\mathbf{K}}$. As can be seen from the figure, the length of an 'velocity-arrow' is constant along the K_y axis indicating a constant velocity. The velocity vectors are all normal to the constant Fermi energy contours, as they should be.

Figures 2.1 and 2.2 illustrate the velocity distribution of semi-Dirac dispersion. Fig. 2.2 also shows the evolution of the constant energy contours with change in Fermi energy.

2.4 Fermi-surface velocity averages for the semi-Dirac dispersion

Apart from being interesting itself, the average of the Fermi surface velocity will prove to be useful in later calculations, and also in the semi-classical expression for the conductivity tensor, given by $\sigma_{\alpha\beta} = e^2 \tau D(\varepsilon)\langle v_\alpha v_\beta \rangle$, where $D(\varepsilon)$ is the density of states. Due to the anisotropy in the semi-Dirac dispersion, the average Fermi-surface velocities will be differ-

ent in different directions. Hence $\langle v_x^2 \rangle$ and $\langle v_y^2 \rangle$, the averages of the Fermi surface velocities squared in the non-relativistic and the relativistic directions respectively, are separately computed. They are defined as follows

$$\langle v_{x(y)}^2 \rangle \;\; = \;\; \frac{1}{2\pi^2 \hbar D(\varepsilon)} \int dk_t \frac{v_{x(y)}^2}{|v_k|}, \tag{2.9}$$

Using Eq. 2.4 and Eq. 2.6 in Eq. 2.9, one obtains

$$\langle v_x^2 \rangle \;\; = \;\; \frac{4I_3}{I_1} \frac{\varepsilon}{m}, \tag{2.10a}$$

$$\langle v_y^2 \rangle \;\; = \;\; \frac{I_2}{I_1} \frac{\varepsilon_0}{m}, \tag{2.10b}$$

where I_2 and I_3 are given by

$$I_2 \;\; = \;\; \int_0^1 dk_x' (1 - k_x'^4)^{\frac{1}{2}} \approx 0.8740, \tag{2.11a}$$

$$I_3 \;\; = \;\; \int_0^1 dk_x' \frac{k_x'^6}{(1 - k_x'^4)^{\frac{1}{2}}} \approx 0.7189, \tag{2.11b}$$

From Eq. 2.10a it is observed that $\langle v_x^2 \rangle$ depends linearly on the the energy ε. For a non-relativistic parabolic dispersion, the average Fermi surface velocity shows the same kind of mathematical relationship with energy. In our problem x is the non-relativistic direction, hence the equivalence. $\langle v_y^2 \rangle$, the average Fermi-surface velocity squared in the relativistic direction, assumes a constant value as is evident from Eq. 2.10b. This agrees with the fact that the average Fermi surface velocity is constant for a linear Graphene-like dispersion. From Eq. 2.10a and Eq. 2.10b it is observed that the ratio of $\langle v_x^2 \rangle$ to $\langle v_y^2 \rangle$ scales as $\varepsilon/\varepsilon_0$, which is small (for the VO$_2$ system only very small doping levels will remain within the energy range represented by the semi-Dirac dispersion, so $\frac{\varepsilon}{\varepsilon_0} \sim 10^{-4}$ or less). In other words, for VO_2 like semi-Dirac system the average velocity in the relativistic direction (y) is much larger than that in the non-relativistic direction (x). The high anisotropy in the average Fermi surface velocities is a characteristic of the semi-Dirac dispersion and not

shared by either Dirac or parabolic dispersion.

3. TIGHTBINDING DESCRIPTION OF THE SEMI-DIRAC DISPERSION

In this section a tight-binding model is developed for the semi-Dirac dispersion. A tight-binding model gives a simple description of the behavior of an electron inside a material. Assuming that the atoms are arranged in a periodic structure, the tight-binding model utilizes the fact that there are overlaps of the wave functions of an electron at different sites of the lattice.

In the following is given a 3-band tight-binding model of spinless fermions (corresponding to the half-metallic VO_2 trilayer) on a square-lattice, defined by the Hamiltonian

$$\mathcal{H} = \sum_{\alpha=1}^{3}(\sum_i \epsilon_\alpha n_{i,\alpha} + \sum_{<i,j>} t_\alpha(c_{i,\alpha}^\dagger c_{j,\alpha} + h.c.)) \qquad (3.1)$$
$$+\lambda_1 \sum_{<i>}(c_{i,1}^\dagger c_{i+\hat{x},3} - c_{i,1}^\dagger c_{i+\hat{y},3} + h.c.)$$
$$+\lambda_2 \sum_{<i>}(c_{i,2}^\dagger c_{i+\hat{x},3} - c_{i,2}^\dagger c_{i+\hat{y},3} + h.c.)$$

with $\epsilon_3 >> \epsilon_1, \epsilon_2$, so that there are two overlapping bands 1 and 2, with no coupling between them. Instead, they couple through the third band, through a coupling which changes sign under rotation by 90 degrees. Such a coupling can be shown to arise by symmetry between d and s orbitals. However, since the third band is far from the Fermi energy, it can be taken as dispersionless. Furthermore, without affecting any essential physics, it is assumed that $t_1 = -t_2 = t$ and $\lambda_1 = \lambda_2 = t'$. Thus in momentum space, the

Hamiltonian becomes a 3×3 matrix:

$$H = \begin{pmatrix} \widetilde{\varepsilon}_{1k} & 0 & V_k \\ 0 & \widetilde{\varepsilon}_{2k} & V_k \\ V_k & V_k & \varepsilon_3 \end{pmatrix} \tag{3.2}$$

where the dispersions and coupling are given by

$$\widetilde{\varepsilon}_{1k} = \varepsilon_1 + 2t(\cos k_x + \cos k_y) \tag{3.3a}$$

$$\widetilde{\varepsilon}_{2k} = \varepsilon_2 - 2t(\cos k_x + \cos k_y) \tag{3.3b}$$

$$V_k = 2t'(\cos k_x - \cos k_y). \tag{3.3c}$$

Supposing orbital 3 to be distant in energy, the three-orbital problem can be downfolded to a renormalized two orbital problem which becomes (neglecting a parallel shift of the two remaining bands)

$$H = \begin{pmatrix} \widetilde{\varepsilon}_{1k} & \frac{V_k^2}{\varepsilon_3} \\ \frac{V_k^2}{\varepsilon_3} & \widetilde{\varepsilon}_{2k} \end{pmatrix} \tag{3.4}$$

The eigenvalues $E_{k\pm}$ of H are given by

$$E_{k\pm} = \frac{\widetilde{\varepsilon}_{1k} + \widetilde{\varepsilon}_{2k}}{2} \pm \frac{1}{2}\sqrt{(\widetilde{\varepsilon}_{1k} - \widetilde{\varepsilon}_{2k})^2 + 4[\frac{V_k^2}{\varepsilon_3}]^2} \tag{3.5}$$

The two energy bands given by Eq. 3.5 will be equal and hence touch at a point when the expression inside the square root sign is zero. $(\widetilde{\varepsilon}_{1k} - \widetilde{\varepsilon}_{2k})^2 + 4[\frac{V_k^2}{\varepsilon_3}]^2 = 0$ implies each of the squared terms being zero, as given by the following equations.

$$\widetilde{\varepsilon}_{1k} - \widetilde{\varepsilon}_{2k} = 0 \tag{3.6a}$$

$$V_k = 0 \tag{3.6b}$$

From Eq. 3.3c and Eq. 3.6b one obtains $k_y = k_x$(Only the first quadrant is considered without any loss of generality; without that restriction there will be four such points in the Brillouin zone.) That is, the two bands touch at the point $\vec{k}_{sd} \equiv (k_0, k_0)$ along the (1,1) lines where $\widetilde{\varepsilon}_{1k_0} = \widetilde{\varepsilon}_{2k_0}$, otherwise the two bands lie on either side of the touching point(the Fermi energy). From Eq. 3.3c, Eq. 3.6a and Eq. 3.6b one obtains the following expression for k_0:

$$k_0 = \cos^{-1}(\frac{\varepsilon_2 - \varepsilon_1}{8t}). \tag{3.7}$$

For k_0 to have a real solution, the argument of the inverse cosine function in the right side of Eq. 3.7 should be less than one. That imposes some (not very stringent) restrictions on $\varepsilon_1 - \varepsilon_2$ and t. The Hamiltonian given by Eq. 3.4 is expanded about $\vec{k}_{sd}$ along (1,1) direction, and the direction transverse to it. To that end $\widetilde{\varepsilon}_{1k}, \widetilde{\varepsilon}_{2k}$, and V_k are expanded along both the directions. Expanding $\widetilde{\varepsilon}_{1k}, \widetilde{\varepsilon}_{2k}$, and$V_k^2/\varepsilon_3$ in the (1,1) direction, the following expressions are obtained

$$\widetilde{\varepsilon}_{1k} \approx \frac{\varepsilon_1 + \varepsilon_2}{2} - (2\sqrt{2}t\sin k_{x_0})\delta k_{\parallel} \tag{3.8a}$$

$$\widetilde{\varepsilon}_{2k} \approx \frac{\varepsilon_1 + \varepsilon_2}{2} + (2\sqrt{2}t\sin k_{x_0})\delta k_{\parallel} \tag{3.8b}$$

$$V_k^2/\varepsilon_3 = 0, \tag{3.8c}$$

where $\delta k_{\parallel}$ is the distance along $(1,1)$ direction. Expanding the same quantities along the orthogonal direction it is found that the first order changes in $\widetilde{\varepsilon}_{1k}$ and $\widetilde{\varepsilon}_{2k}$ are zero, but that in V_k is nonzero. Hence unlike Eq. 3.8c, V_k^2/ε_3 is given by

$$V_k^2/\varepsilon_3 \approx \frac{8t'^2}{\widetilde{\varepsilon}_3}\sin^2 k_{x_0}\delta k_{\perp}^2, \tag{3.9}$$

where $\delta k_{\perp}$ is the distance along the orthogonal direction. Defining two constants m, and v as $\frac{\hbar^2}{2m} \equiv \frac{8t'^2}{\widetilde{\varepsilon}_3}\sin^2 k_{x_0}$, and $\hbar v \equiv 2\sqrt{2}t\sin k_{x_0}$[The motivation for doing so will be clear

from Eq. 3.12], Eq. 3.8 and Eq. 3.9 become

$$\widetilde{\varepsilon}_{1k} \approx \frac{\varepsilon_1 + \varepsilon_2}{2} + \hbar v \delta k_{\parallel} \tag{3.10a}$$

$$\widetilde{\varepsilon}_{2k} \approx \frac{\varepsilon_1 + \varepsilon_2}{2} - \hbar v \delta k_{\parallel} \tag{3.10b}$$

$$V_k{}^2/\varepsilon_3 = 0 \tag{3.10c}$$

and

$$V_k{}^2/\varepsilon_3 \approx \frac{\hbar^2}{2m} \delta k_{\perp}^2. \tag{3.11}$$

Using Eq. 3.10 and Eq. 3.11 in Eq. 3.4, the following expression for the Hamiltonian is obtained

$$H = \begin{pmatrix} \frac{\varepsilon_1 + \varepsilon_2}{2} + \hbar v \delta k_{\parallel} & \frac{\hbar^2}{2m} \delta k_{\perp}^2 \\ \frac{\hbar^2}{2m} \delta k_{\perp}^2 & \frac{\varepsilon_1 + \varepsilon_2}{2} - \hbar v \delta k_{\parallel} \end{pmatrix} \tag{3.12}$$

Relabeling $\hbar \delta k_{\perp}$ as q_1 and $\hbar \delta k_{\parallel}$ as q_2, and ignoring a constant shift in energy in the diagonal elements of the Hamiltonian in Eq. 3.12, it takes the following form

$$H = \begin{pmatrix} v q_2 & q_1^2/2m \\ q_1^2/2m & -v q_2 \end{pmatrix} \tag{3.13}$$

where q_2 and q_1 denote the distance from $\vec{k}_{sd}$ along the $(1,1)$ symmetry direction, and the orthogonal $(1,\bar{1})$, respectively. The Fermi velocity v and effective mass m can be related explicitly to the tight binding model parameters, and also calculated by standard ab initio techniques. The eigenvalues of H are given by

$$E_{q\pm} \rightarrow \pm\sqrt{(q_1^2/2m)^2 + (v q_2)^2}. \tag{3.14}$$

In terms of Pauli matrices Eq.3.13 can be written in the following way:

$$H = \tau_z(vq_2) + \frac{1}{2m}(q_1)^2\tau_x.$$

(3.15)

Another observation is that the *same bands $E_{q\pm}$* can be obtained from related but distinct low-energy models, such as

$$H_2 = \begin{pmatrix} vq_2 & iq_1^2/2m \\ -iq_1^2/2m & -vq_2 \end{pmatrix}$$

(3.16)

and

$$H_3 = \begin{pmatrix} 0 & q_1^2/2m + ivq_2 \\ q_1^2/2m - ivq_2 & 0 \end{pmatrix}$$

(3.17)

Although the bands resulting from H_2 and H_3 are the same, the eigenfunctions are different and are intrinsically complex for H_2 and H_3 unlike the eigenfunctions of the Hamiltonian given by Eq. 3.13. This particular aspect will be revisited in chapter 7.

4. SEMI-DIRAC SYSTEM IN A MAGNETIC FIELD

One of the issues of most interest to semi-Dirac systems is the behavior in a magnetic field. In this chapter the effect of the magnetic field on the semi-Dirac electrons will be described. This chapter draws on the papers [42] and [66] mentioned in the references.

4.1 Landau Like Quantized Energy Levels

The quantized energy levels of an electron with a parabolic dispersion in a magnetic field are called the Landau levels (L.L s). For the parabolic dispersion, the dependence of the L.L s on the magnetic field and the quantum number n have been worked out. In this section an expression for the Landau like energy levels for the semi-Dirac dispersion are found. The cyclotron orbit that a semi-Dirac electron would follow in a magnetic field is calculated and the phenomenon of Faraday rotation is investigated.

Making the usual substitution $\vec{q} \rightarrow \vec{p} + \frac{e}{c}\vec{A}$ with momentum operator $\vec{p}$ and vector potential $\vec{A}$ in the Hamiltonian given by Eq. 3.15, the Landau gauge $\vec{A} = B(-x_2, 0, 0)$ is found to be the most convenient here. The Hamiltonian in Eq. 3.15 then becomes

$$
\begin{aligned}
H &= \tau_z(vq_2) + \frac{1}{2m}(p_1 - \frac{e}{c}Bx_2)^2\tau_x \\
&= \tau_z(-i\hbar v\frac{\partial}{\partial x_2}) + \frac{\hbar^2}{2m}(p_1 - \frac{e}{c}Bx_2)^2\tau_x,
\end{aligned}
\tag{4.1}
$$

where q_1 and q_2 are the momentum space co-ordinates of the corresponding real space co-ordinates x_1 and x_2 respectively. A length scale L is introduced in the above problem, which will simplify the subsequent calculations. Also the dimensionless variable $\tilde{x}_2$ is introduced, such that $x_2 = L\tilde{x}_2$, and $x_1 = L\tilde{x}_1$. With the introduction of the length scale

the Hamiltonian in Eq. 4.1 becomes

$$
\begin{aligned}
H & = (-i\hbar \frac{v}{L})\tau_z \frac{\partial}{\partial \tilde{x}_2} + \frac{1}{2m}(p_1 - \frac{e}{c}BL\tilde{x}_2)^2 \tau_x \\
& = (-i\hbar \frac{v}{L})\tau_z \frac{\partial}{\partial \tilde{x}_2} + \frac{1}{2m}(\frac{e}{c}BL)^2(\tilde{x}_2 - \frac{p_1}{\frac{e}{c}BL})^2 \tau_x.
\end{aligned}
\tag{4.2}
$$

The length scale L is determined in such a way that the first two terms of Eq. 4.2 have the same dimension. To that end $\frac{\hbar v}{L}$ in the first term is equated to $\frac{1}{m}(\frac{eBL}{c})^2$ in the second term. The length scale thus obtained is

$$
L = \frac{mv\hbar}{(\frac{eB}{c})^2}.
\tag{4.3}
$$

In the following it is shown that the length scale in Eq. 4.3 can be obtained in a rather natural way. A natural unit of momentum $p = 2mv$ has already been defined in the context of semi-Dirac dispersion. The corresponding length scale is $l = \hbar/p$. Introducing the atomic unit of magnetic field $B_\circ$ such that $\mu_B B_\circ = 1$ Ha, and the dimensionless field $b = B/B_\circ$, it can be shown that

$$
L = (\frac{1}{\sqrt{2}\gamma b})^{\frac{2}{3}} l,
\tag{4.4}
$$

where γ is the dimensionless ratio of the two natural energy scales: $\gamma = \mu_B B_\circ/\varepsilon_0$, ε_0 being the energy scale previously introduced in the context of the semi-Dirac dispersion. For the case of trilayer VO_2, γ does not differ greatly from unity. With the length scale defined above, and introducing a new dimensionless variable $u \equiv \tilde{x}_2 - \frac{p_1}{\frac{e}{c}BL}$, the Hamiltonian in Eq. 4.2 reduces to

$$
H = \hbar \frac{v}{L}(-i\frac{\partial}{\partial u}\tau_z + u^2 \tau_x), .
\tag{4.5}
$$

The only dimensional factor appearing in Eq. 4.5 is the overall multiplicative factor $\hbar \frac{v}{L}$. Using Eq. 4.4 for L, $\hbar \frac{v}{L}$ becomes $(\sqrt{2}\gamma b)^{\frac{2}{3}}\varepsilon_0$. Hence the Hamiltonian in Eq. 4.5 can also

be written as

$$H = (\sqrt{2}\gamma b)^{\frac{2}{3}}\varepsilon_0(-i\frac{\partial}{\partial u}\tau_z + u^2\tau_x) \tag{4.6}$$

$$\equiv (\sqrt{2}\gamma b)^{\frac{2}{3}}\varepsilon_0 h.$$

The dimensionless Hamiltonian h in Eq. 4.6 is given by

$$h = -i\frac{\partial}{\partial u}\tau_z + u^2\tau_x. \tag{4.7}$$

The goal is to find out the eigenvalues of h. The problem of diagonalization is simplified considering h^2 instead of h as is shown below. Using the properties of the Pauli matrices, e.g., $\tau_x^2 = \tau_z^2 = I$, $\tau_z\tau_x = -\tau_x\tau_z = i\tau_y$ etc, one can show

$$h^2 = -\frac{\partial^2}{\partial u^2} + \frac{1}{4}u^4 + \frac{1}{2}\tau_y[\frac{\partial}{\partial u}, u^2]. \tag{4.8}$$

Using the fact that $[\frac{\partial}{\partial u}, u^2] = 2u$, Eq. 4.8 reduces to

$$h^2 = -\frac{\partial^2}{\partial u^2} + \frac{1}{4}u^4 + u\tau_y. \tag{4.9}$$

τ_y having eigenvalues of ± 1, finding the eigenvalues of h^2 is equivalent to finding the eigenvalues of the following two operators

$$h^2 = -\frac{\partial^2}{\partial u^2} + \frac{1}{4}u^4 \pm u \tag{4.10}$$

It is instructive to note that h^2 appearing in Eq. 4.10 can be written as $Q^\dagger Q$, where $Q = -i\frac{\partial}{\partial u} + i\frac{u^2}{2}$, a linear combination of u and its conjugate variable $p_u \equiv -i\frac{\partial}{\partial u}$, or $QQ^\dagger$ depending on whether the plus or the minus sign is considered in Eq. 4.10. The operator Q is analogous to the ladder operator a that appears in the context of the harmonic oscillator. For an harmonic oscillator, the operators a and $a^\dagger$ obey the commutation rule $[a, a^\dagger] = 1$. It can be shown by a straightforward calculation that the commutator of Q and $Q^\dagger$ is given

by $[Q, Q^\dagger] = -2u$. The difference in the two commutation relations is obvious. In case of a harmonic oscillator, the commutator of the ladder operators is a constant, whereas it is not so for the semi-Dirac problem. The Hamiltonian for the harmonic oscillator, when expressed in terms of the ladder operators, is given as $H = a^\dagger a + \frac{1}{2}$; whereas for the semi-Dirac problem, the Hamiltonian squared as obtained in Eq. 4.10 can be written as $h^2 = Q^\dagger Q$. Apart from an additive constant $\frac{1}{2}$, they are formally similar. One important difference is, in case of the harmonic oscillator the Hamiltonian itself is written in terms of the ladder operators; whereas in case of semi-Dirac, it is the Hamiltonian squared which is written in terms of the operators Q, and $Q^\dagger$. The eigen-equation for the Hamiltonian in Eq. 4.10 is given by

$$Q^\dagger Q \phi_n(u) = (-\frac{\partial^2}{\partial u^2} + \frac{1}{4}u^4 + u)\phi_n(u) = \varepsilon_n \phi_n(u), \tag{4.11}$$

and a similar equation replacing $Q^\dagger Q$ on the left of Eq. 4.11 by $QQ^\dagger$, with the plus sign before u on the right side of the same equation replaced by a minus sign.

4.1.1 Solving the Eigenvalue problem by WKB Method

The eigenvalue problem in Eq. 4.11 is similar to solving for a Schrodinger equation with a linear plus a quartic potential. The eigenvalue problem in Eq. 4.11 can not be solved exactly due to the presence of the quartic potential term $\frac{1}{4}u^4$. For some general results one must resort to an approximate method. The 'Wentzel Kramers Brillouin' or WKB method is such an approximate method, which allows one to compute the eigen-energies without needing first to solve the Schrodinger's equation. It is based on casting the wave-function under certain approximations in such a way that the energy quantization comes out as a requirement of uniqueness of the wave-function. Following is a brief description of the WKB method.

4.1.2 WKB Method

For simplicity and also due to the relevance to the problem at hand, in the following only the one dimensional case is considered. A higher dimensional generalization, although not required for our problem, is straight forward. The one dimensional Schrodinger equation can be written as

$$\frac{d^2\psi}{dx^2} = -\frac{p^2}{\hbar^2}\psi,$$ (4.12)

where

$$p(x) = \sqrt{2m(E - V(x))}.$$ (4.13)

x denotes the space variable; E, the eigenvalue and V, the potential. It is noted that p in Eq. 4.13 reduces to the conventional free particle momentum when $V(x) = 0$. p is in general a function of x. Writing $\psi(x) = A(x)e^{i\phi(x)}$ for the wave-function $\psi(x)$, and after substituting that in Eq. 4.12, equating the real and the imaginary parts separately one obtains the following coupled equations for the amplitude and the phase functions $A(x)$ and $\phi(x)$ respectively.

$$\frac{A''}{A} = (\phi')^2 - \frac{p^2(x)}{\hbar^2},$$ (4.14)

$$(A^2\phi')' = 0.$$ (4.15)

The solution to Eq. 4.15 is easy and is given by

$$A^2\phi' = C,$$ (4.16)

where C is a constant. Next it is assumed that $\frac{A''}{A}$ is a small quantity, which is a reasonable assumption if A is slowly varying function of x. Then the left side of Eq. 4.14 is ≈ 0 and

the following is obtained

$$\phi' = \pm\frac{p}{\hbar}.$$ (4.17)

Solving for ϕ,

$$\phi = \pm\frac{1}{\hbar}\int p(x).$$ (4.18)

Using Eq. 4.18 in Eq. 4.16, the following is obtained

$$A = \frac{C}{\sqrt{p(x)}}.$$ (4.19)

Combining Eq. 4.19 and Eq. 4.18 the following expression is obtained for the wave-function

$$\psi(x) \equiv Ae^{i\phi(x)} \approx \frac{C}{\sqrt{p(x)}}e^{\pm\frac{i}{\hbar}\int p(x)dx}.$$ (4.20)
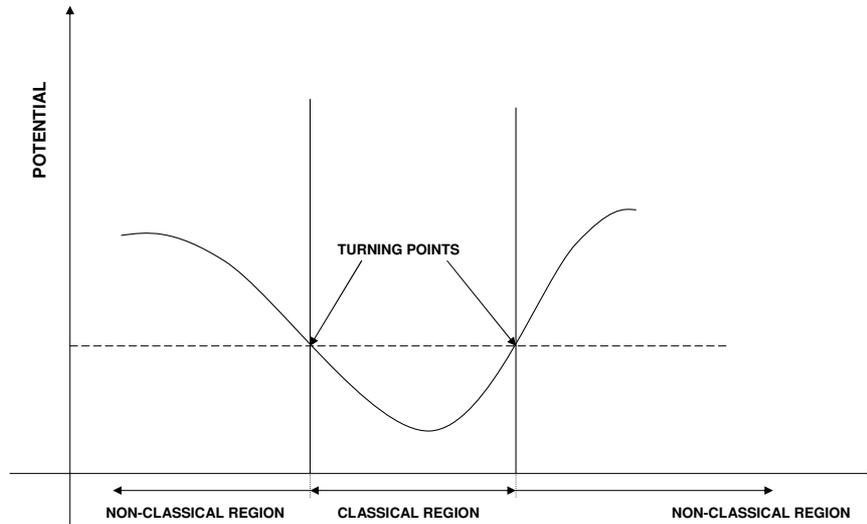
Fig. 4.1: Illustrating classical and nonclassical regions, as well as turning points

$p(x)$ in Eq. 4.20 can be real or imaginary depending on whether x is in the classical

region or not. By classical region one means the range of the space variable x, in which the total energy of the particle E is greater than $V(x)$. The range of x, in which $E < V(x)$ is called the nonclassical region. In the non-classical region, $p(x)$ given by Eq. 4.13 is imaginary. Hence in the nonclassical region Eq. 4.20 reduces to

$$\psi(x) \approx \frac{C}{\sqrt{|p(x)|}} e^{\pm \frac{1}{\hbar} \int |p(x)| dx}. \tag{4.21}$$

In Fig.4.1 the classical region, the non-classical region, and turning points (values of x where the total energy is equal to the potential energy) are shown. In the following one of the turning points is considered: the right turning point. Shifting the origin to there and referring to Eqs. 4.20 and 4.21 one can write the wave-function for the classical ($x < 0$) and the non-classical ($x > 0$) regions as follows

$$\psi(x) \approx \frac{1}{\sqrt{p(x)}} [B e^{\frac{i}{\hbar} \int_x^0 p(x') dx'} + C e^{-\frac{i}{\hbar} \int_x^0 p(x') dx'}], x < 0 \tag{4.22a}$$

$$\approx \frac{1}{\sqrt{|p(x)|}} D e^{-\frac{1}{\hbar} \int_0^x |p(x')| dx'}, x > 0. \tag{4.22b}$$

4.1.3 Patching Function

The wave-functions given by Eq. 4.22 has a serious problem: they blow up at the turning points, where $p(x) = 0$. So it is suspected although the wave-functions given by Eq. 4.22 are good approximations away from the turning point and well into the classical and the non-classical regions, a different patching function is needed for the region around the turning point. In the following it is described how that patching function is obtained. Referring to Fig.4.2, the potential function is Taylor-expanded about the turning point as follows:

$$V(x) \approx E + V'(0)x, \tag{4.23}$$

POTENTIAL

LINARIZED POTENTIAL

ACTUAL POTENTIAL

RIGHT TURNING POINT

CLASSICAL REGION   NON-CLASSICAL REGION
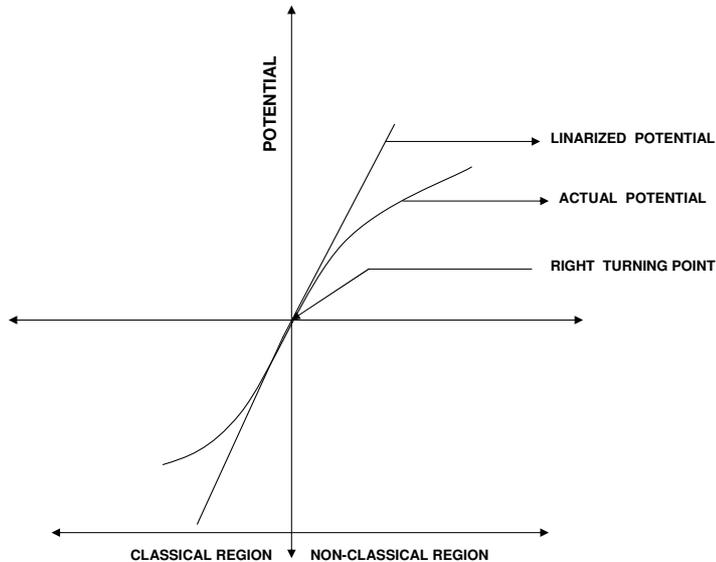
Fig. 4.2: Zooming in on one of the turning points

where E is the total energy, and $V'(0)$ denotes the slope of the potential at $x = 0$. Inserting Eq. 4.23 in Eq. 4.12, the following is obtained

$$\frac{d^2\psi_{\text{patch}}}{dx^2} = -\beta^3 x \psi_{\text{patch}},\tag{4.24}$$

where ψ_{patch} is the patching function valid near the turning point and β is a constant given by $\beta \equiv [\frac{2m}{\hbar^2} V'(0)]^{\frac{1}{3}}$. Eq. 4.24 goes by the name 'Airy's equation'. [Absorbing the constant β in the variable x, one could cast Eq. 4.24 in a form more recognizable as a Airy's equation, for example, $\frac{d^2\psi}{dz^2} = -z\psi$, where z is the new variable βx.] The linearly independent solutions of Eq. 4.24 are given by the functions $Ai(\beta x)$ and $Bi(\beta x)$. The most general solution of the Airy's equation will involve both the functions. But the fact that $Bi(\beta x)$ blows up for large values of x does not qualify it as a physical solution for ψ_{patch}: after all, the patching function should match with the exponentially decaying expression for the wave function in the nonclassical region given by Eq. 4.22b. Hence for the turning point under question, the solution for the patching function will involve $Ai(\beta x)$ only. In the
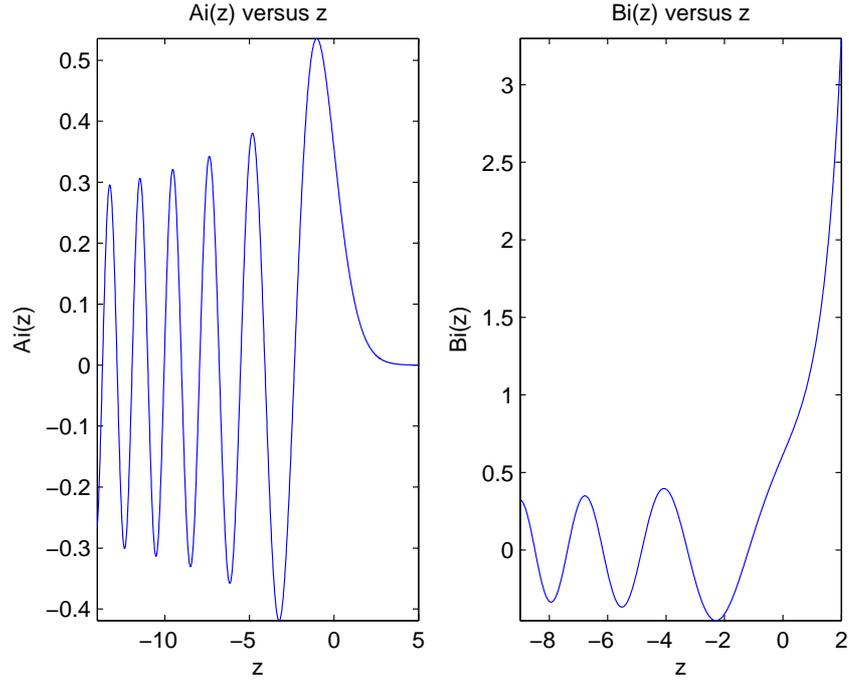
Fig. 4.3: The Airy's functions Ai(z) and Bi(z)

following only the classical region $(x < 0)$ is considered, since that will help us obtain the WKB quantization condition. The wave function assumes an uninteresting exponentially decaying form in the non-classical region $(x > 0)$. In the following it is verified that the asymptotic expression for the Airy function $Ai(\beta x)$ in the classical region matches with Eq. 4.22b. The reason for considering an asymptotic expression for the Airy function in the classical region is that it is a solution for the wave function around the right turning point which is rather far away from the core of the classical region. Inserting Eq. 4.23 in Eq. 4.13, the following is obtained

$$p(x) \approx \hbar \beta^{\frac{3}{2}} \sqrt{-x}. \tag{4.25}$$

27

Using Eq. 4.25 for $p(x)$ in Eq. 4.22a, the following is obtained

$$\psi(x) \approx \frac{1}{\sqrt{\hbar}\alpha^{\frac{3}{4}}(-x)^{\frac{1}{4}}}[Be^{i\frac{2}{3}\hbar(-\alpha x)^{\frac{3}{2}}} + Ce^{-i\frac{2}{3}\hbar(-\alpha x)^{\frac{3}{2}}}] \tag{4.26}$$

The asymptotic expression for ψ_{patch} is:

$$\psi_{\text{patch}}\ Ai(\beta x) \approx \frac{1}{\sqrt{\pi}(-\beta x)^{\frac{1}{4}}}\sin[\frac{2}{3}(-\beta x)^{\frac{3}{2}} + \frac{\pi}{4}], x \ll 0. \tag{4.27}$$

Comparing Eq. 4.26 and Eq. 4.27 it is observed that they agree as expected with the choices of $B = \sqrt{\frac{\hbar\alpha}{\pi}}\frac{1}{2i}e^{i\frac{\pi}{4}}$ and $C = -\sqrt{\frac{\hbar\alpha}{\pi}}\frac{1}{2i}e^{-i\frac{\pi}{4}}$. Hence Eq. 4.27 gives the wave function for the classical region. In Eq. 4.27 the term $\frac{2}{3}(-\beta x)^{\frac{3}{2}}$ appearing in the argument of the sine function is nothing but the integral $\int_x^0 p(x')dx'$, where $p(x)$ is given by Eq. 4.25. As for the upper limit of integration, one can replace 0 by a more generic symbol x_2, corresponding to the right turning point as shown in Fig.4.1. Finally dropping the pre factors, in Eq. 4.27 only the sine function is written as

$$\sin[\frac{1}{\hbar}\int_x^{x_2} p(x')dx' + \frac{\pi}{4}] \tag{4.28}$$

[With the goal of obtaining the WKB quantization condition it will suffice to focuss on the sine function only.] Eq. 4.28 does not depend on a specific choice of origin. In an exactly similar way expanding the potential $V(x)$ about the left turning point as shown in Fig.4.1, a very similar expression as Eq. 4.28 will be arrived at. The only difference will be in the limits of integration in the integral appearing inside the argument of the sine function: instead of having $\int_x^{x_2} p(x')dx'$ one will have $\int_{x_1}^x p(x')dx'$, where x_1 is the co-ordinate of the left turning point. Hence for the left turning point, the expression that would correspond to to Eq. 4.28 is given as follows

$$\sin[\frac{1}{\hbar}\int_{x_1}^x p(x')dx' + \frac{\pi}{4}] \tag{4.29}$$

The expressions given by Eq. 4.28 and Eq. 4.29 should correspond to the same wave function: the wave function being unique(up to a sign)should not depend on how it is arrived at. As a wave function is unique up to a sign, the argument of the sine function in Eq. 4.29 can be multiplied with an overall negative sign. [Any special assumption is not being made here. It's just that without the negative sign one doesn't get the quantization condition in its desired form.] With that little adjustment, Eq. 4.29 is transformed into

$$\sin[-\frac{1}{\hbar}\int_{x_1}^{x} p(x')dx' - \frac{\pi}{4}]$$ (4.30)

Considering the equivalence of Eq. 4.28 and Eq. 4.30, and using the fact that two sine functions differ at most by a sign if their arguments differ by an additive constant $n\pi$(where n is an integer), the following WKB energy quantization condition is obtained

$$\int_{x_1}^{x_2} p(x)dx = (n + \frac{1}{2})\pi\hbar,$$ (4.31)

n being an integer. This finishes the description of the WKB method. Next it is described how the method is applied in the context of the semi-Dirac problem.

4.1.4   Results obtained with the help of WKB method

With an aim to solving the eigenvalue problem in Eq. 4.11 it is noted that every eigenfunction of h given by Eq. 4.7 is also an eigenfunction of h^2, and that although the potential given by Fig.4.4 is negative in the interval $(0,4^{1/3})$, the eigenvalues ε_n^2 must be non-negative. In the following it is described how the WKB method is applied to compute the eigenvalues. Initially neglecting the linear term in the potential, the WKB condition given by Eq. 4.31 becomes

$$\int_{-\sqrt{2}\varepsilon_n^{\frac{1}{4}}}^{\sqrt{2}\varepsilon_n^{\frac{1}{4}}} \sqrt{E_n - \frac{1}{4}u^4}du = (n + \frac{1}{2})\pi,$$ (4.32)
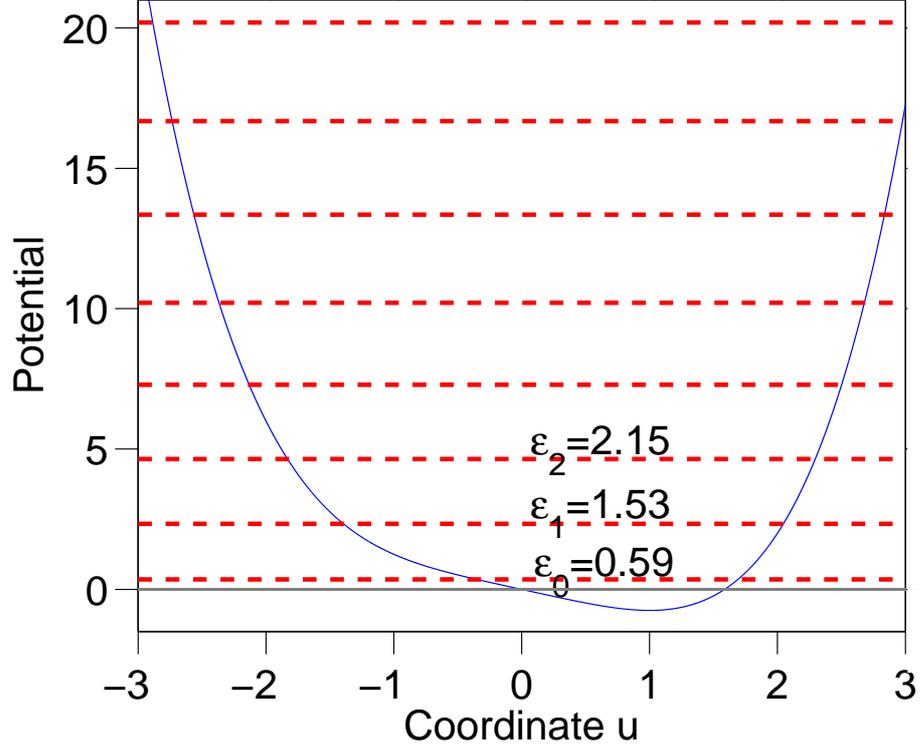
Fig. 4.4: Potential energy function $\frac{1}{4}u^4 + u$ for the one-dimensional Schrodinger equation and the resulting quantized energy levels for h^2 obtained by the WKB method. The lowest three energy eigenvalues ε_n's are given explicitly.

which can be solved in closed form to give the eigenvalues for the quartic potential as

$$\varepsilon_n^2 = [3\sqrt{\frac{\pi}{2}}\frac{\Gamma(\frac{3}{4})}{\Gamma(\frac{1}{4})}]^{4/3}(n+\frac{1}{2})^{\frac{4}{3}} = 1.3765(n+\frac{1}{2})^{\frac{4}{3}}. \tag{4.33}$$

The linear perturbation corrects the eigenvalues only to second order, which is a small correction as verified by direct numerical solution, which gets successively smaller for higher eigenvalues. [This has been verified by numerical solution of the eigenvalue problem in Eq. 4.11.] Therefore the semiDirac system has eigenvalues in a magnetic field which scale as $B^{2/3}$ (from Eq. 4.6) and increase as $(n+\frac{1}{2})^{2/3}$(from Eq. 4.33) as n gets large. Both

aspects lie between the behaviors for conventional Landau levels (linear in B, proportional the $n + \frac{1}{2}$) and the Dirac point behavior (proportional to $\sqrt{B\,n}$), as might have been anticipated. Some low-lying eigenvalues of h^2 are shown in Fig.4.4 against the potential well. It is noted that there is no zero-energy solution as in the graphene problem.

4.2 Faraday Rotation in the context of the semi-Dirac system

4.2.1 The semiclassical equation of motion

The semiclassical equation of motion of an electron in a magnetic field $\vec{B}$ is given by

$$\hbar \frac{d\vec{k}}{dt} = -\frac{e}{c} \vec{v}_k \times \vec{B}. \tag{4.34}$$

Using Eq. (2.6) for $\vec{v}_k$ in Eq. (4.34), one obtains the following expressions

$$\frac{dK_x}{dt} = -\omega_0 K_y, \tag{4.35a}$$

$$\frac{dK_y}{dt} = 2\omega_0 K_x^3, \tag{4.35b}$$

where K_x and K_y are the dimensionless variables associated with momentum introduced before, and ω_0 is given by

$$\omega_0 = \frac{eBv^2}{c\varepsilon}, \tag{4.36}$$

where B is the magnetic field, and ε, the Fermi energy. Combining Eqs. Eq. (4.35a) and Eq. (4.35b), the following differential equation is obtained

$$\frac{d^2 K_x}{dt^2} = -2\omega_0^2 K_x^3, \tag{4.37}$$

In order to solve this second order differential equation, we multiply both sides of the equation by $\dot{K}_x$ ($\dot{K}_x$ denotes the derivative of K_x w.r.t time). Both the right and the left sides of the equation can then be written as a total derivative of time, which can be

31

integrated to give

$$\dot{K}_x{}^2 = -\omega_0^2 K_x^4 + C, \tag{4.38}$$

where the constant C can be determined from the condition that $\dot{K}_x = 0$ when $K_x = (K_x)_{\text{max}}$. This follows from the fact that K_y is equal to 0 when $\dot{K}_x = 0$, as can be seen from Eq. (4.35a); and from the semiDirac dispersion given by Eq. 2.2, $K_y = 0$ corresponds to $K_x = (K_x)_{\text{max}} = \sqrt{\frac{\varepsilon}{\varepsilon_0}}$. Hence Eq. 4.38 becomes

$$\dot{K}_x = \omega_0 \sqrt{(K_x)_{\text{max}}^4 - K_x^4}, \tag{4.39}$$

4.2.2 The cyclotron frequency, solutions for K_x and K_y as functions of time, and the cyclotron orbit

Integrating Eq. 4.39, one obtains K_x as a function of time. Once K_x is known, K_y can be obtained from Eq. 4.35b. Before showing the detailed results for that, it is observed that the time period can be obtained simply by integrating Eq. 4.39 from $-(K_x)_{\text{max}}$ to $(K_x)_{\text{max}}$ for the variable K_x. The time period (T) thus obtained is

$$\omega_0 T = \frac{4I_1}{(K_x)_{\text{max}}} = 4I_1\sqrt{\varepsilon/\varepsilon_0}, \tag{4.40}$$

where I_1 is given by Eq. 2.5. From Eq. 4.40, the fundamental cyclotron frequency $\omega_c \equiv \frac{2\pi}{T}$ is obtained as

$$\omega_c/\omega_0 = \frac{\pi}{2} I_1^{-1} (\varepsilon/\varepsilon_0)^{-\frac{1}{2}}. \tag{4.41}$$

The cyclotron frequencies for the parabolic and the linear dispersion cases are given by $(\frac{\mu_B B}{\hbar} = \frac{eB}{mc})$ and $\frac{eBv^2}{c\varepsilon}$ respectively(μ_B is the Bohr magneton). Comparing with Eq. 4.41 it is observed that the cyclotron frequencies for all the three cases(the parabolic, linear, and semi-Dirac) depend linearly on the magnetic field. The cyclotron frequency is independent

32

of the Fermi energy for parabolic dispersion, whereas it varies as $\varepsilon^{-\frac{1}{2}}$ for the semiDirac dispersion and as ε^{-1} for the linear Dirac dispersion. One important aspect of the semi-Dirac dispersion is that the semi-Dirac dispersion being anisotropic in the momentum space can have harmonics of the fundamental cyclotron frequency given by Eq. 4.41. This feature is absent in the Dirac or the two dimensional parabolic dispersion where the energy momentum dispersion is isotropic giving rise to only one value for the cyclotron frequency.

Next, In order to find the solution to Eq. 4.39 in closed form, a new variable K_x' is introduced defined as $K_x' = \frac{K_x}{(K_x)_{\max}}$. Eq. 4.39 is rewritten in terms of the new variable as follows

$$\dot{K_x'} = \omega_0'\sqrt{1 - K_x'^4}, \tag{4.42}$$

where ω_0' is given by

$$\omega_0' = (K_x)_{\max}\omega_0 = \sqrt{\frac{\varepsilon}{\varepsilon_0}}\omega_0 \tag{4.43}$$

The solution to Eq. 4.42 can be given in closed form in terms of elliptic integrals. To that end Eq. 4.42 is written in the integral form as follows

$$\int \frac{dK_x'}{\sqrt{1 - K_x'^4}} = \omega_0' \int t \tag{4.44}$$

The solution of the above equation is given by

$$\frac{1}{\sqrt{2}}F(\arcsin \frac{\sqrt{2}K_x'}{\sqrt{1 + K_x'^4}}, \frac{1}{\sqrt{2}}) = \omega_0't, \tag{4.45}$$

where the function F is the elliptic integral of the first kind. It has two arguments and is defined as follows

$$F(\varphi, k) = \int_0^\varphi \frac{dw}{\sqrt{1 - k^2 \sin^2 w}} \tag{4.46}$$

The implicit expression in Eq. 4.45 is solved for the variable K'_x (there is command in Matlab to do that). K'_x and K'_y are plotted w.r.t the dimensionless time variable $t' \equiv \omega'_0 t$ in Fig.4.5. K'_x and K'_y have an inverse relationship as far as evolution with time is concerned:
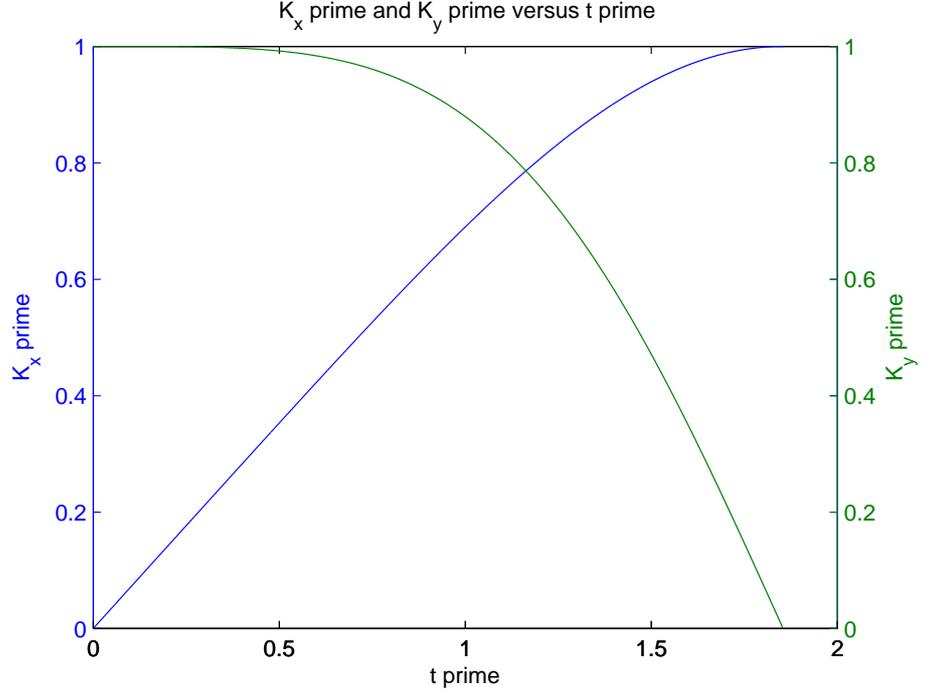
Fig. 4.5: K'_x and K'_y versus the dimensionless time variable t'

as one of them increases, the other one decreases. Their rates of change w.r.t time are also not the same. As can be seen from Fig.4.5, near $t' = 0$, K'_x changes much more rapidly than K'_y, which stays approximately flat for a while. This is reversed near the end where K'_x is close to one and K'_y is close to zero. The differential equation for the cyclotron orbit is obtained by dividing Eq. 4.35b by Eq. 4.35a. Solving for that, we obtain the semi-Dirac constant energy contour as an expression for the cyclotron orbit, which is expected, since the energy of an electron does not change when it moves under the influence of magnetic

34

field.

Angle of rotation of the plane
Of polarization
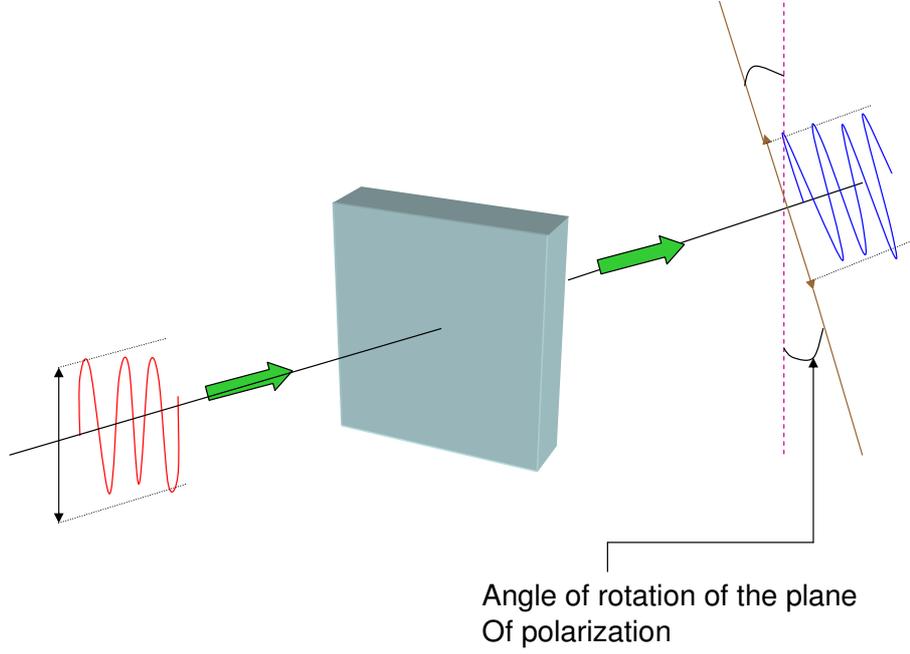
Fig. 4.6: Faraday rotation [36]

The Faraday rotation Fig.4.6 is the phenomenon of rotation of polarization of light after passing a medium in the presence of the magnetic field. This was first discovered by Michael Faraday, which helped to establish the relationship between light and electromagnetism. The Faraday rotation angle is given by the expression [36]

$$\theta(\omega, B) = Z_0 f_s(\omega) Re[\sigma_{xy}(\omega, B)], \tag{4.47}$$

where Z_0 is the impedance of the vacuum, f_s is the spectrally featureless function specific to the substrate, and σ_{xy} is the dynamic Hall conductivity. According to the Drude formula the dynamic Hall conductivity is given by [36]

$$\sigma_{xy} = \frac{-2\mathcal{D}}{\pi} \frac{\omega_c}{\omega_c^2 - (\omega + \frac{i}{\tau})^2}, \tag{4.48}$$

35

where $\mathcal{D}$ is the Drude weight, given by $\mathcal{D} = \frac{\pi}{6}e^2 D(\varepsilon)\langle v^2 \rangle$. Taking the real part of Eq. 4.48 and using it in Eq. 4.47 we obtain

$$\theta(\omega, B) = \frac{-2Z_0 f_s(\omega)\mathcal{D}\omega_c}{\pi} I(\omega), \tag{4.49}$$

where $I(\omega)$ is given by

$$I(\omega) = \frac{\omega_c^2 - \omega^2 + \frac{1}{\tau^2}}{(\omega_c^2 - \omega^2 + \frac{1}{\tau^2})^2 + \frac{4\omega^2}{\tau^2}} \tag{4.50}$$

Extremizing $I(\omega)$ and inserting the resulting expression for $I(\omega)$ in Eq. 4.49 we obtain the following expression for the maximum value of the Faraday rotation angle θ

$$\theta(\omega, B) = \frac{-Z_0 f_s(\omega)\mathcal{D}\omega_c\tau^2}{2\pi((\omega_c^2\tau^2 + 1)^{\frac{1}{2}} - 2)}, \tag{4.51}$$

The Drude weight $\mathcal{D} \sim \varepsilon$ for Dirac dispersion (since $D(\varepsilon) \sim \varepsilon$, and $\langle v^2 \rangle$ is a constant). The Dirac cyclotron frequency $\omega_c \sim \varepsilon^{-1}$. Hence the product $\mathcal{D}\omega_c$ that appears in the numerator of Eq. 4.51 is independent of the doping level for Dirac dispersion. For semi-Dirac dispersion, $\mathcal{D} \sim \varepsilon^{\frac{1}{2}}$, which follows from the fact that the product $D(\varepsilon)\langle v^2 \rangle \sim D(\varepsilon)\langle v_y^2 \rangle$, where v_y is the speed in the relativistic direction, and that $D(\varepsilon)\langle v_y^2 \rangle \sim \varepsilon^{\frac{1}{2}}$. The last step follows by combining Eq. 2.4 and Eq. 2.10b. For the same dispersion $\omega_c \sim \varepsilon^{-\frac{1}{2}}$ (from Eq. 4.41). Hence, like Dirac dispersion, $\mathcal{D}\omega_c$ for the semi-Dirac dispersion is independent of the doping energy. For two dimensional parabolic dispersion, ω_c is independent of the doping energy, but $\mathcal{D} \sim \varepsilon$. Hence $\mathcal{D}\omega_c$ depends on the doping energy. This is a significant difference when compared to the Dirac and the semi-Dirac dispersion.

For Dirac and semi-Dirac systems the dependence of the Faraday angle on the doping level arises from the term $\omega_c\tau$ in the denominator of Eq. 4.51, whereas the numerator is independent of doping. For those dispersions one can fine tune the Fermi energy to obtain a large value of the Faraday angle by bringing the term $\omega_c\tau$ close to three, so that the term $(\omega_c^2\tau^2 + 1)^{\frac{1}{2}} - 2$ appearing in denominator goes to zero causing a significant value for

the Faraday angle.

5. FEATURES OF THE SEMI-DIRAC DISPERSION

5.1 Introduction

In this section a study of the low energy behavior of a semi-Dirac system is presented. That includes Hall coefficient, magnetic susceptibility and heat capacity. Results for plasma frequency versus doping level are also provided. Some new behavior along with somewhat conventional results are found. In the next chapter some results for Klein tunneling of semi-Dirac particles are given. While for several properties semi-Dirac behavior is intermediate and thus unique, it may become quite different for certain properties.

5.2 Hall Coefficient

The Hall effect is the building up of voltage transverse to the direction of the flow of the current when magnetic field is applied in a bar of a material. Classically the Hall effect can be thought of as a result of the deflecting Lorentz force that an electron encounters in the presence of the magnetic field. As an indicator of the intensity of this effect one defines a quantity called the Hall coefficient (R_H), which is the ratio of the transverse electric field and the product of the current and the magnetic field. For a given current the Hall coefficient gives a measure of how strong the transverse electric field is, or in other words how strongly an electron is deflected. Without considering the details of the band structure the Hall coefficient turns out to be a rather simple expression given as $R_H = \frac{-1}{nec}$, where n is the carrier concentration. With the help of Bloch Boltzman transport theory, in the following it is shown how to obtain an energy-momentum dispersion dependent expression for the Hall coefficient [37]. It is also shown even with as exotic a dispersion as semi-Dirac dispersion one obtains $R_H = \frac{-1}{nec}$! Following an argument based on mathematical and

geometrical features of the Fermi surface, it is proven that the above result holds for a class of energy momentum dispersion relation.

5.2.1 Bloch-Boltzman Transport theory

In transport theory the collective motions of electrons is considered. Electrons move due to the application of the electric and the magnetic field or the presence of a temperature gradient. The existence of a temperature gradient is ignored in computing the Hall coefficient. In Boltzman transport theory an important quantity is the local distribution function $F(\mathbf{r}, \mathbf{k})$ of electrons. $F(\mathbf{r}, \mathbf{k}) d\mathbf{r} d\mathbf{k}$ gives the number of electrons in the phase-space volume $d\mathbf{r} d\mathbf{k}$. In steady state $F(\mathbf{r}, \mathbf{k})$ is given by

$$F(\mathbf{r}, \mathbf{k}) = f(\varepsilon(\mathbf{k} - \hbar^{-1}\mathbf{F}_{\text{ext}}\tau)), \tag{5.1}$$

where $f(\varepsilon)$ and $\mathbf{F}_{\text{ext}}$ are the Fermi-Dirac distribution and external force respectively. τ is relaxation time. The Fermi-Dirac distribution $f(\varepsilon)$ is given by

$$f(\varepsilon) = 1 + e^{\frac{\varepsilon - \mu}{k_B T}}{}^{-1}, \tag{5.2}$$

where the standard notations for energy, chemical potential and Boltzman's constant have been used. The external force $\mathbf{F}_{\text{ext}}$ is the Lorentz force given by

$$\mathbf{F}_{\text{ext}} = -e\mathbf{E} - e\mathbf{v}(\mathbf{k} + e\mathbf{E}) \times \mathbf{B}. \tag{5.3}$$

The local distribution in Eq. 5.1 can be physically interpreted being same as the Fermi-Dirac distribution at an earlier time $t-\tau$, when the momentum of the electron was $\mathbf{k} - \mathbf{F}_{\text{ext}}\tau$. [During the time interval τ, the the momentum changes by $\mathbf{F}_{\text{ext}}\tau$, which is a consequence of the semi-classical equation of motion $\frac{d\mathbf{p}}{dt} = \frac{d\hbar\mathbf{k}}{dt} = \mathbf{F}$.] It is assumed that there has been no collision in the time interval τ, and that the electrons maintain a quasi-equilibrium

distribution after the collision. The current can be written as

$$j_\alpha = -\frac{e}{\Omega} \Sigma_k v_\alpha(\mathbf{k}) F(\mathbf{r}, \mathbf{k}). \tag{5.4}$$

The same current assumes the following form when expressed as a function of the electric and the magnetic field [37]

$$j_\alpha = \sigma_{\alpha\beta} E_\beta + \sigma_{\alpha\beta\gamma} E_\beta B_\gamma, \tag{5.5}$$
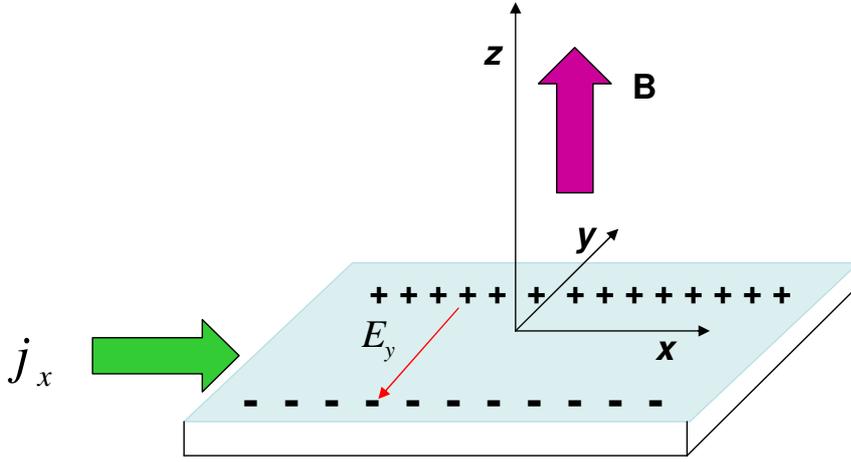
Fig. 5.1: The arrangement for the Hall effect. The applied magnetic field is in the z direction and the current flows along x.

where $\sigma_{\alpha\beta}$ and $\sigma_{\alpha\beta\gamma}$ are tensors. A two-dimensional system described by the co-ordinates x and y is considered. The current flows initially along the x-direction as shown in Fig.5.1. A magnetic field B is applied along the z-direction. Setting j_y , the current along y, in Eq. 5.5 to be zero (at equilibrium), the Hall coefficient R_H is obtained as

$$R_H = \frac{\sigma_{xyz}}{\sigma_{xx}\sigma_{yy}}. \tag{5.6}$$

After Taylor expanding Eq. 5.1 w.r.t the parameter τ, the resulting expression is inserted in Eq. 5.4, and the final expression is compared to Eq. 5.5. One obtains

$$\sigma_{xyz} = \frac{1}{2\pi^2}\int d\mathbf{k}[v_y(v_y\frac{\partial}{\partial k_x} - v_x\frac{\partial}{\partial k_y})](-\frac{\partial f}{\partial \varepsilon_\mathbf{k}}) \tag{5.7a}$$

$$\sigma_{xx} = \frac{1}{2\pi^2}\int d\mathbf{k}v_x^2(-\frac{\partial f}{\partial \varepsilon_\mathbf{k}}) \tag{5.7b}$$

$$\sigma_{yy} = \frac{1}{2\pi^2}\int d\mathbf{k}v_y^2(-\frac{\partial f}{\partial \varepsilon_\mathbf{k}}) \tag{5.7c}$$

The factor $(-\frac{\partial f}{\partial \varepsilon_\mathbf{k}})$ in the above equations arises as a result of Taylor expansion and in the low temperature limit is approximately equal to $-\delta(\varepsilon - \varepsilon_\mathbf{k})$. Using the identity $\int d\mathbf{k}\delta(\varepsilon - \varepsilon_\mathbf{k}) = \int dk_l|v_k^{-1}|$, where dk_l is the length along the Fermi-contour of the semi-Dirac dispersion, we obtain

$$\sigma_{xyz} = \frac{1}{2\pi^2}\int dk_l|v_k^{-1}|[v_y(v_y\frac{\partial}{\partial k_x} - v_x\frac{\partial}{\partial k_y})] \tag{5.8a}$$

$$\sigma_{xx} = \frac{1}{2\pi^2}\int dk_l|v_k^{-1}|v_x^2 \tag{5.8b}$$

$$\sigma_{yy} = \frac{1}{2\pi^2}\int dk_l|v_k^{-1}|v_y^2. \tag{5.8c}$$

It is shown in the following that Eq. 5.8a is the area A_v spanned by the velocity vector over the Fermi surface[38]. With the co-ordinates depicted in Fig.5.2, the following identity is obtained

$$v_k^{-1}(v_y\frac{\partial}{\partial k_x} - v_x\frac{\partial}{\partial k_y})v_x = v_k^{-1}[(\mathbf{v}\times\hat{z}).\nabla]v_x \tag{5.9}$$

$$= [(\hat{v}\times\hat{z}).\nabla]v_x$$

$$= [\hat{t}.\nabla]v_x$$

$$= dv_x$$

To derive the last line of Eq. 5.9, the fact that $\hat{t}.\nabla$ is the change 'd' along the Fermi contour

Area enclosed by the Fermi surface $= \int k_y dk_x$

Area enclosed by the velocity vector$= \int v_y dv_x$
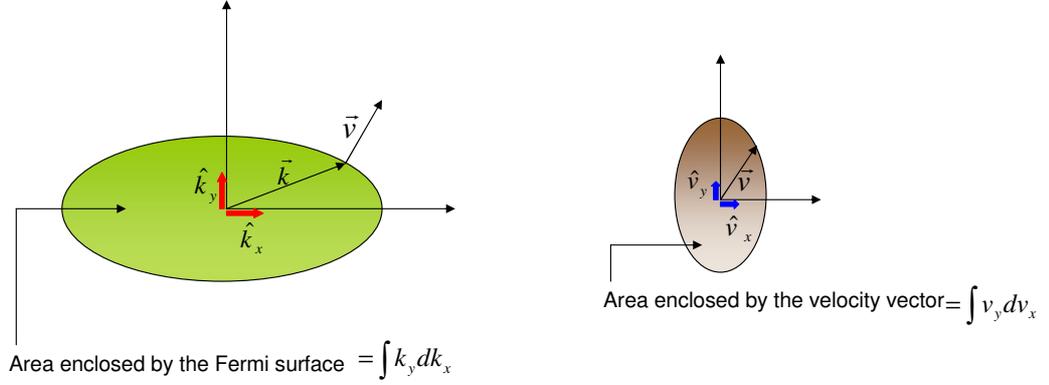
Fig. 5.2: The areas enclosed by the Fermi-contour as well as the closed curve described by the velocity vector defined on the Fermi contour

is used. Using Eq. 5.9 in Eq. 5.8a, the following expression for σ_{xyz} is obtained.

$$\sigma_{xyz} = \int v_y dv_x. \tag{5.10}$$

Eq. 5.10 is the area enclosed by the curve generated by the velocity vector at the Fermi contour, as one traverses along the Fermi-contour. This is a nice geometrical interpretation of σ_{xyz}. In the following the expressions for σ_{xx} and σ_{yy} are also simplified. The velocity $\mathbf{v_k} \sim \nabla_\mathbf{k} \varepsilon_\mathbf{k}$ at the Fermi contour is perpendicular to the line element $d\mathbf{k}_l$. But $\nabla_k \varepsilon \cdot d\mathbf{k} = 0$ implies

$$\frac{dk_y}{dk_x} = \frac{-v_x}{v_y}. \tag{5.11}$$

Using Eq. 5.11 in the expression for $|d\mathbf{k}_l|$ given as $|d\mathbf{k}_l| = (1 + (\frac{dk_y}{dk_x})^2)^{\frac{1}{2}}$, the following is

obtained

$$|d\mathbf{k}_l| = \frac{|v_k|}{v_y}dk_x, \tag{5.12}$$

where the fact that $|v_k| = \sqrt{v_x^2 + v_y^2}$ is used. Using Eq. 5.11 and Eq. 5.12 in Eq. 5.8b and in Eq. 5.8c, one obtains

$$\sigma_{xx} = \frac{1}{2\pi^2}\int dk_y v_x \tag{5.13a}$$

$$\sigma_{yy} = \frac{1}{2\pi^2}\int dk_x v_y \tag{5.13b}$$

Using Eq. 5.10, Eq. 5.13 in Eq. 5.6, the following is obtained

$$R_H = \frac{\frac{1}{2\pi^2}v_y dv_x}{(\frac{1}{2\pi^2}\int dk_y v_x)(\frac{1}{2\pi^2}\int dk_x v_y)}. \tag{5.14}$$

$\frac{1}{2\pi^2}\int dk_y v_x$ in the denominator of Eq. 5.14 can be recast as an integration over the velocity variable instead of over the momentum variable by executing an integration by parts as follows

$$\frac{1}{2\pi^2}\int dk_y v_x = \frac{1}{2\pi^2}[v_x k_y|_i^f - \int_i^f k_y dv_x], \tag{5.15}$$

where i and f are as indicated in Fig.5.3. [The semi-Dirac dispersion is symmetric both in the x and the y directions. Hence the limits of the integrals appearing in Eq. 5.15 (and also in Eq. 5.14) can be restricted to the first quadrant.]

Referring to Fig.5.3, k_y at i and v_x at f are zero. Hence Eq. 5.15 assumes the following form.

$$-\frac{1}{2\pi^2}\int dk_y v_x = \frac{1}{2\pi^2}\int_i^f k_y dv_x \tag{5.16}$$
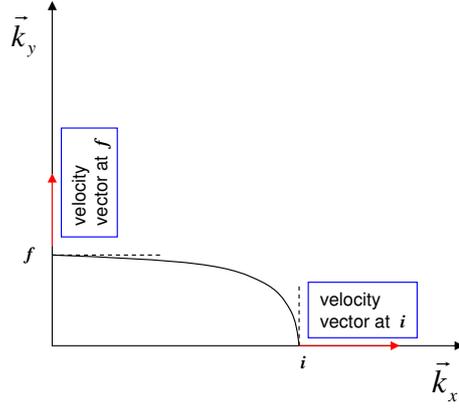
Fig. 5.3: One quarter of the semi-Dirac contour. The velocities at i and f are directed along k_x and k_y axis respectively.

Inserting Eq. 5.16 in Eq. 5.14 the following is obtained

$$R_H = \frac{-\frac{1}{2\pi^2} v_y dv_x}{\left(\frac{1}{2\pi^2} \int k_y dv_x\right)\left(\frac{1}{2\pi^2} \int v_y dk_x\right)}. \tag{5.17}$$

Next, it is noted that the carrier density n is proportional to the area swept by the vector **k** as **k** moves along the Fermi surface, which is same as the area enclosed by the Fermi surface as shown in Fig.5.2. Hence n is given by

$$n = \frac{1}{2\pi^2} \int k_y dk_x \tag{5.18}$$

Hence the quantity $R^H n$ is given by:

$$R^H n = -\frac{\int k_y dk_x \int v_y dv_x}{\int k_y dv_x \int v_y dk_x}. \tag{5.19}$$

Eq. 5.19 is the key result of this section. It will help in proving that $R^H n = -1$ for the semi-Dirac dispersion. It will also help establishing a general relationship between the energy-momentum dispersion and the quantity $R^H n$.

5.2.2 A theorem relating the energy-momentum dispersion and $R^H n$ being -1

*Under the assumptions that the Fermi surface is not too complicated and that there exists a pair of orthogonal axes in the k-space such that they are normal to the Fermi surface at the points they intersect the Fermi surface, if any component of the velocity vector is proportional to the corresponding component of the **k** vector throughout the Fermi surface, $R^H n$ will be equal to -1.* It is explained in the following how the theorem follows from Eq. 5.19. From Eq. 5.19 it is observed if the y component of the velocity vector is proportional to that of the **k** vector, $R^H n$ will be equal to -1. There is nothing special about the k_x or the k_y axis. If any component of the velocity vector is proportional to the corresponding component of the **k** vector, $R^H n$ will be equal to -1. For graphene, the energy momentum dispersion $\sim \sqrt{k_x^2 + k_y^2}$, which results in $v_y \sim k_y(k_x^2 + k_y^2)^{-1/2} = k_y \varepsilon_{Fermi}^{-1}$, where ε_{Fermi} is the energy at the Fermi contour. Since $v_y \propto k_y$ for the Dirac dispersion, $R^H n$ is equal to -1 for that case. For a simpler dispersion like the parabolic dispersion, both the components of the velocity vector are proportional to those of the **k** vector. Hence $R^H n$ is also -1 for that. For the semiDirac dispersion v_y evaluated on the Fermi surface turns out to be proportional to k_y(Eq. 2.7). [On the Fermi contour $\sqrt{K_X^4 + K_Y^2}$ is a constant.] Hence $R^H n = -1$. This is a rather surprising result given the complexity of the semi-Dirac dispersion. Eq. 5.19 was arrived at by assuming that the Fermi contour is normal to the k_x and k_y axes as shown in Fig.5.3. Hence if it turns out, for a particular choice of mutually orthogonal axes the above-mentioned condition is not satisfied, that does not immediately rule out $R^H n$ being -1. One should try to find a pair of orthogonal axes which are normal to the Fermi-contour. In case either that does not exist or the curvature of the F.S is not as simple as shown in Fig.5.3, the validity of the theorem may be compromised. In order to emphasize the point that the result is not true in general an hypothetical energy momentum dispersion, say, $\varepsilon_k = ak_x^4 + bk_y^4$ is invoked. For this dispersion $v_y \propto k_y^3$. Hence the requirement that v_y should be proportional to k_y is violated. It can be shown by direct calculation that $R^H n = -.8488 \neq 1$ for this problem. Hence it has been shown that the Hall coefficient times the carrier density is a topologically invariant quantity for a certain

class of band structures, whose F.S's are not too complicated.

5.3   Heat Capacity

It is shown that the heat capacity for the non-interacting *two*-dimensional semi-Dirac electron gas without any external potential is equal to that of the *three*-dimensional non-interacting electron gas with the parabolic energy-momentum dispersion at both the low and the high temperature ends. Relative to the natural energy scale ε_0 introduced at the beginning, the low and the high temperatures can be considered. The low temperature heat capacity per particle for the semiDirac dispersion is :

$$c_v = \frac{2I_1}{3} m k_B^2 \sqrt{\frac{\varepsilon}{\varepsilon_0}},\tag{5.20}$$

which is calculated using Sommerfeld expansion [44](I_1 is given in Eq. 2.5). It is observed that the heat capacity in Eq. 5.20 is proportional to $\sqrt{\varepsilon}$. A similar type of dependence with energy is observed for the three dimensional electron gas. The major difference between the heat capacity for a three dimensional electron gas and two dimensional semi-Dirac electron gas is in the prefactors. This difference disappears quite nicely in the high temperature end as is shown in the following. At high temperature, the heat capacity for the three dimensional electron gas is given by $\frac{3}{2} k_B$. In order to emphasize a technique that will be used for the semi-Dirac problem a derivation of the above result for the three-D electron gas is first outlined in the following. The Hamiltonian for the parabolic three dimensional Hamiltonian is given by $H_{\text{parabolic}} = \frac{1}{2m}(p_x^2 + p_y^2 + p_z^2)$. It can be shown that $\frac{\partial H}{\partial p_i} = \frac{p_i}{m}$ [where $i = x, y, z$]. Hence $H_{\text{parabolic}}$ can be written as

$$H_{\text{parabolic}} = \frac{1}{2}(p_x \frac{\partial H_{\text{parabolic}}}{\partial p_x} + p_y \frac{\partial H_{\text{parabolic}}}{\partial p_y} + p_z \frac{\partial H_{\text{parabolic}}}{\partial p_z}).\tag{5.21}$$

Next by equipartition theory, the ensemble average of each of $p_x \frac{\partial H}{\partial p_x}, p_y \frac{\partial H}{\partial p_y},$ and $p_z \frac{\partial H}{\partial p_z}$ is $k_B T$ [43]. Hence taking the ensemble average of the Hamiltonian in Eq. 5.21, one obtains

$$< H_{\text{parabolic}} >= \frac{3}{2} k_B T. \qquad (5.22)$$

Taking the derivative of $< H_{\text{parabolic}} >$ w.r.t T one obtains the expression for the heat capacity as $\frac{3}{2} k_B$. The classical semi-Dirac Hamiltonian is given by

$$H_{\text{sD}} = \sqrt{\frac{p_x^4}{4m^2} + v^2 p_y^2} \qquad (5.23)$$

It is a two dimensional system, hence p_z is absent in Eq. 5.23. Taking the derivative of H_{sD} w.r.t p_x and p_y the following identity is established.

$$H_{\text{sD}} = \frac{1}{2} p_x \frac{\partial H_{\text{sD}}}{\partial p_x} + p_y \frac{\partial H_{\text{sD}}}{\partial p_y} \qquad (5.24)$$

Next the equipartition theorem is used to obtain an expression for the ensemble average of H_{sD}. One obtains

$$< H_{\text{sD}} >= \frac{1}{2} k_B T + k_B T = \frac{3}{2} k_B T \qquad (5.25)$$

Taking the derivative of the above expression w.r.t T one obtains $c_v = \frac{3}{2} k_B$ for the heat capacity for the semi-Dirac dispersion. It is noted that it is exactly same as that of a three dimensional non-interacting gas with parabolic dispersion. This result has also been veri-fied by computing the heat capacity for the semi-Dirac dispersion directly starting from the Boltzmann distribution. This is rather an interesting result. In the low temperature limit the semi-Dirac heat capacity has the same energy dependence as the three dimensional parabolic system. In the high temperature end of the spectrum the heat capacities are identical. A two dimensional semi-Dirac system effectively behaves as a three dimensional system. The appearance of this third degree of freedom can have potential technological applications. For example, larger the heat capacity of the material, the better is its ability

to maintain the desired temperature. So a semi-Dirac system can function more efficiently as compared to other two dimensional systems so far as maintaining a fixed temperature is concerned.

5.4   Plasmon frequency

5.4.1   Random Phase Approximation and Lindhard Dielectric function

The plasmon oscillation can be thought of as the oscillation of negatively charged electrons in the background of positively charged ions. The plasmon oscillation frequency can be determined with the help of classical Maxwell's equations modeling electrons sloshing back and forth in a positively charged background. So plasmon excitation can be thought of as a result of the variation of the charge density. In the following it is outlined how one can obtain the Linhard susceptibility expression starting from density-density Green's function and also obtain an expression for the dielectric constant making an approximation known as the 'Random Phase Approximation'. The density-density Green's function is given by [69]

$$X(\mathbf{q}, t) = i < GS|T\hat{\rho}_{\mathbf{q}}(t)\hat{\rho}_{\mathbf{q}}^{\dagger}(0)|GS >, \tag{5.26}$$

where $|GS>$ is the ground state wave function. T indicates the time ordering, and $\mathbf{q}$ stands for the momentum vector. The density operator $\hat{\rho}_{\mathbf{q}}(t)$ can be expressed as a sum of the Fourier components as follows

$$\hat{\rho}_{\mathbf{q}}(t) = \sum_{\mathbf{k}} c_{\mathbf{k}}^{\dagger}(t)c_{\mathbf{k}+\mathbf{q}}^{\dagger}(t), \tag{5.27}$$

where $c^{\dagger}$ and c are the creation and the destruction operators for the electron. The physical interpretation of the density density Green's function is it creates a particle-hole pair and let it propagate in time. Spin is ignored in the calculation. Using Eq. 5.27 in Eq. 5.26 one

obtains

$$X(\mathbf{q}, t) = i \sum_{\mathbf{k}} < GS | c_{\mathbf{k}}^{\dagger}(t) c_{\mathbf{k+q}}(t) c_{\mathbf{k'+q}}^{\dagger} c_{\mathbf{k'}} | GS > . \tag{5.28}$$

Approximating the $|GS>$ by a non-interacting one, as well as applying Wick's theorem, Eq. 5.28 in the zeroth order approximation can be written as

$$X_0(\mathbf{q}, t) = 2i \sum_{\mathbf{k}} G_0(\mathbf{k+q}, t) G_0(\mathbf{k}, -t), \tag{5.29}$$

where $G_0(\mathbf{k}, t)$ is a non-interacting Green's function.
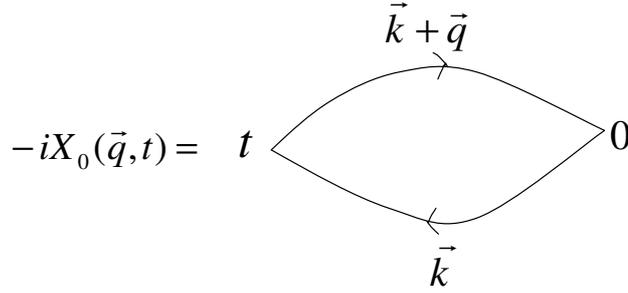
Fig. 5.4: Diagram showing the density density Green's function iX_0 given by Eq. 5.29.

Eq. 5.29 can diagrammatically be represented as in Fig.5.4. The solid lines correspond to free single particle Green's functions. $\mathbf{k}$ and $\mathbf{q}$ are the internal and the external momenta respectively. A hole is a particle moving backward in time. Because the two arrows in the diagram are oppositely directed, one of them is a particle and the other is hole. Hence the bubble is also called as a particle-hole or polarization loop. Taking the Fourier transform

of Eq. 5.29 one obtains

$$
\begin{aligned}
X_0(\mathbf{q}, \omega) &= \int_{-\infty}^{\infty} dt e^{-i\omega t} X_0(\mathbf{q}, t) \\
&= \sum_{\mathbf{k}} \int \frac{d\epsilon}{2\pi} G_0(\mathbf{k+q}, \epsilon + \omega) G_0(\mathbf{k}, \epsilon),
\end{aligned}
\tag{5.30}
$$

where $G_0(\mathbf{k}, \epsilon)$ is given by

$$
G_0(\mathbf{k}, \epsilon) = \frac{1}{\epsilon - \varepsilon_{\mathbf{k}} + i\delta \text{sign}(\varepsilon_{\mathbf{k}})}
\tag{5.31}
$$

$\varepsilon_{\mathbf{k}}$ in Eq. 5.31 is the energy corresponding to the unperturbed Hamiltonian. Using the expression for the Green's function given by Eq. 5.31 in Eq. 5.30, one obtains

$$
X_0(\mathbf{q}, \omega) = -2\Sigma_{\mathbf{k}} \int \frac{d\epsilon}{2\pi i} \frac{1}{\epsilon + \omega - \varepsilon_{\mathbf{k+q}} + i\delta \text{sign}(\varepsilon_{\mathbf{k+q}})} \cdot \frac{1}{\epsilon - \varepsilon_{\mathbf{k}} + i\delta \text{sign}(\varepsilon_{\mathbf{k}})}.
\tag{5.32}
$$

In order to evaluate the integral given by Eq. 5.32 the observation is made when $\varepsilon_{\mathbf{k+q}}$ and $\varepsilon_{\mathbf{k}}$ are both positive, the poles of both the Green's functions appearing in Eq. 5.32 have poles in the lower half of the complex ϵ plane. Hence the contour of integration can be chosen in the upper half of the complex ϵ plane, resulting in the integral being zero. A similar result holds for the case when $\varepsilon_{\mathbf{k+q}}$ and $\varepsilon_{\mathbf{k}}$ are both negative.(The contour then needs to be chosen in the lower half of the complex ϵ plane, both the poles being in the upper half.) A nontrivial result follows when $\varepsilon_{\mathbf{k+q}}$ and $\varepsilon_{\mathbf{k}}$ are of opposite sign. In that case the contour integrations in Eq. 5.32 give the following result

$$
X_0(\mathbf{q}, \omega) = -2\Sigma_{\mathbf{k}} [\frac{\theta(\varepsilon_{\mathbf{k+q}})\theta(-\varepsilon_{\mathbf{k}})}{\epsilon + \omega - \varepsilon_{\mathbf{k+q}} + i\delta} - \frac{\theta(-\varepsilon_{\mathbf{k+q}})\theta(\varepsilon_{\mathbf{k}})}{\omega - \varepsilon_{\mathbf{k+q}} + \varepsilon_{\mathbf{k}} - i\delta}].
\tag{5.33}
$$

It is noticed either the first or the second term of Eq. 5.33 is nonzero. For finite temperature scenario the theta function is be replaced by the Fermi-Dirac distribution function f. $\theta(-\varepsilon_{\mathbf{k}})$ is replaced by $f(\varepsilon_{\mathbf{k}})$, the reason being $\theta(-\varepsilon_{\mathbf{k}})$ is non-zero when $\varepsilon_{\mathbf{k}} < 0$.(The chemical potential has been chosen to be the origin of the energy.) $\theta(\varepsilon_{\mathbf{k}})$ is replaced

by $1 - f(\varepsilon_{\mathbf{k}})$ for obvious reason. After some algebraic manipulation The real part of X_0, also called Lindhard susceptibility function, is given by

$$\chi_0(\mathbf{q}, \omega) \equiv Re X_0(\mathbf{q}, \omega) = \int \frac{d^2 k}{(2\pi)^2} \frac{f(\varepsilon_{\mathbf{k}}) - f(\varepsilon_{\mathbf{k+q}})}{\hbar\omega + \varepsilon_{\mathbf{k}} - \varepsilon_{\mathbf{k+q}}}. \tag{5.34}$$
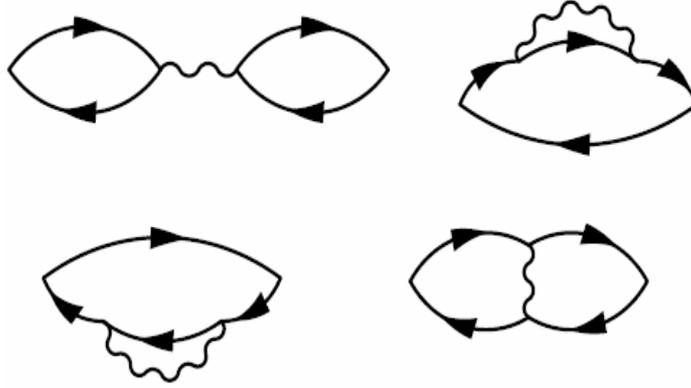
Fig. 5.5: First order diagrams for X
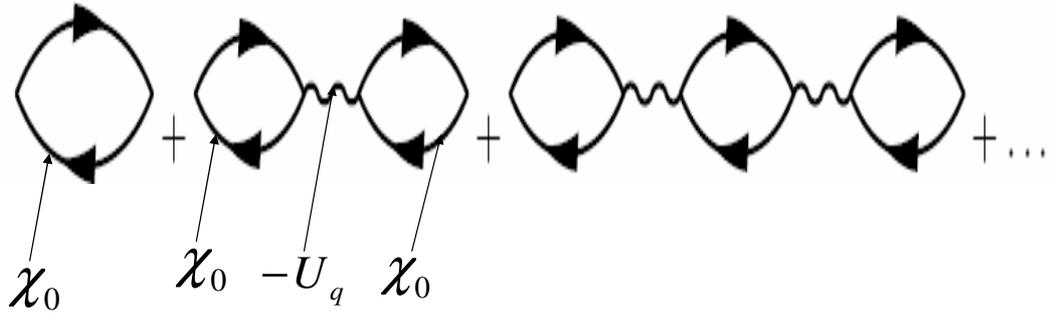
Fig. 5.6: RPA diagram for χ

The stage is set to discuss the Random Phase Approximation (RPA) technique. χ_0

Eq. 5.34 gives the zeroth order approximation for the susceptibility χ. In the following it is shown how to obtain a better approximation of χ through RPA. The first order diagrams as shown in Fig.5.5 are considered. Not all the diagrams contribute equally for small q and ω. In the first diagram the variable q is a free variable. Each wiggly line corresponds to the potential $U_{\mathbf{q}}$, which goes as q^{-1} or q^{-2} depending on whether the system is a three or a two dimensional one. So, in the first diagram there is a divergence coming from q appearing in $U_{\mathbf{q}}$. As for the other diagrams, the singularities arising from the potential $U_{\mathbf{q}}$ gets integrated out. Hence the for small q, it is the first diagram which contributes most among all the first order diagrams. In the RPA approximation all such diagrams are collected ignoring others as shown in Fig.5.6. Hence χ_{RPA} is given as

$$
\begin{aligned}
\chi_{RPA} &= \chi_0(\mathbf{q}, \omega) + \chi_0(\mathbf{q}, \omega)[-U_{\mathbf{q}}\chi_0(\mathbf{q}, \omega)] + \chi_0(\mathbf{q}, \omega)[-U_{\mathbf{q}}\chi_0(\mathbf{q}, \omega)]^2 + ... \quad (5.35) \\
&= \frac{\chi_0(\mathbf{q}, \omega)}{1 + U_{\mathbf{q}}\chi_0(\mathbf{q}, \omega)}
\end{aligned}
$$

The pole of χ_{RPA} gives the Plasma excitation frequency. To build an intuitive understanding of that, the expression for the effective screened potential is considered in the following. Variation of the charge density at one point creates an electric field at another point in space, where the charge density gets influenced thereby. The effective screened interaction energy due to the charge density fluctuation can be written as

$$
\begin{aligned}
U_{RPA}(\mathbf{q}, \omega) &= U_{\mathbf{q}} + U_{\mathbf{q}}[-\chi_0(\mathbf{q}, \omega)U_{\mathbf{q}}] + U_{\mathbf{q}}[-\chi_0(\mathbf{q}, \omega)U_{\mathbf{q}}]^2 + ... \quad (5.36) \\
&= \frac{U_{\mathbf{q}}}{1 + U_{\mathbf{q}}\chi_0(\mathbf{q}, \omega)}
\end{aligned}
$$

It is noted that the effective potential in the RPA approximation gets screened by the factor $1 + U_{\mathbf{q}}\chi_0(\mathbf{q}, \omega)$. A dielectric constant is defined to be a measure of the screening. Hence the RPA expression for the dielectric constant is given by

$$
\varepsilon(\mathbf{q}, \omega) = 1 + U_{\mathbf{q}}\chi_0(\mathbf{q}, \omega). \quad (5.37)
$$

Plasma oscillation takes place in the absence of any external potential. If $U_{\mathbf{q}} = 0$, the denominator of U_{RPA} in Eq. 5.36, i,e $\varepsilon(\mathbf{q}, \omega)$ is also zero in order to keep U_{RPA} finite. Hence the plasmon frequency for the semiDirac system can be computed by setting $\varepsilon(\mathbf{q}, \omega)$ to zero.

5.4.2   The Plasma Frequency for the Semi-Dirac Dispersion

In this section an expression for the Plasma frequency for the semi-Dirac dispersion is obtained. Expanding $\varepsilon_{\mathbf{k+q}}$ in Eq. 5.34 for small $\mathbf{q}$ (only this limit is considered), the numerator in Eq. 5.34 assumes the following low temperature expression

$$f(\varepsilon_{\mathbf{k}}) - f(\varepsilon_{\mathbf{k+q}}) = \vec{v}_k \cdot \vec{q}\delta(\varepsilon_{\mathbf{k}} - \varepsilon). \tag{5.38}$$

Expanding the denominator as well, Eq. 5.34 becomes

$$\chi_0(\mathbf{q}, \omega) = \int \frac{d^2k}{(2\pi)^2} \vec{v}_k \cdot \vec{q}(\frac{1}{\hbar\omega} + \frac{\vec{v}_k \cdot \vec{q}}{(\hbar\omega)^2})\delta(\varepsilon_{\mathbf{k}} - \varepsilon). \tag{5.39}$$

The Coulomb potential $v(\mathbf{q})$ for a two dimensional system is given by

$$v(\mathbf{q}) = \frac{2\pi e^2}{\kappa q}, \tag{5.40}$$

where $q = \sqrt{q_x^2 + q_y^2}$, and κ is the background dielectric constant of the medium. Using Eq. 5.39 and Eq. 5.40 in Eq. 5.37, and setting Eq. 5.37 to zero, the plasmon frequency for the semi-Dirac energy dispersion is obtained as

$$(\hbar\omega_p)^2 = \frac{8gI_3}{\pi} \frac{e^2 q \varepsilon_0}{\kappa} F(\theta), \tag{5.41}$$

where $F(\theta)$ is given by

$$F(\theta) = \xi^{\frac{3}{2}}(\cos^2\theta + \frac{1}{4}\xi^{-1}\frac{I_2}{I_3}\sin^2\theta), \tag{5.42}$$

and I_2, I_3 are given by Eq. 2.11a and in Eq. 2.11b respectively. ε_0 is the energy scale defined earlier and the polar coordinates q, θ have been introduced. θ denotes the angle that the plasmon wave-vector makes with the non-relativistic axis of the semi-Dirac dispersion. It is recalled that the dimensionless Fermi energy variable is defined as $\xi \equiv \frac{\varepsilon}{\varepsilon_0}$. $\omega_p \propto \sqrt{q}$ is the characteristic of a two-dimensional system.
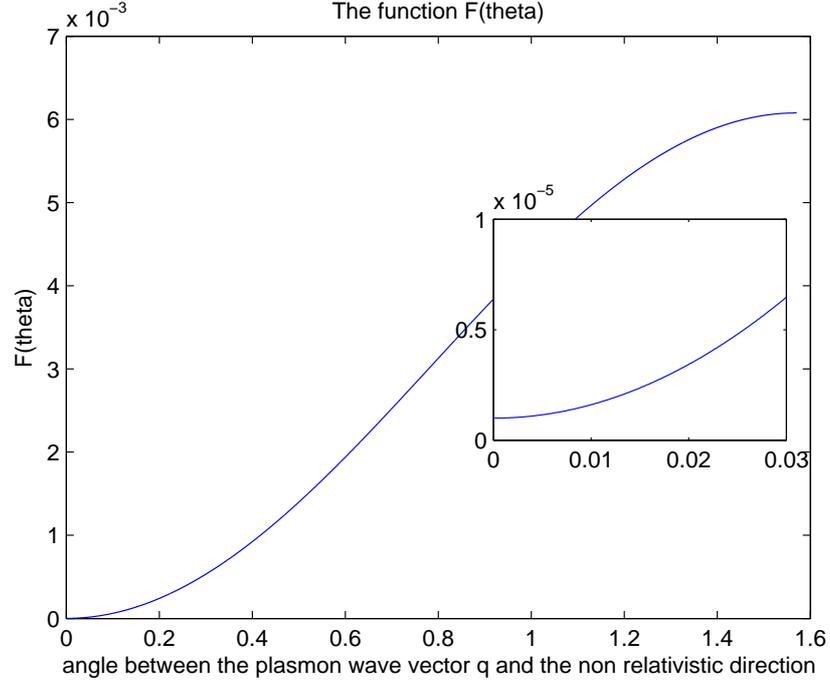
Fig. 5.7: Angular dependence of the function F

The function $F(\theta)$ is plotted against θ in Fig. 5.7. Using Eq. 2.4 for the semiDirac density of states and Eq. 2.10a and Eq. 2.10b for the average Fermi surface velocities squared, Eq. 5.41 takes the following form

$$(\hbar\omega_p)^2 \quad = \quad g\pi \frac{e^2 q \hbar D(\varepsilon)}{\kappa}(\langle v_x^2 \rangle \cos^2\theta + \langle v_y^2 \rangle \sin^2\theta), \qquad (5.43)$$

As was mentioned at the end of section I, the average velocity in the relativistic direction

(y) is significantly higher than that in the non-relativistic direction (x). From Eq. 5.43 it is seen that the plasmon frequency is maximum when $\theta = \frac{\pi}{2}$, i,e, when the wave vector oscillates along the relativistic direction. For the plasmon oscillation along the non-relativistic direction, the oscillation frequency is much smaller in magnitude as compared to the previous case. There exists a high anisotropy between the relativistic and the non-relativistic directions in this respect. This bears the signature of the semi-Dirac dispersion and is in sharp contrast to the two dimensional parabolic and the Dirac dispersions, for which the Plasmon frequencies are isotropic.

5.5 Magnetic susceptibility

In this section the magnetic susceptibilities for the semi-Dirac dispersion are considered. The Pauli paramagnetic susceptibility is given by

$$\chi_{para} = \mu_B^2 D(\varepsilon), \tag{5.44}$$

where $D(\varepsilon)$ is the density of states. Using Eq. 2.4 for the semi-Dirac density of states, Eq. 5.44 reduces to

$$\chi_{para} = \frac{2\mu_B^2 m}{\pi^2 \hbar^2} \sqrt{\xi}, \tag{5.45}$$

where $\xi \equiv \frac{\varepsilon}{\varepsilon_0}$ is the dimensionless variable as mentioned before. For a non-interacting Fermi liquid the orbital susceptibility is given by[40].

$$\chi_{orb} = -\frac{m^2 \mu_B^2}{12\pi^3 \hbar^4} \int d^2\mathbf{k} [\frac{\partial^2 \varepsilon_{\mathbf{k}}}{\partial k_x^2} \frac{\partial^2 \varepsilon_{\mathbf{k}}}{\partial k_y^2} + 2(\frac{\partial^2 \varepsilon_{\mathbf{k}}}{\partial k_x \partial k_y})^2 \tag{5.46}$$
$$+\frac{3}{2}(\frac{\partial \varepsilon_{\mathbf{k}}}{\partial k_x} \frac{\partial^3 \varepsilon_{\mathbf{k}}}{\partial k_x \partial k_y^2} + \frac{\partial \varepsilon_{\mathbf{k}}}{\partial k_y} \frac{\partial^3 \varepsilon_{\mathbf{k}}}{\partial k_y \partial k_x^2})]\delta(\varepsilon - \varepsilon_{\mathbf{k}})$$

Using Eq. 2.2 For $\varepsilon_{\mathbf{k}}$ in Eq. 5.47 and doing the integral the following is obtained.

$$\chi_{orb} = -\frac{2\sqrt{2}I_4}{3\pi^3}\frac{\mu_B^2 m^{\frac{3}{2}}v}{\hbar^2\varepsilon^{\frac{1}{2}}}, \tag{5.47}$$

where the integral I_4 is given by $\int_0^1 d\alpha(-33\alpha^{10}+41\alpha^6-9\alpha^2)(1-\alpha^4)^{\frac{-1}{2}}$, α being a dummy variable. Evaluating the numerical value for I_4 and using the dimensionless variable ξ, Eq. 5.47 reduces to

$$\chi_{orb} = -\frac{.0798}{\pi^3}\frac{m\mu_B^2}{\hbar^2}\frac{1}{\sqrt{\xi}} \tag{5.48}$$

It is observed that the orbital susceptibility for the semi-Dirac band structure is always diamagnetic. The absolute value of the ratio of the paramagnetic to the orbital susceptibilities(i,e the ratio of Eq. 5.45 to Eq. 5.48)of the semi-Dirac dispersion is given by

$$\left|\frac{\chi_{para}}{\chi_{orb}}\right| \approx 100\xi \tag{5.49}$$

This ratio is small due to the presence of ξ, which is small for the VO_2 system as was mentioned before. Hence it is concluded that the orbital magnetic susceptibility for the semi-Dirac dispersion dominates the paramagnetic susceptibility. This result is distinct qualitatively from both the Dirac and the parabolic dispersion cases. For the doped Dirac dispersion the orbital susceptibility vanishes identically. For conventional two dimensional parabolic dispersion the orbital susceptibility is calculated using Eq. 5.47, and turns out to be 6π times smaller than its paramagnetic susceptibility. Hence the unusually large orbital susceptibility can be considered a characteristic feature of the semi-Dirac dispersion.

6. KLEIN PARADOX AND THE SEMI-DIRAC DISPERSION

In this chapter results for Klein tunneling of semi-Dirac particles are given. Several observations about Klein tunneling for the particle-hole symmetric semi-Dirac system are presented. The problem is given an extra richness by introducing a variable angle that the barrier makes with respect to the anisotropic dispersion. Comparisons are made with both other types of point Fermi surface systems (conventional zero-gap semiconductors and graphene).

6.1   background

The Klein paradox, is the complete transmission of a relativistic electron through a potential barrier even when the barrier is arbitrarily high. This strange phenomenon was discovered by Oskar Klein in 1929[49][48]. It is an impossibility for a parabolic energy-momentum dispersion. In that case the probability density outside the potential barrier decreases exponentially with the increase of the barrier height. In the following Klein tunneling is described and a possible explanation of this seemingly paradoxical phenomenon is given in terms of electron-hole pair production mechanism. A relativistic electron is considered with energy E and mass m in an one dimensional potential as given in Fig.6.1[48]. It is noticed in the energy range $m < E < V - m$, the particle and the hole continuum overlaps. This happens due to the fact that the potential at $x > 0$ lifts the energies of the hole/positron sea. With the increase of the height of the potential barrier the width of the overlap region increases. Klein found that the reflection R and the transmission coefficient T for this one dimensional problem are

$$R = [\frac{1 - \kappa}{1 + \kappa}]^2, T = \frac{4\kappa}{(1 + \kappa)^2},$$ (6.1)
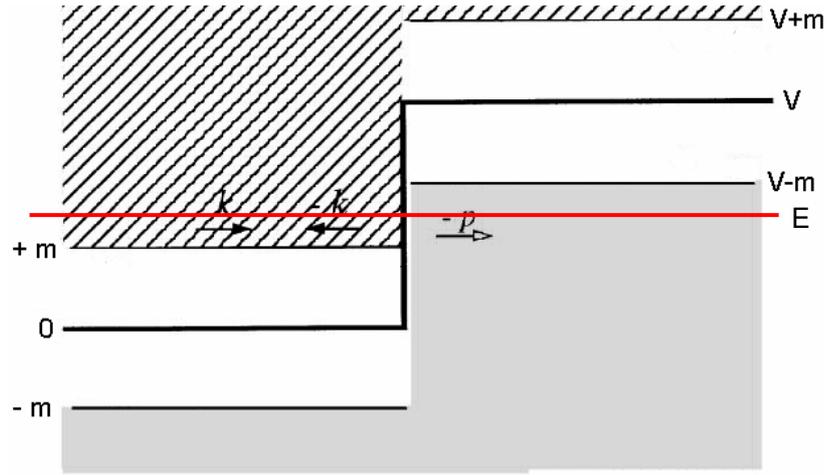
Fig. 6.1: An electron scattering off a step potential. The hatched region is the electron-continuum and the grey region corresponds to the hole continuum. k and p are the momenta of the incident and the transmitted electrons respectively.

where κ is given by

$$\kappa = \frac{p}{k}\frac{E+m}{E+m-V}. \tag{6.2}$$

k is the momentum of the incident particle. p, the momentum of the transmitted particle, obeys the following relativistic expression

$$p = \sqrt{(V-E)^2 - m^2}. \tag{6.3}$$

Using the expression $v_g = \frac{dE}{dp}$ for the group velocity v_g, one obtains

$$v_g = \frac{p}{E-V}. \tag{6.4}$$

A very interesting observation is made at this point. When $E < V$, v_g is negative if p is assumed to be positive. From the problem definition, for $x > 0$ propagation to the right is expected; but a negative v_g does not indicate that. Hence one needs to use a negative sign on the right side of Eq. 6.3. An electron with a negative momentum is equivalent to a hole

58

with a momentum going to the right. Hence there will be a flux of holes moving to the right causing a transmission current. With the discovery of graphene an opportunity to verify
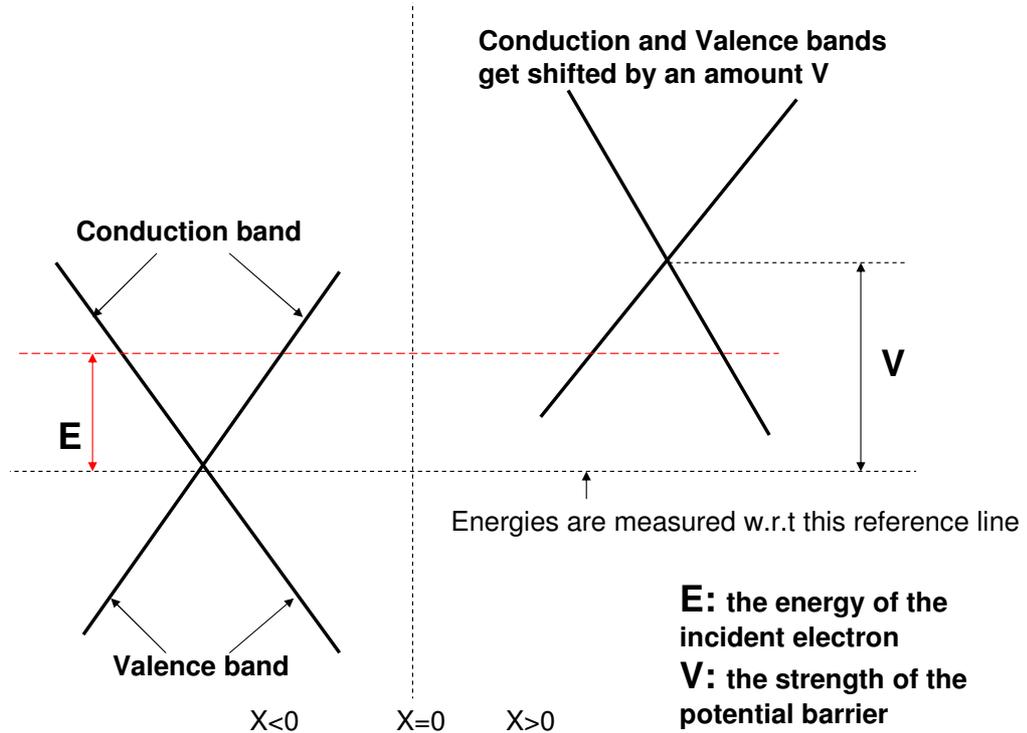
Fig. 6.2: graphene Valence and Conduction band picture in the context of Klein tunneling.

the Klein phenomenon presented itself. Electron in graphene is described by massless Dirac equation. Since the graphene dispersion is massless, any energy of the incident electron E less than V causes the overlap of the particle-hole continua at the two sides of the potential barrier. In other words, the conduction band in the $x < 0$ region and the valence band in the $x > 0$ region are accessible to the energy E as shown in Fig. 6.2 rendering Klein tunneling to be possible. Next the semi-Dirac dispersion is considered: Is Klein tunneling possible for the semi-Dirac dispersion? A semi-Dirac dispersion is a zero-gap, electron-hole symmetric dispersion. Hence both it's valence and the conduction bands are accessible at an energy less than the potential barrier. But as much as the Klein tunneling is about the overlap of the particle-hole continua, it is also about the mathematical form

of the dispersion. For example, the Klein tunneling does not happen in bilayer graphene although it is a zero-gap, electron-hole symmetric dispersion. In the following the Klein tunneling for the semiDirac dispersion is investigated, and interesting results are brought into light, which are not characteristics of either the Dirac or the parabolic dispersion.

Substituting the momenta variables by the corresponding differential operators, the tight-binding Hamiltonian corresponding to the semiDirac dispersion in Eq. 3.13 can be written as

$$H = v\hat{p}_y\tau_z + \frac{\hat{p}_x^2}{2m}\tau_x \tag{6.5}$$

where τ's are the Pauli matrices and $\hat{p}_{x(y)}$ are the momenta operators given by $-i\partial/\partial x(y)$. To get the essential physics keeping the mathematics as simple as possible, the special case of **normal incidences** of a semi-Dirac quasi-particle with a potential barrier of width d inclined at an angle α with respect to the x(nonrelativistic) axis is considered, as shown in Fig.6.3. A set of orthogonal axes ξ and η, ξ making an angle α w.r.t the x axis is defined. The potential has a width d along the ξ axis and is infinitely extended along the η axis. It is assumed that the energy of the incident semi-Dirac quasi-particle is much smaller than the barrier potential. There are three regions of interest: to the left of the barrier where the potential is zero; the middle with nonzero potential; and to the right of the barrier where the potential is also zero. They are referred to as regions I, II, and III respectively. The wave-functions in these regions are denoted by Ψ_I, Ψ_{II}, Ψ_{III} respectively. The momenta operators along the x and the y(relativistic) directions can be written in terms of the variables ξ and η as follows:

$$\begin{aligned}
\hat{p}_x &= \hat{p}_\xi \cos\alpha - \hat{p}_\eta \sin\alpha \\
\hat{p}_y &= \hat{p}_\xi \sin\alpha - \hat{p}_\eta \cos\alpha,
\end{aligned} \tag{6.6}$$

where $\hat{p}_{\xi(\eta)}$ are the momenta operators given by $-i\partial/\partial\xi(\eta)$. Since only the normal incidence is considered the η degree of freedom can be eliminated from the problem. Hence

60
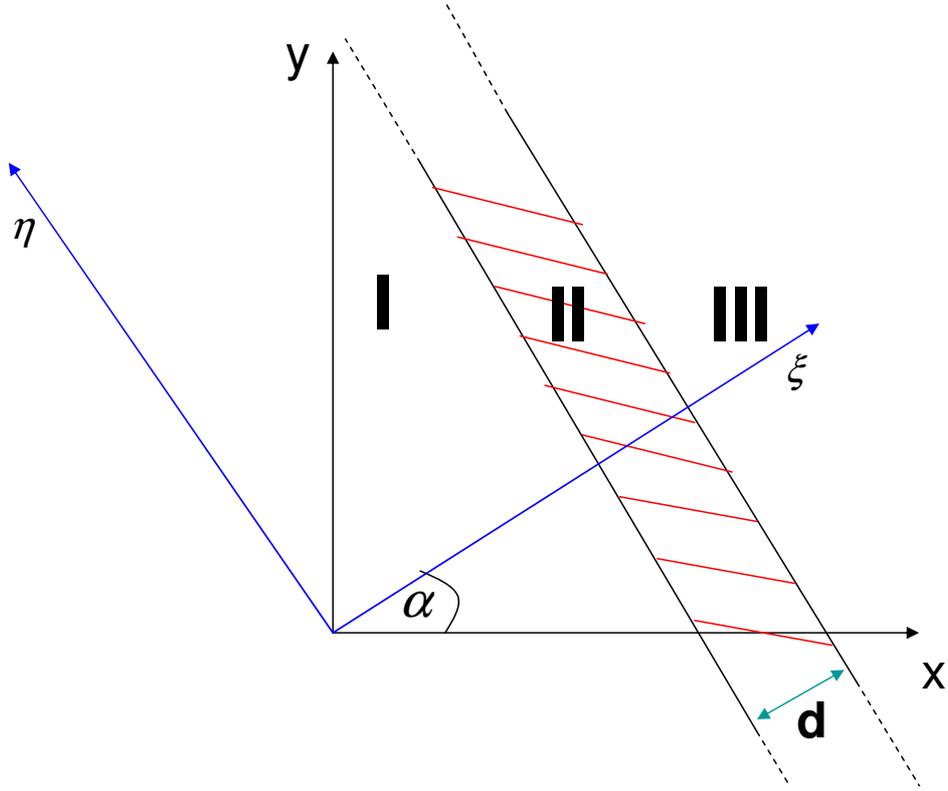
Fig. 6.3: The top view of the potential barrier is shown. It extends infinitely in one direction, but limited to a spatial length d in the orthogonal direction. An electron with energy E and making an angle alpha with the non-relativistic direction is incident normally on the potential.

the Hamiltonian in Eq. 6.5 takes the following form:

$$H = \hat{p}_\xi v \sin \alpha \tau_z + \frac{1}{2m}\hat{p}_\xi^2 \cos^2 \alpha \tau_z. \tag{6.7}$$

For a finite value of α the forward propagating wave, which is of the form $e^{ik\xi}$ times a spinor, is an admissible eigenstate of the Hamiltonian. With that ansatz the Hamiltonian in Eq. 6.7 becomes

$$H = vk \sin \alpha [\tau_z + \tan \theta \tau_x], \tag{6.8}$$

where $\tan\theta = \frac{\cos^2\alpha}{\sin\alpha}\frac{k}{2mv}$. When $\mathbf{k}$ goes to $-\mathbf{k}$(as is the case when one considers the backward propagating wave $e^{-ik\xi}$ instead of the forward propagating wave $e^{ik\xi}$), aside from the positive multiplicative factor $\hbar vk$ the Hamiltonian in Eq. 6.7 goes from $\tau_z + \tan\theta\tau_x$ to $-[\tau_z - \tan\theta\tau_x]$.

6.2   The Derivation of the Resonance Condition

The time independent Schrodinger equation in a given potential can be written as

$$h\psi = (E - V)\psi, \tag{6.9}$$

where h is the part of the Hamiltonian without the potential V. In regions I and III, $E - V$ is positive. Hence the positive eigenvalue solutions as given by Eq. .25b in the Appendix for the forward propagating wave and by Eq. .27b for the backward propagating wave need to be considered in those regions. In region II, V being much larger than E results in $(E - V)$ being negative. Hence the negative eigenvalue solutions as given by Eq. .25c and Eq. .27c appearing in the appendix are of importance in that region. k's in regions I and III are equal and is denoted by k_1. k is denoted by k_2 in region II. k_1 and k_2 are given by

$$vk_1 \sin\alpha(\cos\theta_1)^{-1} = E, \tag{6.10a}$$

$$vk_2 \sin\alpha(\cos\theta_2)^{-1} = V_0 - E, \tag{6.10b}$$

where θ_1 and θ_2 are given by

$$\tan\theta_{1(2)} = \frac{\cos^2\alpha}{\sin\alpha}\frac{k_{1(2)}}{2mv} \tag{6.11}$$

Finally, the wave functions in the three regions are

$$\Psi_I = e^{ik_1\xi}\begin{pmatrix}\cos(\theta_1/2)\\\sin(\theta_1/2)\end{pmatrix}$$

$$+re^{-ik_1\xi}\begin{pmatrix}\sin(\theta_1/2)\\\cos(\theta_1/2)\end{pmatrix}, -\infty < x < 0,$$

$$\Psi_{II} = t_1 e^{ik_2\xi}\begin{pmatrix}\sin(\theta_2/2)\\-\cos(\theta_2/2)\end{pmatrix}$$

$$+r_1 e^{-ik_2\xi}\begin{pmatrix}\cos(\theta_2/2)\\-\sin(\theta_2/2)\end{pmatrix}, 0 < x < d,$$

$$\Psi_{III} = t_2 e^{ik_1\xi}\begin{pmatrix}\cos(\theta_1/2)\\\sin(\theta_1/2)\end{pmatrix}, d < x < \infty,$$

(6.12)

where r, t_1, r_1 and t_2 are constants. It is noticed that in the regions I and II both the forward and backward traveling (reflected) waves are present. In region III only the forward traveling but no reflected wave is considered. The absolute square of t_2 gives the transmission coefficient. t_2 is solved for matching the wave functions at the boundaries $y = 0$ and $y = d$, and the following expression for $|t_2|^2$ is obtained:

$$|t_2|^2 = \frac{(\sin\theta_2\cos\theta_2\cos\theta_1)^2}{A^2 + B^2 - 2AB\cos k_2 d}, \tag{6.13}$$

where A and B are given by:

$$A = [\sin((\theta_2 - \theta_1)/2)\cos\theta_2 \tag{6.14}$$

$$+ \sin(\theta_2 + \theta_1)/2]\cos((\theta_2 - \theta_1)/2)$$

$$B = \sin\theta_2\sin^2((\theta_2 + \theta_1)/2)$$

It can be shown when

$$\cos k_2 d = 1, \qquad (6.15)$$

the denominator in Eq. 6.13 becomes exactly equal to the numerator. The resonance condition as given by Eq. 6.15 implies

$$k_2 d = 2n\pi, \qquad (6.16)$$

where n is an integer. From Eq. 6.10b and Eq. 6.16 the following condition for complete transmission of an incident wave is obtained:

$$(2\pi v/d)(n^2 \sin^2 \alpha + n^4 \cos^4 \alpha (\pi/mvd)^2)^{\frac{1}{2}} \qquad (6.17)$$

$$= V_0 - E$$

Eq. 6.17 gives the resonance condition when α is not equal to $\pi/2$. For $\alpha = \pi/2$, θ_1 and θ_2 as given by Eq. 6.11 are zero, which makes $|t_2|^2$ given by Eq. 6.13 indeterminate ($\frac{0}{0}$ form). Hence Eq. 6.17 can not directly be used for that case. $\alpha = 0$ case will also need separate consideration, one of the reasons being $\tan \theta$ appearing in the Hamiltonian given by Eq. 6.8 becomes infinite when α is equal to zero. The other important reason is, as will be seen, the Hamiltonian admits evanescent as well as propagating wave solutions when α is set to zero.

6.3 Special Cases

Case I. $\alpha = \frac{\pi}{2}$

As for the special cases, first the potential is considered to be perpendicular to the relativistic direction ($\alpha = \frac{\pi}{2}$). With the ansatz of the forward propagating wave $e^{ik_y y}$, the

64

Hamiltonian in Eq. 6.5 takes the following form in the $\mathbf{k}$ space:

$$H = vk_y\tau_z, \tag{6.18}$$

the eigenvalues of which are $\pm vk_y$. With the backward propagating wave ansatz $e^{-ik_y y}$ the Hamiltonian in Eq. 6.5 reduces to a matrix, which is the negative of the one appearing in Eq. 6.18, and hence with the same eigenvalues; but the eigenfunctions being reversed.

The wave-functions in the three regions are

$$\Psi_I = e^{ik'_1 y}\begin{pmatrix} 1 \\ 0 \end{pmatrix} + r'e^{-ik'_1 y}\begin{pmatrix} 0 \\ 1 \end{pmatrix}, -\infty < y < -d, \tag{6.19}$$

$$\Psi_{II} = t'_1 e^{ik'_2 y}\begin{pmatrix} 0 \\ 1 \end{pmatrix} + r'_1 e^{-ik'_2 y}\begin{pmatrix} 1 \\ 0 \end{pmatrix}, -d < y < d,$$

$$\Psi_{III} = t'_2 e^{ik'_1 y}\begin{pmatrix} 1 \\ 0 \end{pmatrix}, d < y < \infty,$$

where r', t'_1, r'_1 and t'_2 are constants. k'_1 and k'_2 are given by $\hbar k'_1 = E$ and $\hbar k'_2 = V - E$ respectively. Following the previous discussion about the sign of $E - V$ appearing on the right side of Eq. 6.9, eigenvalues of appropriate signs and corresponding eigenfunctions are considered for different regions (regions I, II and III). The absolute square of t'_2 gives the transmission coefficient. Matching the wavefunctions at the boundaries $y = 0$ and $y = d$, the following is obtained:

$$|t'_2|^2 = |e^{-i(k'_1 + k'_2)d}|^2, \tag{6.20}$$

which is equal to 1. So it is seen that in case the potential is in the relativistic direction there is complete transmission for the normal incidence. Now k'_2 gets large as the potential V gets large. But k'_2 being in the argument of an oscillatory function given by Eq. 6.20, the transmission coefficient $|t'_2|^2$ remains 1, which assures complete transmission even when

the potential barrier is large.

Case II.$\alpha = 0$

Next the potential is considered to be perpendicular to the x (the non-relativistic direction). The Hamiltonian admits **propagating as well as evanescent** wave solutions. The y-component of the momentum k_y is zero since the particle is incident normally. For the propagating waves $e^{\pm ik_x x}$ The Hamiltonian in Eq. 6.5 takes the following form in the **k** space:

$$H = \frac{k_x^2}{2m}\tau_x, \tag{6.21}$$

the eigenvalues of which are $\pm\frac{k_x^2}{2m}$. For the evanescent wave of the form $e^{\pm k_x x}$, Eq. 6.5 becomes the negative of the Hamiltonian given by Eq. 6.21, the eigenvalues remaining unchanged. The eigenfunction corresponding to the positive-eigenvalue of one of the Hamiltonians is the same as the eigenfunction corresponding to the negative-eigenvalue of the other Hamiltonian and *vice versa*.

The energy of the incident particle for both the propagating and the evanescent cases are the same:$(E = \frac{k_x^2}{2m})$. Considering the propagating waves first, for regions I and III like before one takes into account the positive eigenvalue solution of the Hamiltonian given by Eq. 6.21 and as for region II, the negative eigenvalue solution of the same Hamiltonian. As for the evanescent waves, appropriate eigenfunctions are used for regions I $II$and III keeping in mind that the Hamiltonian is negative of that of the propagating case. k_x's in regions $\{I,III\}$ and II are denoted by k_1'' and k_2'' respectively, where k_1'' and k_2'' are given

by $\sqrt{2mE}$ and $\sqrt{2m|V-E|}$ respectively. The wave functions in the three regions are

$$\Psi_I = e^{ik_1''x}\begin{pmatrix}1\\1\end{pmatrix} + r''e^{-ik_1''x}\begin{pmatrix}1\\1\end{pmatrix} \qquad (6.22)$$

$$+ t'''e^{k_1''x}\begin{pmatrix}1\\-1\end{pmatrix},$$

$$-\infty < x < -d,$$

$$\Psi_{II} = t_1''e^{ik_2''x}\begin{pmatrix}1\\-1\end{pmatrix} + r_1''e^{-ik_2''x}\begin{pmatrix}1\\-1\end{pmatrix}$$

$$+ t_1'''e^{k_2''x}\begin{pmatrix}1\\1\end{pmatrix} + r_1'''e^{-k_2''x}\begin{pmatrix}1\\1\end{pmatrix},$$

$$-d < x < d,$$

$$\Psi_{III} = t_2''e^{ik_1''x}\begin{pmatrix}1\\1\end{pmatrix} + r_2'''e^{-k_1''x}\begin{pmatrix}1\\-1\end{pmatrix},$$

$$d < x < \infty,$$

where $r'', t''', t_1'', r_1'', t_1''', r_1''', t_2'', r_2'''$ are constants. In Eq. 6.22, for regions I and III the evanescent waves are constructed in such a way that they don't blow up when $|x|$ becomes large. There is no backward traveling wave in region III. $|t_2''|^2$ is the transmission coefficient. Equating the wave functions and its derivatives at the boundaries $x = 0$ and $x = d$, the following is obtained for the transmission coefficient

$$|t_2''|^2 = |\frac{4ik_1''k_2''e^{-ik_2''d}}{e^{-k_2''d}(k_2'' + ik_1'')^2 - e^{k_2''d}(k_2'' - ik_1'')^2}|^2. \qquad (6.23)$$

Eq. 6.23 is the same as what appears in [39] in the context of the tunneling probability for the bilayer graphene dispersion. k_2'' gets large as the potential V gets large. Because of the presence of the exponential factor $e^{k_2''d}$ in the denominator, the transmission coefficient given by Eq. 6.23 goes to zero as the potential goes to infinity. So there is no transmission when the potential is in the non relativistic direction and the particle is incident normally.

6.4 Summary of Klein Tunneling in the Context of Semi-Dirac Band structure
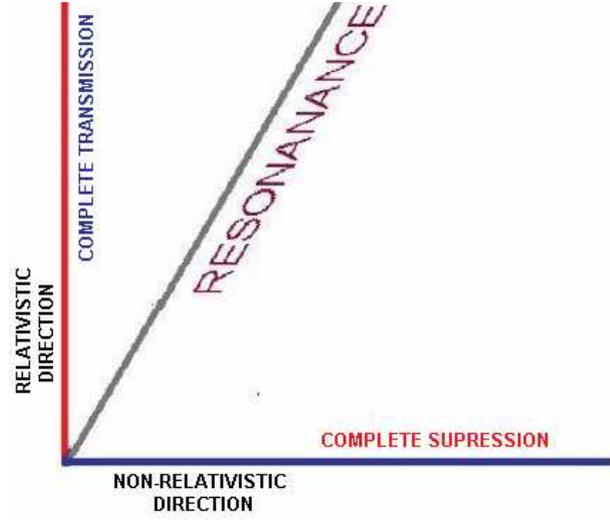
Fig. 6.4: Complete transmission for various orientations of the potential

The summary of our study is diagrammatically represented in Fig. 6.4. It is concluded as far as normal incidences are concerned, the semiDirac material is perfectly transmitting if the potential is along the direction in which the energy momentum dispersion is relativistic, but opaque for the orientation of the potential in the non-relativistic direction. If the potential barrier is aligned at a finite angle w.r.t the non-relativistic direction one obtains a resonance condition for complete transmission as given by Eq. 6.17.

7. TOPOLOGICAL ASPECT OF THE SEMI-DIRAC BAND STRUCTURE: CALCULATION OF BERRY'S PHASE

7.1   Introduction

In this section Berry's phase[58] associated semi-Dirac dispersion is discussed. Berry's phase is a topological phase. As the Hamiltonian is changed adiabatically by varying a parameter, in addition to an overall dynamic phase, the eigenfunction of the Hamiltonian acquires the Berry's phase. For determining the Berry's phase, the parameter is brought back to its initial value. In other words the parameter describes a loop in the parameter space. In most cases Berry's phase is zero. It can be nonzero if there is a degeneracy in the spectrum of the Hamiltonian. Berry's phase for ordinary parabolic dispersion is zero. It has also been discussed in the context of Dirac dispersion[52] and turns out to be nonzero for that case.

Berry's phase (γ_n) for the n_{th} band is given as

$$\gamma_n = \int \int_S \mathbf{B}_n(\mathbf{k}).\mathbf{dS}, \tag{7.1}$$

where S is the area enclosed by the loop in the parameter space, and $\mathbf{B}_n$ is the Berry's curvature corresponding to the n_{th} band, described in the following. Let $|n>$ be the nth eigenstate of the Hamiltonian. The corresponding Berry's connection $\mathbf{A}_n$ is defined as

$$\mathbf{A}_n = -Im < n|\nabla n > . \tag{7.2}$$

Berry's curvature for the n_{th} band is the curl of $\mathbf{A}_n$ ($\nabla \times \mathbf{A}_n$), which can also be written

as

$$\mathbf{B}_n = -Im \sum_{n' \neq n} \frac{<n|\nabla H|n'> \times <n'|\nabla H|n>}{(E_{n'} - E_n)^2} \tag{7.3}$$

In Eq. 7.3, the summation is restricted to different bands only $(n \neq n')$. If it happens to be the case that the energies of the two different bands n and n' are equal, $(i.e, E_{n'} = E_n)$, in other words there is a degeneracy in the spectrum of the Hamiltonian, the denominator in Eq. 7.3 becomes zero. It is less likely that the off-diagonal terms in the Hamiltonian matrix appearing in the numerator will also be zero. Under that circumstance the Berrry's curvature will have a singularity. Referring to Eq. 7.1, a singularity in Berrry's curvature would imply the Berry's phase γ_n being non-zero[The property of a delta function is recalled here].

7.2 Berry's phase for the Dirac dispersion

It was mentioned before that Berry's phase for the Dirac dispersion is non-zero. A derivation of that is given in the following [52]. The Hamiltonian for the Dirac dispersion is given as

$$H = \hbar v k \tilde{h}_D, \tag{7.4}$$

where $\tilde{h}_D$ is the matrix given by

$$\tilde{h}_D = \begin{pmatrix} 0 & e^{-i\theta_{\mathbf{k}}} \\ e^{i\theta_{\mathbf{k}}} & 0, \end{pmatrix} \tag{7.5}$$

The phase $\theta_{\mathbf{k}}$ appearing in Eq. 7.5 is given as

$$\theta_{\mathbf{k}} = \arctan \frac{k_y}{k_x}. \tag{7.6}$$

The normalized eigenstates of the Hamiltonian in Eq. 7.5 are $\frac{1}{\sqrt{2}} \begin{pmatrix} 1 \\ e^{i\theta_{\mathbf{k}}} \end{pmatrix}$ and $\frac{1}{\sqrt{2}} \begin{pmatrix} -e^{-i\theta_{\mathbf{k}}} \\ 1 \end{pmatrix}$ with the eigenvalues 1 and -1 respectively. Plugging the eigenfunction with negative eigenvalue in Eq. 7.2, the Berry's connection for the lower band of the Dirac dispersion is obtained as

$$\mathbf{A} = -\frac{1}{2}\nabla_{\mathbf{k}}\theta_{\mathbf{k}}. \tag{7.7}$$

$\nabla_{\mathbf{k}}$ correspond to the gradient w.r.t $\mathbf{k}$. Using Eq. 7.6 for $\theta_{\mathbf{k}}$ in Eq. 7.7 an explicit expression for the Berry's connection of the semi-Dirac Hamiltonian is obtained

$$\mathbf{A} = -\frac{1}{2k}\hat{\theta}, \tag{7.8}$$

where $\hat{\theta}$ is the direction shown in Fig.7.2. The Berry's connection given by the curl of
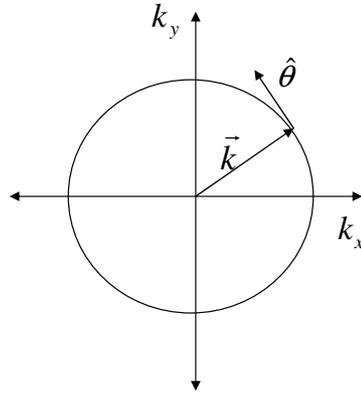
Fig. 7.1: The square contour along which the integration the Berry's connection is integrated.

Eq. 7.8 vanishes identically everywhere except at $(k_x, k_y) = (0,0)$ as can be checked by a

straightforward calculation. Both the Berry's connection and curvature blow up at $\mathbf{k} = \mathbf{0}$. The Berry's phase can be computed by integrating $\mathbf{A}$ around a contour containing the point of singularity. Since the result is independent of the shape of the contour, a circle of radius k is chosen as shown in Fig. and $\mathbf{A}$ is integrated along it. Now $\mathbf{A}$ given by Eq.7.8 being proportional to $\frac{1}{k}$ and the length of the circular contour being proportional to k, the integral of $\mathbf{A}$ along the circular contour gives a finite number, which turns out to be π considering the right numerical factors in obtaining the result. This value of Berry's phase is obtained for the eigenfunction with the negative eigen value. A similar calculation with the eigenfunction corresponding the positive eigen value will give $-\pi$ for the Berry's phase.

7.3   Berry's phase for the semiDirac dispersion

As mentioned at the end of the Ch.3, semi-Dirac dispersion follows from more than one Hamiltonian. To investigate the Berry's phase problem the semi-Dirac Hamiltonian given by Eq. 3.17 is chosen to facilitate the comparison with Dirac Hamiltonian. With the dimensionless variables K_x and K_y and the energy scale ε_0 defined at the beginning of Ch.2, one can write Eq. 3.17 as

$$H = \varepsilon_0 (K_x^4 + K_y^2)^{\frac{1}{2}} \tilde{h}_{sD}, \tag{7.9}$$

where $\tilde{h}_{sD}$ is the matrix given by

$$\tilde{h}_{sD} = \begin{pmatrix} 0 & e^{-i\theta_{\mathbf{K}}} \\ e^{i\theta_{\mathbf{K}}} & 0, \end{pmatrix} \tag{7.10}$$

The phase $\theta_{\mathbf{K}}$ appearing in Eq. 7.10 is given as

$$\theta_{\mathbf{K}} = \arctan \frac{K_y}{K_x^2}. \tag{7.11}$$

The eigenstates of the Hamiltonian in Eq. 7.10 are $\begin{pmatrix} 1 \\ e^{i\theta_{\mathbf{K}}} \end{pmatrix}$ and $\begin{pmatrix} -e^{-i\theta_{\mathbf{K}}} \\ 1 \end{pmatrix}$ with the eigenvalues 1 and -1 respectively. Plugging the eigenfunction with negative eigenvalue in Eq. 7.2, the Berry's connection for the lower band of the semi-Dirac dispersion is obtained as

$$\mathbf{A} = -\frac{1}{2}\nabla_{\mathbf{K}}\theta_{\mathbf{K}}. \tag{7.12}$$

$\nabla_{\mathbf{K}}$ correspond to the gradient w.r.t $\mathbf{K}$. Using Eq. 7.11 for $\theta_{\mathbf{K}}$ in Eq. 7.12 an explicit expression for the Berry's connection of the semi-Dirac Hamiltonian is obtained

$$\mathbf{A} = -\frac{\hbar}{4mv}[-\frac{2K_yK_x}{K_x^4 + K_y^2}\hat{i} + \frac{K_x^2}{K_x^4 + K_y^2}\hat{j}]. \tag{7.13}$$

The Berry's connection given by the curl of Eq. 7.13 vanishes identically everywhere except at $(K_x, K_y) = (0,0)$ as can be checked by a straightforward calculation. Does the Berry's curvature remain zero even at $(K_x = 0, K_y = 0)$? The vector field $\mathbf{A}$ blows up at that point as can be seen from Eq. 7.13, but that does not necessarily imply that the Berry's connection also has a singularity there. To explain this point, an example from the electrostatics is borrowed. The electric field $\mathbf{E}$ due to a point charge q is given by $\mathbf{E} = \frac{q}{r^2}\hat{r}$, where r denotes the distance from the charge. It blows up at $r = 0$. This is also reflected in one of the Maxwell's equations, viz., $\nabla.\mathbf{E} = \rho$(the charge density). For a point charge ρ assumes the form of a delta function. But the curl of the electric field due to the same point charge does not have a delta function singularity at $r = 0$. In fact $\nabla \times \mathbf{E} = \mathbf{0}$ everywhere **including** at $r = 0$. This becomes clear when the definition of a curl of a vector field is considered in terms of a limiting process. $\nabla \times \mathbf{E}$ is defined as $\nabla \times \mathbf{E} \equiv \lim_{\mathbf{A}_{\text{loop}} \to \mathbf{0}} \frac{\oint \mathbf{E}.\mathbf{dl}}{\mathbf{A}_{\text{loop}}}$, where A_{loop} is the area of the loop enclosing the point under consideration, which in this case is the $r = 0$ point. This definition of curl becomes the conventional expression for curl involving derivatives of various components of the vector field, when the derivatives **are defined** at the point under consideration. Considering a

circular loop (the result holds for other types of loops too), $\mathbf{E}$ is always perpendicular to the the line element $d\mathbf{l}$, resulting in the line integral in the definition of curl mentioned above to be zero, irrespective of how small the loop is, i.e, how close one is to the point $r = 0$ under question. Hence it is concluded that $\nabla \times \mathbf{E} = \mathbf{0}$ at $r = 0$.

In order to compute the Berry's curvature for the semi-Dirac dispersion at the point $K_x = K_y = 0$ the following expression is used for $\nabla \times \mathbf{A}$

$$\nabla \times \mathbf{A} \equiv \lim_{\mathbf{A}_{\text{loop}} \to \mathbf{0}} \frac{\oint \mathbf{A}.d\mathbf{l}}{\mathbf{A}_{\text{loop}}}. \tag{7.14}$$

In the following the numerator of Eq. 7.14 is evaluated for a square contour. The square
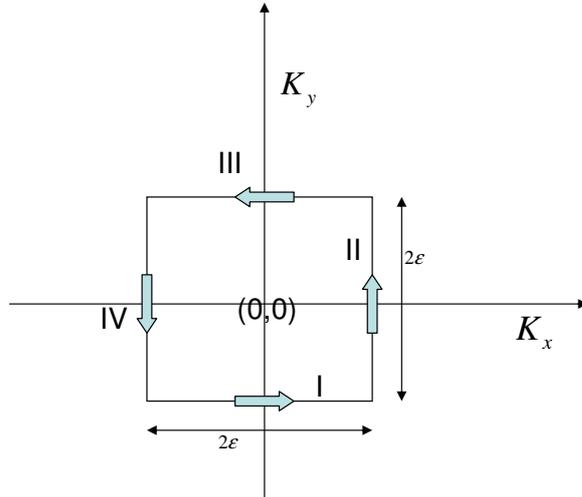
Fig. 7.2: The square contour along which the integration the Berry's connection is integrated.

contour has four sides marked by the Roman letters I through IV, as shown in Fig.7.2. Using Eq. 7.13, and the line element $d\mathbf{k} = \frac{\mathbf{p}}{\hbar}d\mathbf{K}$, where p is the usual momentum scale associated with the semi-Dirac dispersion, the line integral of the Berry's connection $\mathbf{A}$

can be written explicitly as

$$\oint \mathbf{A}.\mathbf{dk} = -\frac{1}{2}[-\frac{2\mathbf{K_y}\mathbf{K_x}}{\mathbf{K_x^4} + \mathbf{K_y^2}}\mathbf{dK_x} + \frac{\mathbf{K_x^2}}{\mathbf{K_x^4} + \mathbf{K_y^2}}\mathbf{dK_y}]. \tag{7.15}$$

In the following Eq. 7.15 is evaluated for all the sides of the square of Fig.7.2. Along the side I, $K_y = -\epsilon$, a constant, which implies that $dK_y = 0$ in Eq. 7.15 and K_x varies from $-\epsilon$ to ϵ. Hence the integral in Eq. 7.15 becomes $-\epsilon \int_{-\epsilon}^{\epsilon} \frac{K_x dK_x}{K_x^4 + \epsilon^2}$, which gives a zero since the integrand is an odd function. In a very similar similar way one can show that the line integral is zero along the side III of the square. As for the side II, $K_x = \epsilon$, a constant, implying $dK_x = 0$. Hence from Eq. 7.15 one obtains $\int_{-\epsilon}^{\epsilon} \frac{\epsilon^2 dK_y}{\epsilon^4 + K_y^2}$. This is non-zero, but of opposite sign compared to the contribution from side IV. Hence when the contributions from the sides II and IV are added it gives zero. Hence the line integral along the square contour is zero, irrespective of the size of the square, indicating that the Berry's curvature as given by Eq. 7.14 is zero for the semi-Dirac Hamiltonian. Other closed contours like a rectangle or a trapezoid have been tried, all of them confirming the line integral being zero. Finally an argument is given, which is based on transporting an eigenfunction along a closed contour. The Berry's phase can be obtained by a continuous transportation of the eigenfunction of the Hamiltonian over a closed contour. If the sign of the eigenfunction reverses after it comes back to the same point it started from, the Berry's phase is non-trivial. In case the eigenfunction maintains the sign, the Berry's phase is zero. One starts with an eigenstate of the Hamiltonian, and transports it along a closed loop. In the problem of the Dirac dispersion one needs to worry about the continuity of the eigenfunction at $k_x = 0$, where there is a discontinuity in $\theta_\mathbf{k}$ given by $\arctan \frac{k_y}{k_x}$.($\arctan \frac{k_y}{k_x} = -\frac{\pi}{2}$ or $\frac{\pi}{2}$ depending on whether k_x approaches 0 from the left or the right side of zero respectively.) No such problem exists for semi-Dirac dispersion. For semi-Dirac, due to the presence of K_x^2 instead of K_x in the expression for $\theta_\mathbf{K}$ given by Eq. 7.11, $\theta_\mathbf{K}$ is continuous at $K_X = 0$. What that means is when an eigenstate of the semi-Dirac Hamiltonian given by Eq. ?? is transported along a circle it's phase does not face a discontinuity. So when it comes back

to where it started, the sign of the eigenfunction does not get changed. This is a clear indication of Berry's phase being zero.

7.4   conclusion

In this chapter the topological aspect of the semi-Dirac dispersion was discussed. The finding is somewhat surprising: semi-Dirac dispersion, which has a point Fermi surface like a Dirac dispersion, and more complex (in terms of anisotropy) as compared to the Dirac dispersion, is topologically simpler than the latter. That was verified by direct calculation as well as by transporting an eigenfunction around a closed loop. It was mentioned at the end of chapter 3 that a semi-Dirac Hamiltonian can have various forms. For a 'real' semi-Dirac Hamiltonian the Berry's phase is trivially zero. In this chapter it is shown that the result holds even when the Hamiltonian is complex.

8. THE ENERGY LEVEL STATISTICS FOR THE SEMIDIRAC DISPERSION

8.1   Introduction

In this chapter Quantum Chaos and its relevance to the semi-Dirac dispersion is discussed. Quantum Chaos is a relatively new idea which began with serious investigations by Michael Berry, Gutzwiller and other proponents in the field. In the following, a brief description of the basic concepts of Quantum Chaos is given. The discovery of the classical Chaos theory[67], a very important one in contemporary physics, was a severe blow to the predictive power of Newtonian mechanics. With the help of Newton's law one can predict the trajectory of an object accurately, given its initial position and the velocity. But with the advent of the Chaos theory things did not remain that simple any more. According to Michael Berry[57], "Chaos is instability that persists, so that motion, although strictly determined, is so sensitive that prediction is effectively impossible. With chaos, there is no regularity, no strict repetition. The weather is a familiar example. Another is the erratic rotation of one of the satellites of the planet Saturn, namely Hyperion, a potato-shaped rock about the size of New York City." After the Chaos theory, the determinism remained purely in the mathematical sense: in a chaotic system if one could specify the initial conditions with infinite accuracy, a trajectory could be determined precisely. Two trajectories with very small differences in their initial conditions will evolve very differently over time. So for all practical purposes the notion of predictability is seriously compromised. However, there seems to be a very interesting connection between the classical chaos and quantum mechanics.

8.2   Connection between Classical Chaos and Quantum mechanics

Due to the works of Bohr, Heisenberg, Schrodinger and others Quantum mechanics was developed in the 1920's, which revolutionized the way physics was thought before that: it became impossible to talk about trajectories any more. One could only predict the probability of an event with the help of Schrodinger's equation. As an alternative to the Schrodinger equation approach, Richard Feynman introduced the path integral technique[53], according to which the probability amplitude of a particle to go from a point A to another point B is a function of all the possible paths that the particle can take between A and B. Different paths are weighted differently, the greatest weight being associated with the classical path, i,e the path which satisfies the Euler Lagrange equation or in simpler terms Newton's law of motion. The path integral technique allows one to think in terms of paths for solving quantum mechanical problems. Path integral has a deep philosophical significance in the sense that it unifies the classical and the quantum mechanics. The classical limit of quantum mechanics is achieved as the Planck's constant $\hbar$ goes to 0 as explained below. $\hbar$ in essence is the quantum of action. According to the Feynman path integral technique[53], the propagator is given by:

$$K(b,a) = \int_a^b Dx e^{\frac{i}{\hbar}S},$$

(8.1)

where S is the action given by $\int L dt$, L being the Lagrangian of the system. As $\hbar$ goes to zero, the phase factor in Eq.8.1 oscillates rapidly and the greatest contribution to the path integral comes from the path which has the zero first order variation(stationary phase approximation). It can be shown that the path for which the above criterion is met is the classical trajectory of the particle. That is how Newton's law enters in the formulation of quantum mechanics. It can be shown in the semiclassical approximation ($\hbar \to 0$), the non-relativistic propagator takes the following approximate expression[25]:

$$K(b,a) \approx (2\pi i\hbar)^{-\frac{1}{2}}(-|\frac{\partial^2 S}{\partial x_b \partial x_a}|)^{-\frac{1}{2}} e^{\frac{i}{\hbar}S},$$

(8.2)

where x_a and x_b denote the co-ordinates of the points A and B respectively. In a system whether there is chaos or not depends on how the potential function and its derivatives behave over a region. An analogy can be drawn w.r.t the stability of a dynamical system. Stability is determined by the sign of the second derivative of the potential. The positive sign of the second derivative indicates stability, whereas the negative sign indicates the lack of it. Through the expression $\frac{\partial^2 S}{\partial x_b \partial x_a}$ appearing in Eq.8.2, the derivatives of the potential enter into the expression of the semi-classical propagator; and the potential itself enters through the action function S. Hence Eq.8.2 establishes a link between classical chaos and quantum mechanics. This relationship leads to many interesting consequences. The presence of chaos in the corresponding classical problem leaves its quantum signature, for example, in the statistics of the spacing of the consecutive energy levels. In the subsequent sections this particular aspect of quantum chaos is described in details and how it plays out for the semi-Dirac dispersion is investigated. Before going into that this section is concluded by mentioning one fascinating aspect of quantum chaos: even when chaos is present in the system, quantum mechanics is able to make precise predictions. For example, the problem of scattering of an electron by a complicated (chaotic) potential field can in theory be solved both classically and quantum mechanically. But the difference between the two is more fundamental than just being different in their predictions. By use of classical mechanics one is not even able to make sensible predictions about the physical observables due to the sensitive dependence of the trajectories to the initial conditions, whereas the quantum mechanical expressions are not beset with such problems for computing the same physical quantities. In a sense quantum mechanics takes care of the philosophical questions about the issue of predictability which had beset the field of physics after the advent of Chaos theory. Hence Michael Berry pointed out [57], 'There is no Quantum Chaos', and instead of calling it Quantum Chaos coined the term 'Quantum Chaology'.

8.3   Energy Level Statistics

The study of energy level statistics first originated in the context of nuclear physics, where the Hamiltonian could not be specified exactly. Wigner came up with the idea that one does not need to know about the details of a Hamiltonian other than the fact that the elements of the Hamiltonian matrix are random. This line of thought culminated in 'Random Matrix Theory'[54, 55, 56] which deals with the the energy level statistics of a random matrix. Wigner showed that for a random matrix, the distribution of eigenvalues(as opposed to the spacing between the consecutive eigenvalues, which will be discussed in the subsequent sections) take the shape of a semi-circle, which is known as the Wigner's semi-circle law. This is pretty remarkable because of its universality: Wigner's semi-circle law does not depend on any specific distribution that the elements of the random matrix follow. The energy level statistics turns out to be a powerful tool even when the Hamiltonian is known completely. The universality behavior of the statistics of the normalized energy level spacings can be exploited to ascertain whether chaos is present in the system or not. There are primarily two different types of universal distribution function for the normalized energy level spacing: Poisson and Gaussian Orthogonal Ensemble (GOE). The Poisson distribution is given by the expression: e^{-s}, where s is the normalized energy level spacing. [The normalization procedure(also called the 'unfolding process') will be described in details later.] The GOE distribution is given by $\frac{\pi}{2}se^{-\frac{\pi}{4}s^2}$. If the billiards has less symmetry in it, either due to a less symmetric boundary or because of an energy momentum dispersion lacking in a specific symmetry, the latter being the case for the semi-Dirac dispersion, the statistics is no more either of the two types of distributions mentioned above. The distribution in that case is a superposition of N independent GOE distributions[68], the mathematical form for the resulting distribution being given by $\frac{\partial^2}{\partial s^2}[erfc(\frac{\sqrt{\pi}}{2}\frac{s}{N})]^N$, where $erfc$ denotes the complementary error function, which is written in an integral form as $erfc(z) = \frac{2}{\sqrt{\pi}}\int_z^\infty dte^{-t^2}$. N is an integer. For $N = 1$ the distribution reduces to the conventional GOE distribution. For $N = 2$, the distribution starts from a non-zero value at $s = 0$. [The distributions considered in this chapter will primarily fall into Poisson,

GOE, or superposition of independent GOEs corresponding to $N = 2$]. The three types distributions are shown in Fig.8.1.

Various statistics for the variable s
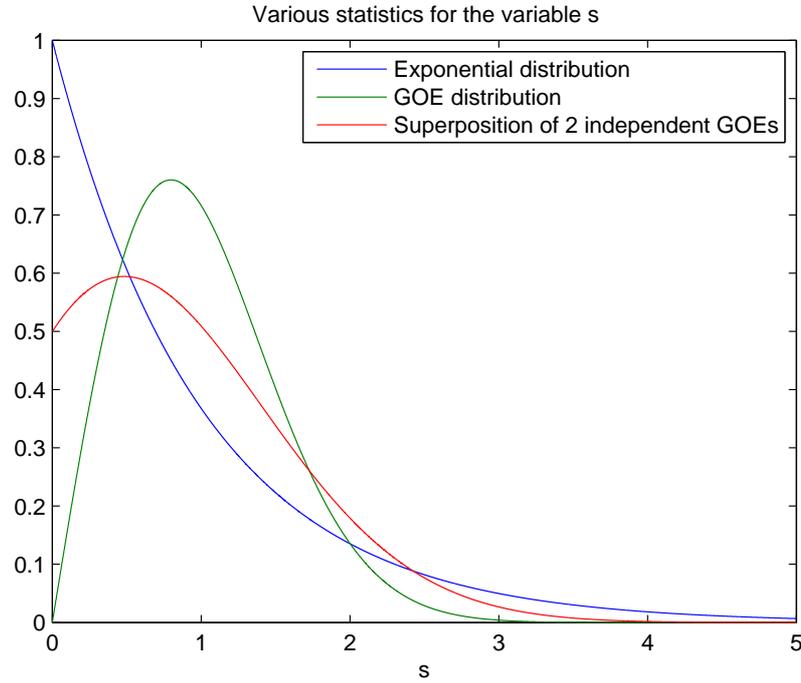
Fig. 8.1: Distributions of s

When chaos is present in the corresponding classical problem, the normalized level spacings of the quantum energies follow the GOE (or superposition of independent GOEs) distribution as opposed to the Poisson distribution, which corresponds to a problem without chaos[59]. The GOE(or superposition of independent GOEs) distribution is qualitatively different from the Poisson distribution in the feature that the former goes to a maximum for a non-zero value of s, whereas the latter peaks at $s = 0$, s being proportional to the energy level spacing. That means the energy levels corresponding to the GOE (or superposition of independent GOEs) distribution repel each other. Hence it can

be said that the energy level repulsion is a feature of a chaotic system. The energy level repulsion indicates that the energies are not distributed randomly. When the energy levels are distributed randomly, it can mathematically be proved that s follows a Poisson distribution[25]. Summarizing, the presence of energy level repulsion is a signature of chaos, whereas the absence thereof is an indicator of regularity in a system. This is rather interesting: although chaos in classical mechanics implies irregularity in the phase space, the energy levels in the corresponding quantum problem are not randomly distributed.

8.4 The quantum billiards

A Quantum billiards[59][60][61] is essentially the system of an electron confined in an infinite potential. With the advent of crystal growth and lithographic techniques, devices in the micro or nanometer scale have been built[59]. They in the low temperature limit can be thought of as physical realizations of Quantum billiards. An electron in such a device is primarily scattered by the device boundary, and not by the impurities. Experimentation on Quantum billiards can be performed with Scanning Tunneling Microscopy[59][63]. The Quantum billiards problem requires solving for Schrodinger's equation for an infinite potential well. For such a problem, the wave function needs to vanish at the boundary, which gives rise to the quantized energies. For different boundary shapes the energy levels will be different. Hence one can construct the statistics for the s variable for different boundaries. It turns out for irregularly shaped boundaries, the energy level statistics is more GOE (or superposition of independent GOEs) type than the Poisson type. Fig.8.2 shows the energy level statistics for various types of billiards. For them, the kinetic energy term in the Hamiltonian is proportional to the Laplacian operator. The corresponding quantum billiards problems are called 'parabolic type', since the Laplacian, when transformed in the momentum space, becomes a quadratic function of the momentum. These results will later be contrasted with those obtained for the quantum billiards corresponding to the semi-Dirac dispersion.
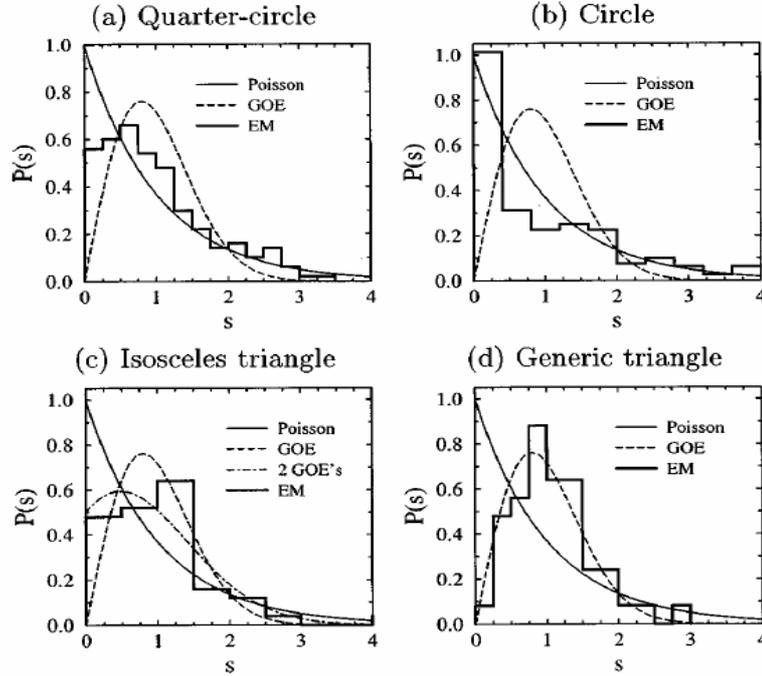
Fig. 8.2: Energy Level Statistics for Quantum billiards of various shapes[59]. The energy momentum relationship in all of them is parabolic.

8.5 Solving for the Energies of the Quantum Billiards by Expansion Method

In quantum billiards the eigen-energies can be calculated exactly only in a very few specific cases, e.g., a parabolic type problem(explained before) with a circular boundary. For the rest of the situations, approximate techniques[62] are necessary. In this section an approximate technique called the expansion method[59] is explained. This method is later used for the quantum billiards problem for the semi-Dirac dispersion. Fig.8.3 describes an arbitrary shaped boundary for the Quantum Billiards problem. Let the domain enclosed by the boundary be denoted by D. The Schrodinger equation for the problem can be

written as:

$$(\hat{H} \equiv -\frac{\hbar^2}{2m}\nabla^2 + V(\mathbf{r}))\Psi = E\Psi, \tag{8.3}$$

where

$$\begin{aligned}
V(\mathbf{r}) &= 0, \mathbf{r} \in D \tag{8.4}\\
&= \infty, \text{otherwise.}
\end{aligned}$$

The quantum mechanical wave-function should vanish at the boundary ∂D of the region D, since the potential is infinite everywhere outside D. In order to solve this problem by the Expansion method, the eigenstates of the Hamiltonian corresponding to a slightly different problem, are considered. For this new problem it is assumed that the potential

is infinite at the enclosing rectangular boundary as given in Fig.8.3. The corresponding eigen-functions are given by

$$\phi_{n_1,m_1} = \sqrt{\frac{2}{a_1}} \sin(\frac{\pi}{a_1} n_1 x_1) \sqrt{\frac{2}{a_2}} \sin(\frac{\pi}{a_2} m_1 x_2), \tag{8.5}$$

where n_1 and m_1 are integers and a_1 and a_2 are the dimensions of the rectangle. x_1 and x_2 correspond to the two orthogonal axes. The region inside the rectangle is divided into regions I and II as shown in the figure. It is assumed that the potential takes a value V_0 in region II. As V_0 approaches ∞, the potential becomes the same as that given by Eq.8.4. Ψ, the solution to Eq.8.3, can be written as a linear combination of ϕ_{n_1,m_1}s appearing in Eq.8.5, since they constitute a complete set of functions.

$$\Psi = \sum_{i,l} C_{i,l} \phi_{i,l}, \tag{8.6}$$

where $C_{i,l}$ are constants. Inserting Eq.8.6 in Eq.8.3, multiplying the resulting expression by ϕ_{n_1,m_1}^*, and ϕ_{n_2,m_2} from the left and the right respectively, and integrating over the rectangular region depicted in Fig.8.3, the following is obtained

$$\sum_{m_1,m_2} (H_{n_1,m_1,n_2,m_2} - E\delta_{n_1,m_1,n_2,m_2})C_{n_1,m_1} = 0, \tag{8.7}$$

where H_{n_1,m_1,n_2,m_2} is given by

$$H_{n_1,m_1,n_2,m_2} = \int \int d^2\mathbf{r}\phi_{n_1,m_1}(\mathbf{r})\hat{H}\phi_{n_2,m_2}(\mathbf{r}), \tag{8.8}$$

$\hat{H}$ being the Hamiltonian operator appearing in Eq.8.3. Using the fact that the potential is zero in region I, but assumes the value V_0 in region II(Fig.8.3), Eq.8.8 can be expressed as

$$H_{n_1,m_1,n_2,m_2} = \frac{\pi^2\hbar^2}{2m}[(\frac{n_1}{a_1})^2 + (\frac{m_1}{a_2})^2]\delta_{n_1,n_2}\delta_{m_1,m_2} + V_0 v_{n_1,n_2,m_1,m_2}, \tag{8.9}$$

where

$$v_{n_1,m_1,n_2,m_2} = \int\int_{II} d^2\mathbf{r}\phi_{n_1,m_1}(\mathbf{r})\phi_{n_2,m_2}(\mathbf{r}). \qquad (8.10)$$

The first term in Eq.8.9 is the kinetic energy term. The orthogonality of the $\phi_{m_1,m_2}(\mathbf{r})$ functions have been used to derive Eq.8.8. The eigen-energies of the Hamiltonian can be found by setting the determinant of the matrix $(H_{n_1,m_1,n_2,m_2} - E\delta_{n_1,m_1,n_2,m_2})$ appearing in Eq.8.7 to zero, which in the following is expressed in an equation form

$$|H_{n_1,m_1,n_2,m_2} - E\delta_{n_1,m_1,n_2,m_2}| = 0. \qquad (8.11)$$

The matrix H_{n_1,m_1,n_2,m_2} is an infinite matrix since each of the suffixes can go from 1 to ∞. For numerical calculations one can not work with an infinite matrix, and hence one needs to truncate H_{n_1,m_1,n_2,m_2} for some finite values of its suffixes. There is no hard and fast rule for how large the truncated Hamiltonian matrix need to be. It depends on the specific problem at hand. At this point it is worth mentioning that the eigenvalues obtained by the expansion method tend to the ideal ones as V_0 tends to ∞. But increasing V_0 without increasing the number of the ϕ_{n_1,m_1}'s in Eq.8.6 might lead to less accurate results. So one needs to use a sufficiently large value of V_0 which will go with a reasonably large number of basis functions ϕ_{n_1,m_1}'s. Of the computed eigenvalues only the lower ones are accurate. A criterion, based on Weyl's formula, regarding how many eigenvalues from the lower end to trust, will be described.

8.6   Weyl's formula

Once the eigen-energies are computed the differences between consecutive energy levels are normalized with the help of Weyl's formula by a technique called 'unfolding'. Weyl's formula counts the number of energy eigenstates less than a given eigen-energy, which is

also the same as the integrated density of states given by [25]

$$N(E) = \frac{1}{(2\pi\hbar)^g} \int dE \int d^g p \, d^g q \, \delta(E - H(p,q)), \qquad (8.12)$$

where g is the geometrical dimension of the problem. $N(E)$ is proportional to the number of states in the phase space constrained by the geometrical boundary of the billiard in the real space and the constant Fermi contour in the momentum space. As an example of how to obtain an expression for $N(E)$, that quantity in the following is derived for the parabolic dispersion. The energy momentum relationship for the parabolic dispersion is $E = \frac{p^2}{2m}$. The Fermi contour is a circle, the area of which is given by $\pi p^2 = \pi 2mE$. Hence the total area of the phase space under consideration is $A(\pi 2mE)$, A being the real space area of the billiard. From Heisenberg's uncertainty principle, the unit of phase space area is h^2, where h is the Planck's constant. [The square coming from the fact that the problem is two-dimensional]. Hence the number of states in the above-mentioned phase space is $\frac{A\pi 2mE}{h^2} = \frac{A}{4\pi}\frac{2mE}{\hbar^2}$. So Eq. 8.12 for the parabolic dispersion reduces to:

$$N(E) = \frac{A}{4\pi}\frac{2mE}{\hbar^2}. \qquad (8.13)$$

The Weyl's expression N_{sD} for the semi-Dirac spectrum is obtained by taking the integral of the expression appearing in Eq. 2.4 (i.e. finding the integrated density of states) and then multiplying that by the real space area A of the billiard

$$N_{sD}(E) = A\frac{(2m)^{\frac{1}{2}}\varepsilon^{\frac{3}{2}}}{\pi^2\hbar^2 v}\frac{2}{3}\int_0^1 \frac{dk'_x}{\sqrt{1 - k'^4_x}}. \qquad (8.14)$$

Next a dimensionless energy variable ϵ is defined as $E = \frac{\hbar^2\pi^2}{2ma^2}\epsilon$. In terms of the new variable $N_{sD}(E)$ becomes

$$N_{sD}(E) = .8740\frac{A}{\alpha a^2}\epsilon^{\frac{3}{2}}. \qquad (8.15)$$

The numerical pre-factor in Eq. 8.15 is obtained by combining the numerical factor and the integral appearing in Eq. 8.14. Using the fact that A, the geometrical area of the circle of diameter a, is given by $\frac{\pi a^2}{4}$, Eq. 8.15 becomes

$$N_{sD}(E) = .8740\frac{\pi}{4\alpha}\epsilon^{\frac{3}{2}}. \tag{8.16}$$

N_{sD} will be used for later calculations.

8.7   The method of the unfolding of the spectra

To compute the energy level statistics, one needs to unfold the spectra first. In the following it is explained what that means and how that is carried out.

In Fig.8.4, N computed from the eigenvalues obtained by actual diagonalization of the Hamiltonian is plotted against the energy E. The shape of the function has the appearance of a staircase and hence called the stair-case function. If there is only one state corresponding to a given energy (that is, no degeneracy), the staircase function increases by one as one moves to the next energy. But it is not so for the case with degeneracies. The jump in the stair-case function at an energy will then be proportional to the degeneracy corresponding to that energy. In order to compute the energy level statistics one can not directly work with this rather rough-looking staircase function. Instead, one considers the Weyl's expression for N given by Eq. 8.13 or Eq. 8.15. Plotting N obtained by direct diagonalization of the Hamiltonian and that obtained from Weyl's expression together, only those eigenvalues are accurate which correspond to the region where the two curves are quite close to each other. There are no hard and fast rules to determine the closeness of the two curves. Depending on the problem at hand a sensible eye-estimate suffices in most of the cases. The difference between the values of N given by Weyl's expression at consecutive energies are defined as the new variable s. The procedure of obtaining the values for s is called unfolding. Since the Weyl's expression is a smooth version of the staircase function, and the staircase function changes by one on an average (assuming
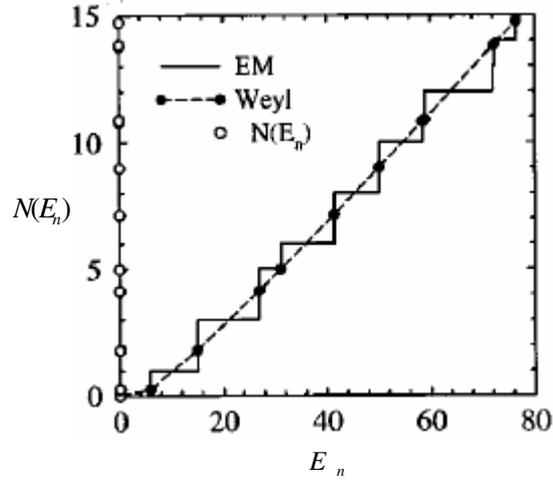
Fig. 8.4: Unfolding of the spectra[59]. The staircase function is obtained by direct calculation of the eigenvalues using a suitable numerical technique like the expansion method(EM). The smooth curve (the dotted line) is obtained from Weyl's formula. E_n are the discrete energy values and $N(E_n)$ are the corresponding points on the Weyl curve. The variable s is defined as the differences in the consecutive $N(E_n)$'s. The Energy momentum relationship for this problem is quadratic.

there are not too many degeneracies) between two consecutive energies, the variable s should have an average value of 1. It's the statistics of s that one is interested in. As mentioned before the probability density function of s has a universal behavior.

8.8 Results for the semi-Dirac dispersion

A quantum billiards problem is considered where the confined electron obeys the semi-Dirac dispersion. The geometry chosen for this problem is a circular one. The interest in a circularly symmetric boundary results from the fact that the semi-Dirac dispersion, itself lacking in the circular symmetry, may produce interesting energy level statistics even when

the boundary is a symmetric one. It is a known fact that the energy level statistics changes from one universality type to another with the change of the shape of the boundary as has been shown in Fig.8.2. But with a given boundary-shape it is of one type for the parabolic as well as the Dirac dispersions. On the contrary, results with a large range of variability follow for the quantum billiards problem with the semi-Dirac dispersion even when the shape of the boundary remains fixed. The Expansion method is employed to find the eigenvalues of the Hamiltonian for this problem. The Hamiltonian for this problem is different from that given by Eq. 8.3, and is given by

$$[\hat{H} \equiv (\sqrt{\frac{\hbar^4}{4m^2}\frac{\partial^4}{\partial x_1^4} - \hbar^2 v^2 \frac{\partial^2}{\partial x_2^2}} + V(\mathbf{r}))]\Psi = E\Psi. \tag{8.17}$$

Assuming that the radius of the circle is a, each side of the enclosing square will also be a. The basis functions are the same as given by Eq. 8.5, with $a_1 = a_2$. Hence the equation corresponding to Eq. 8.8 becomes

$$H_{n_1,n_2,m_1,m_2} = \frac{\pi^2\hbar^2}{2ma^2}\sqrt{m_1^4 + \alpha^2 m_2^2}\delta_{n_1,n_2}\delta_{m_1,m_2} + V_0 v_{n_1,n_2,m_1,m_2}, \tag{8.18}$$

where

$$\alpha = \frac{2mva}{\hbar\pi}, \tag{8.19}$$

and v_{n_1,n_2,m_1,m_2} is given by the following integral

$$v_{n_1,n_2,m_1,m_2} = (\sqrt{\frac{2}{a}})^4 \int\int_{II} d^2\mathbf{r}\sin(\frac{n_1\pi x_1}{a})\sin(\frac{m_1\pi x_2}{a})\sin(\frac{n_2\pi x_1}{a})\sin(\frac{m_2\pi x_2}{a}). \tag{8.20}$$

α as given by Eq. 8.19 is a dimensionless quantity, since the numerator being proportional to the product of a momentum scale (mv) and a length scale (a) has the same dimension as $\hbar$, which is present in the denominator. It can also be shown that α is the ratio of the two energy scales, one, the natural energy scale of the semi-Dirac dispersion $2mv^2$,

and the other the energy scale $\frac{\hbar^2 \pi^2}{2ma^2}$ naturally appearing in the circular quantum billiards problem. To carry out the double integral given by Eq. 8.20 the variables $x_1' \equiv \frac{2x_1}{a}$ and
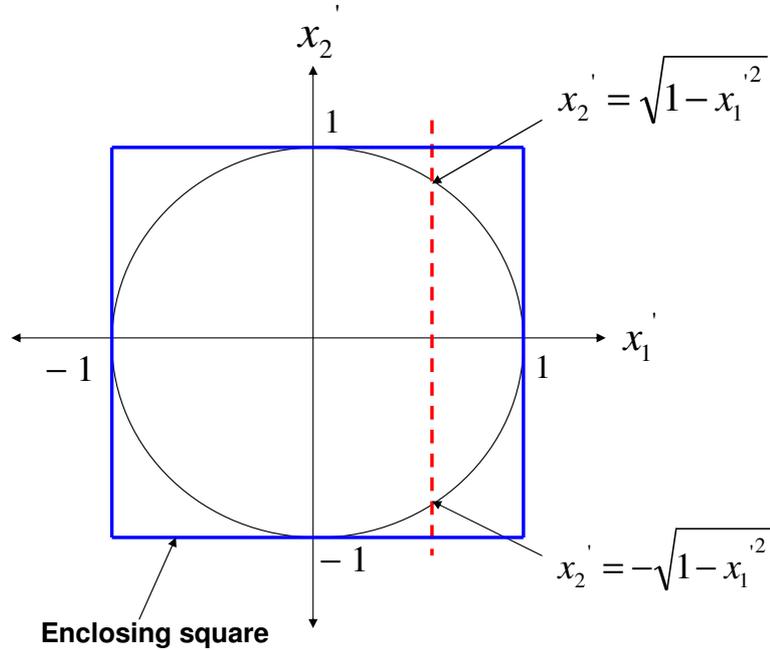
Fig. 8.5: Circular boundary enclosed by a square. The potential is zero inside the circle and non-zero in the region bounded by the arc of the circle and the sides of the square.

$x_2' \equiv \frac{2x_2}{a}$ are introduced[x_1 and x_2 are normalized by the radius of the circle]. The double integral appearing in Eq. 8.20 is done over the region **between** the circular arc and the sides of the square. Fig. 8.5 shows the limits that one needs to use in order to evaluate the double integral as iterated single integrals. Also, the eigenfunctions given by Eq. 8.5 are written w.r.t the origin at the lower left corner of the enclosing square. Shifting the origin at the center of the square and making use of the above mentioned new variables

Eq. 8.20 can be written as follows

$$
\begin{aligned}
v_{n_1,n_2,m_1,m_2} \;=\; & \int_{x'=-1}^{x'=1} dx_1' \int_{x_2'=-1}^{x_2'=1} dx_2' \\
& \sin(\frac{n_1\pi}{2}x_1' + \frac{n_1\pi}{2})\sin(\frac{m_1\pi}{2}x_2' + \frac{m_1\pi}{2})\sin(\frac{n_2\pi}{2}x_1' + \frac{n_2\pi}{2})\sin(\frac{m_2\pi}{2}x_2' + \frac{m_2\pi}{2}) \\
& - \int_{x'=-1}^{x'=1} dx_1' \int_{x_2'=-\sqrt{1-x_1'^2}}^{x_2'=\sqrt{1-x_1'^2}} dx_2' \\
& \sin(\frac{n_1\pi}{2}x_1' + \frac{n_1\pi}{2})\sin(\frac{m_1\pi}{2}x_2' + \frac{m_1\pi}{2})\sin(\frac{n_2\pi}{2}x_1' + \frac{n_2\pi}{2})\sin(\frac{m_2\pi}{2}x_2' + \frac{m_2\pi}{2}).
\end{aligned}
\tag{8.21}
$$

The above equation is written in terms of the difference of two double integrals: one over the entire square, the other over the circular region. A code is written in Java in order to evaluate the double integrals in Eq. 8.21. Java uses the efficient Legender-Gauss technique to carry out the integrations. The Java program is called from within the Matlab environment for diagonalizing the Hamiltonian matrix in Eq. 8.18. If each of the integers n_1, n_2, m_1, m_2 goes from 1 to L, the matrix will be $L \times L \times L \times L$, which can be wrapped into a $L^2 \times L^2$ one, with its number of eigenvalues being L^2. For example when $L = 20$ is chosen, the number of eigenvalues is 400. Next the process of unfolding is carried out to obtain various values for the variable s. In this problem there are two parameters: α and a. Once the energy levels are expressed in the unit of the energy scale $\frac{\pi^2\hbar^2}{2ma^2}$, α is the only free parameter in the problem. In the following it is described how the statistics of the s variable changes with the variation of α. This is an unique feature of the semi-Dirac dispersion. In Dirac and parabolic dispersions the energy level statistics is unique for a given shape of the boundary of the billiard. As it is explored in the following, the statistics for s does not stay the same and hence is not unique as the semi-Dirac parameter space is scanned.

8.8.1   The Statistics for s

One can compute the statistics of s by creating bins for a range of values of s, and constructing a histogram. A histogram consists of bars whose heights are proportional

to the frequencies corresponding to the bins of s. A histogram is an useful tool when only one frequency distribution is visualized. For multiple distributions, histograms will superimpose on each other rendering the visualization almost impossible. For the problem at hand different distributions of s will be obtained for different values of α. Hence a way to visualize them on the same graph is necessary. In the following a method is described which makes that possible. s being a variable whose values are proportional to the difference of the consecutive energy levels, it can assume only discrete values since the energy levels are discrete. Centering each of the discrete values of s, a normalized Gaussian distribution of a given width is constructed. For two values of s, the Gaussians centering each of them will add up. When the two values of s are close to each other the net distribution will be much more accentuated compared to if the values of s are far apart. This procedure will create a net distribution whose profile matches that of a histogram, but is smoother compared to it. Mathematically speaking let $\frac{1}{\sigma\sqrt{2\pi}}e^{\frac{-(s-s_i)^2}{2\sigma^2}}$ be a Gaussian centered at s_i. $s_i, i = 1 \text{to} N$ represent N values of s obtained by unfolding the spectrum of eigenvalues. s represents the continuous variable of the Gaussian. Instead of plotting the histogram, the following expression is plotted.

$$f = \frac{1}{N}\sum_{i=1}^{N}\frac{1}{\sigma\sqrt{2\pi}}e^{\frac{-(s-s_i)^2}{2\sigma^2}} \tag{8.22}$$

The multiplicative factor $\frac{1}{N}$ at the beginning of the expression on the right hand side ensures normalization. The widths of the Gaussians σ are chosen to be equal for all s_i's. There is some flexibility in choosing the exact value for σ. It should be chosen in a way such that f in Eq. 8.22 appears to be smooth. For the calculation at hand, a value of .2 is chosen for σ. f representing a line instead of a histogram, this procedure allows one to plot different f's for different values of α on the same graph. Before showing the plots it's worth while to have a small discussion about α that the plots depend on. α, given by Eq. 8.19, is a dimensionless quantity as mentioned before. α is proportional to the constant mv relevant for the semi-Dirac dispersion. mv determines the eccentricity

of the semi-Dirac dispersion; hence changing α amounts to changing the curvature of the semi-Dirac Fermi surface. The following calculations are restricted to the small value of the α. For this range of α it is shown that the statistics of the variable s displays a very rich behavior. Unlike the parabolic or the Dirac dispersion, the energy level statistics does not always stick to only one type of universality class for a given geometry. The system goes in and out of the these two types sometimes with a very sensitive dependence on α. A possible explanation for this type of behavior is also given at the conclusion. The complete procedure of obtaining a statistics is described in the following for $\alpha = .5$. This will be the first of a series of plots on the energy level statistics of the semi-Dirac dispersion. The purpose of these plots will be to show the rich diversity of the α parameter space. In order to compute the eigen-energies, all the values less than a given energy need to be accounted for. For $\alpha = .5$ that is arbitrarily chosen as 35 in the units of $\frac{\hbar^2}{2ma^2}$. To make sure that all the eigen energies less than that value have been considered the following procedure is resorted to. Ignoring the potential energy and considering the kinetic energy part in Eq. 8.18 only, it is noted in order to obtain all the energies below 35 one would have needed to use $(m_1)_{\mathrm{max}} = 6$, and $(m_2)_{\mathrm{max}} = 70$ approximately. The reason is as follows. In Eq. 8.18, the kinetic energy term(henceforth defined as KE) is given by (in the units of $\frac{\hbar^2}{2ma^2}$)

$$KE = \sqrt{m_1^4 + \alpha^2 m_2^2}\delta_{n_1,n_2}\delta_{m_1,m_2}. \tag{8.23}$$

The above expression attains the maximum value $(KE)_{\mathrm{max}}$ for $(m_1)_{\mathrm{max}} = \sqrt{(KE)_{\mathrm{max}}}$ and $\alpha m_2 = (KE)_{\mathrm{max}}$ approximately. Because when $KE = (KE)_{\mathrm{max}}$, the maximum value of one integer corresponds to the minimum value of the other integer. Strictly speaking, the minimum value of a positive integer for the problem at hand is 1, since the 0 value would make the wavefunction given by Eq. 8.5 to be zero identically, rendering the situation unphysical. But since an estimate is what is sought after in the current situation 0 does the job. It is also due to the approximate nature of the analysis that the potential energy

is ignored to obtain an estimate. Setting $(KE)_{\max}$ to 35, $(m_1)_{\max} = \sqrt{(KE)_{\max}} \approx 6$ and $(m_2)_{\max} = (\alpha)^{-1}(KE)_{\max} = 70$. With these choices of the integers, all the entries of the Hamiltonian matrix for $\alpha = .5$ is computed and the eigenvalues are obtained by diagonalizing the Hamiltonian. Unfolding is carried out next as shown in the following figure. There are two vertical lines in Fig.8.6. The one on the right corresponds to the
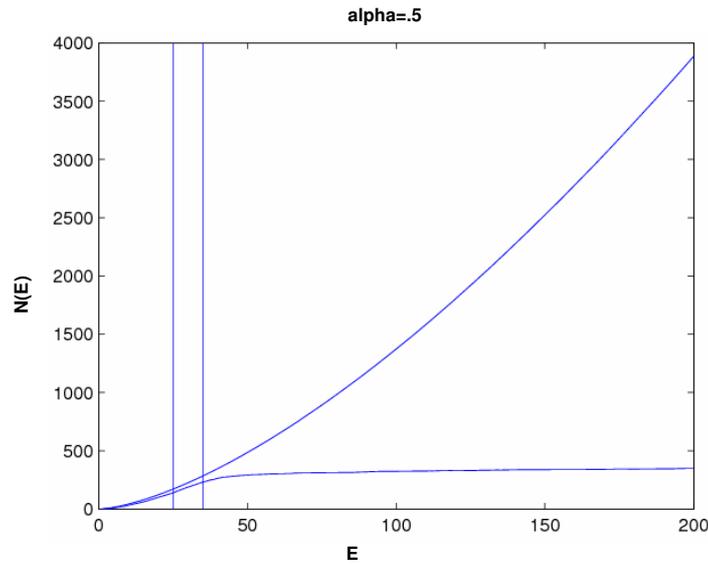
Fig. 8.6: Integrated density of states by direct calculation and from Weyl's formula

energy value equal to 35. The left vertical in Fig.8.6 corresponds to the value of the energy up to which the Weyl's curve follows the integrated density of states as obtained by direct diagonalization of the Hamiltonian matrix rather closely. How 'closely' is subjective and ascertained by eye-estimation. Also there has to be 'enough' number of energies below the left vertical line. For all the calculations presented in the thesis it turns the number of eigenvalues below the left vertical line is around 150. It is assumed the number is sufficient to be able to bring out the necessary features of the statistics. A similar number of eigen-

energies is used for calculations appearing in [59]. In Fig.8.7 the histogram as well as the smooth distribution function of s given by Eq. 8.22 are displayed. They have similarity with a Poisson's distribution. In Fig. 8.7 the s axis starts from .5 instead of 0. That is due
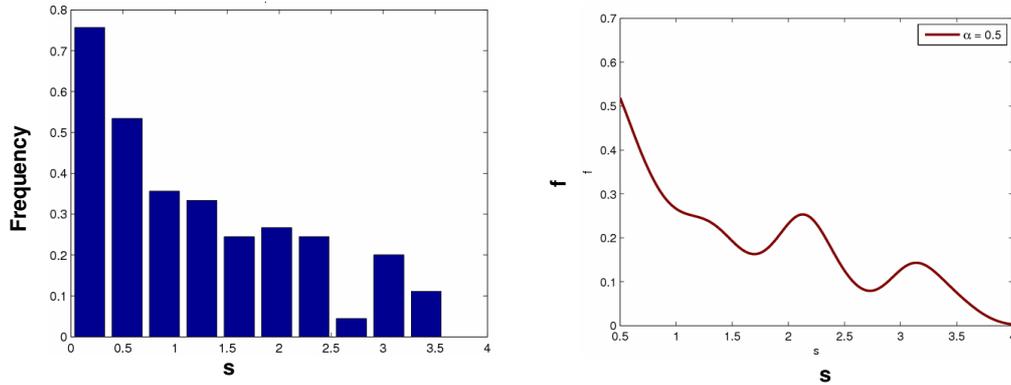
Fig. 8.7: Histogram as well as the smooth distribution for $\alpha = .5$.

to the fact that when the constant frequency corresponding to the bin of a histogram near $s = 0$ is replaced by sum of Gaussians, the latter will show an artificial dip near $s = 0$. It has to do with the shape of a Gaussian function, going to zero for the extreme values of the independent variable it is plotted against. This is also very much in spirit with a histogram plot, in which the frequency corresponding to the first bin can be assigned to any value of s belonging to that bin. Hence, as long as s is not too far away from $s = 0$, beginning the plot slightly from the right of $s = 0$ is reasonable.

To show a distribution which is qualitatively at another extreme, $\alpha = .6$ is chosen. A calculation similar to the one mentioned above is carried out, which includes the right choices of the integers $(m_1)_{\max}$ and $(m_2)_{\max}$ as well as that of V_0. A comparison of the computed integrated density of states with the Weyl's formula is made to ascertain how

96

many eigen-energies can be used. The histogram and the smooth distribution for $\alpha = .6$ are shown in Fig.8.8. It is noted that the distribution for $\alpha = .6$ is of a different nature
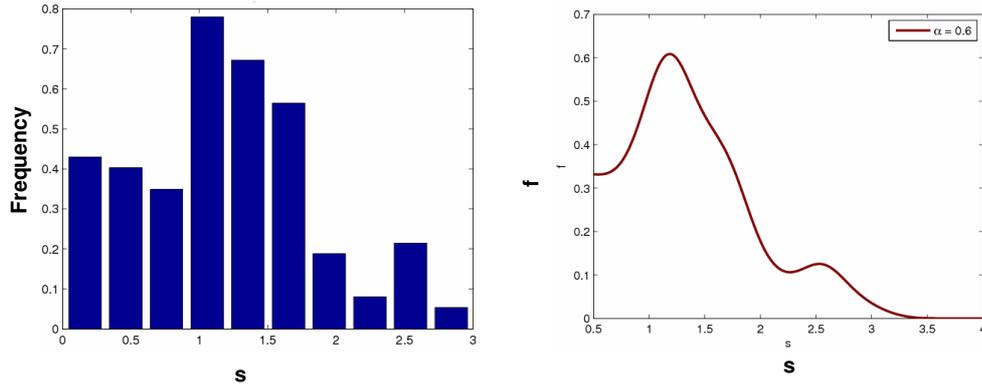
Fig. 8.8: Histogram as well as the smooth distribution for $\alpha = .6$

than that obtained for $\alpha = .5$, which was closer to the exponential distribution. For $\alpha = .6$, the distribution turns out to be closer to the superposition of GOE type of distribution which peaks at a value of s away from 0. It is a rather remarkable result since neither in a parabolic nor in a Dirac quantum billiards does one see two different energy level statistics for the same geometry. But that is possible to achieve in a semi-Dirac system by tuning the parameter α. It is also noted that this qualitative difference in the behavior of the energy level statistics takes place for rather a modest change(about 20 percent) in the value of α. Later it will be shown that a much more dramatic transition is possible in the rich parameter space of α.

To show that the above mentioned transition between the universality classes is not an one-time event but takes place in other regions of the α parameter space too, in Fig.8.9 a range of α between .8 to .9 is considered. It is observed in Fig.8.9 as α increases from .8
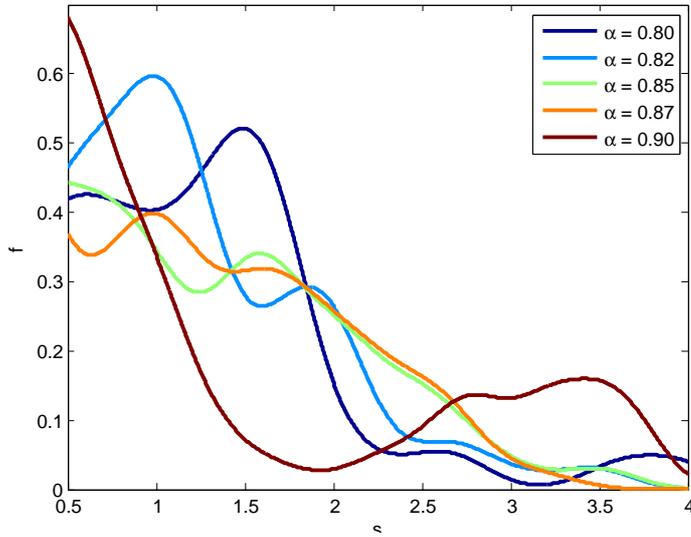
Fig. 8.9: Smooth distribution curves in the range of $\alpha = .8$ to $\alpha = .9$

to .9 the distribution function turns from what is closer to a superposition of GOE's type of distribution with a hump at a non-zero value of s to an exponential distribution, with a maximum close to $s = 0$. Also, it is appropriate to mention at this point that in order to obtain a perfect statistics for the variable s one needs an infinite number of values of s. Limiting the number of values of s to around 150 might cause some deviation, although hopefully not very serious, of the distribution curve from its ideal shape.

Before showing an example of a much more dramatic transition in the α parameter space, a result about the statistics of s is shown in which the distribution curves are insensitive to the changes in the value of α. This result is very different compared to any of the energy level statistics shown so far. In Fig.8.10 distribution curves are plotted for the range of $\alpha = .70$ to $\alpha = .7525$. The results shown in this figure, although intuitive, did not occur for the previously used ranges of the parameter α. It is intuitive since it is very much in line with one's expectation that the distributions should not change much when the parameter α varies very little.
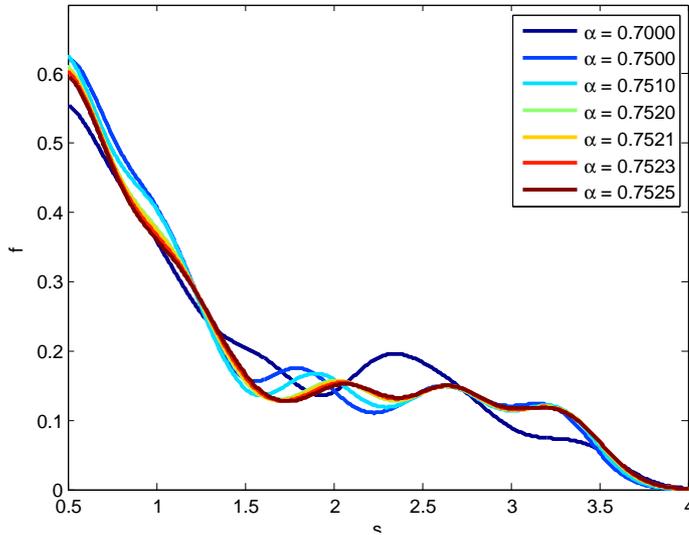
Fig. 8.10: Smooth distribution curves in the range of $\alpha = .7525$ to $\alpha = .7$

As a final example, the distribution functions are plotted for the parameter range $\alpha = .77$ to $\alpha = .78$ in Fig.8.11. The objective is to show a rather sensitive dependence of the distributions on the parameter α. In Fig.8.11 the distributions make transition from Poisson type at $\alpha = .77$ to a phase in which they are beginning to look like superposition of GOE'S type, as can be seen from the humps developing in the distributions for non-zero values of s. The change takes place when α changes by .01, which is about one percent only! It is pointed out although the change is fast in certain ranges of α, it is not discontinuous. That implies that the eigenenergies change continuously with α, there by ensuring the correctness of the results eliminating the possibility of any artifacts of numerical algorithms used for the calculation being responsible for such a special result. Various other regions of the parameter space have also been explored for the semi-Dirac system. The trend in the distribution functions is transitory or monotonic depending on which region in the parameter space one is investigating. As mentioned before, this is rather a special type of behavior for the semi-Dirac system. In Dirac or parabolic systems
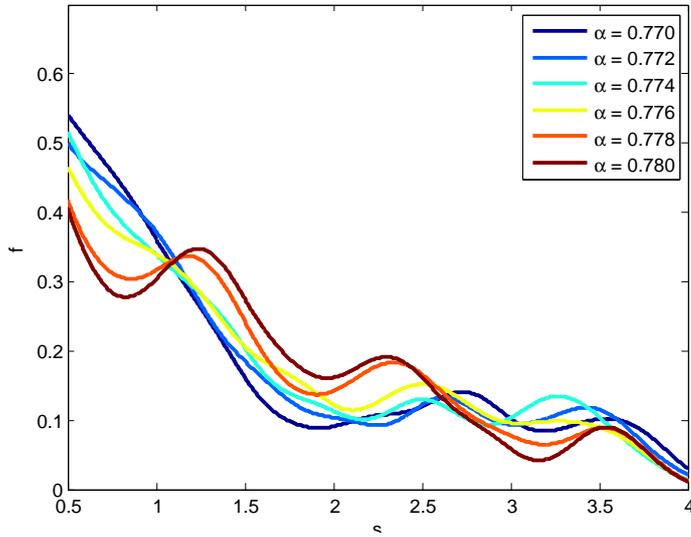
Fig. 8.11: Smooth distribution curves in the range of $\alpha = .77$ to $\alpha = .78$

the transition from one type of distribution to another takes place as the geometrical shape of the billiard is altered. In case of semi-Dirac dispersion, in spite of the fact that the boundary of the billiard is a symmetric one, one sees not only different types of distributions but sometimes the transition from the one to the other is extremely sensitive to the value of α.

8.8.2 Discussion (Future Direction etc.)

In this chapter the quantum chaotic aspects of the semi-Dirac dispersion was discussed. It was shown that the semi-Dirac single parameter space shows a rich behavior of energy level repulsion or the lack of it depending on what region of α is considered. The root cause for such behavior lies in the degeneracy of the eigenvalues of the Hamiltonian given by Eq. 8.8. Depending on the value of the parameter α, the energy levels can show a tendency to be close to each other or not. Of course any degeneracies in this problem are accidental in nature. A few things are worth mentioning at this point. In this chapter for

all the calculations the scalar form of the semi-Dirac Hamiltonian was considered. But one could also work with a tight-binding description of the semi-Dirac Hamiltonian. One could start with a finite size tight-binding semi-Dirac Hamiltonian with a circular boundary, and compute the energy level statistics. It can also be of interest to see how the energy level statistics get modified with the introduction of a magnetic field. For the quantum billiards problem, the translational symmetry is broken. It can be of considerable interest to study the energy level statistics for systems having translational symmetry. In that case the discrete energy levels of the quantum billiards problem will be replaced by energy bands. The energy level statistics of the energy bands can be studied[64] in the following way. Once the electronic structure of a material is obtained, for each k-point in the Brillouin zone there are multiple energy bands with different energy values. So a transition from a billiard problem to a problem with translational symmetry results in more number of energy values, which can be subjected to the statistical considerations, as shown in this chapter. So as much as computing the energy level statistics from the tight-binding semi-Dirac Hamiltonian, and studying the same in the presence of the magnetic field are possible future directions, one can also study the energy level statistics directly from the electronic structure of $TiO2/VO2$ or any other material, where semi-Dirac band structure has been known to appear.

APPENDIX

.1 The eigenvalues and eigenfunctions of a 2 by 2 real matrix

I. The eigenvalues and eigenfunctions of the matrix

$$\tau_z + \tan\theta\,\tau_x \qquad (.24)$$

are given by:

$$\text{eigenfunction:}\begin{pmatrix}\cos(\theta/2)\\\sin(\theta/2)\end{pmatrix}, \qquad (.25a)$$

with the corresponding eigenvalue being: $(\cos\theta)^{-1}$.

$$\text{eigenfunction:}\begin{pmatrix}\sin(\theta/2)\\-\cos(\theta/2)\end{pmatrix}, \qquad (.25b)$$

with the corresponding eigenvalue being: $-(\cos\theta)^{-1}$.

II. For the matrix

$$-[\tau_z - \tan\theta\,\tau_x], \qquad (.26)$$

$$\text{eigenfunction:}\begin{pmatrix}\sin(\theta/2)\\\cos(\theta/2)\end{pmatrix}, \qquad (.27a)$$

with the corresponding eigenvalue being: $(\cos\theta)^{-1}$.

$$\text{eigenfunction:}\begin{pmatrix}\cos(\theta/2)\\-\sin(\theta/2)\end{pmatrix}, \qquad (.27b)$$

with the corresponding eigenvalue being: $-(\cos\theta)^{-1}$.

BIBLIOGRAPHY

[1] K.S. Novoselov *et al.*, Nature **438**, 197 (2005).

[2] A. H. Castro Neto *et al.*, Rev. Mod. Phys. **81**, 109 (2009).

[3] D. Sherrington and W. Kohn, Phys. Rev. Lett. **21**, 153 (1968).

[4] D. J. Singh and W. E. Pickett, Phys. Rev. B (RC) **50**, 11235 (1994).

[5] J. C. Smith, S. Banerjee, V. Pardo, and W. E. Pickett, Phys. Rev. Lett. **106**, 056401 (2011).

[6] Z. Wang, S. Tsukimoto, R. Sun, M. Saito, and Y. Ikuhara, Appl. Phys. Lett. **98**, 104101 (2011).

[7] G. E. Volovik, Pis'ma ZhETF **73**, 182 (2001) [Sov. Phys. JETP **73**, 162 (2001).

[8] G. E. Volovik, *The Universe in a Helium Droplet* (Clarendon Press, Oxford, 2003).

[9] P. Dietl, F. Piéchon, and G. Montambaux, Phys. Rev. Lett. **100**, 236405 (2008).

[10] G. Montambaux, F. Biéchon, J. -N. Fuchs, and M. O. Goerbig, Phys. Rev. B **80**, 153412 (2009).

[11] I. M. Tsidilkovski, *Gapless Semiconductors - a New Class of Materials* (Akademie-Verlag Berlin, Berlin, 1988).

[12] K.S. Novoselov et al., Nature 438, 197 (2005).

[13] A. H. Castro Neto et al Rev. Mod. Phys. **81**, 109 (2009).

[14] T. Ohta, A. Bostwick, T. Seyller, K. Horn and E. Rotenberg, Science 313, 5789 (2006).

[15] C. L. Kane and E. J. Mele, Phys. Rev. Lett. 95, 226801 (2005).

[16] L. Fu and C. L. Kane, Phys. Rev. B 76, 045302 (2007).

[17] I. M. Tsidilkovski, *Gapless Semiconductors* (Akademie-Verlag Berlin, Berlin, 1988).

[18] B. A. Bernevig, T. L. Hughes and S. C. Zhang, Science 314, 1757 (2006).

[19] M. Konig et al, Science 318, 766 (2007).

[20] A. Ohtomo, D.A. Muller, J.L. Grazul and H.Y. Hwang, Nature 419, 378 (2002).

[21] A. Ohtomo and H.Y. Hwang, Nature 423, 427 (2004).

[22] R. Pentcheva and W.E. Pickett, Phys. Rev. B 74, 035112 (2006).

[23] A. Brinkman, M. Huijben, M.V. Zalk, J. Huijben, U. Zeitler, J.C. Maan, M.G.V. der Wiel, G. Rijnder, D.H.A. Blank and H. Hilgenkamp, Nat. Mater. 6, 493 (2007).

[24] N. Reyren et al., Science 317, 5842 (2007).

[25] Chaos in Classical and Quantum Mechanics, Martin C. Gutzwiller, 1990 Springer-Verlag New York Inc.

[26] The Feynman Lectures on Physics, Vol. 3, ch. 13

[27] V. Pardo and W. E. Pickett, *P*hys. Rev. Lett., to be published.

[28] D. J. Griffiths, Introduction to Quantum Mechanics (2nd Edition), (Benjamin Cummings, 2004)

[29] C. M. Bender and S. A. Orszag, Advanced Mathematical Methods for Scientists and Engineers: Asymptotic Methods and Perturbation Theory, (Springer, 1999)

[30] D. J. Thouless et al, Phys. Rev. Lett. 49, 405 (1982).

[31] F. D. M. Haldane, Phys. Rev. Lett. 93, 206602 (2004).

[32] J. E. Moore and L. Balents, Phys. Rev. B 75, 121306 (2007).

[33] V. Pardo and W. E. Pickett, Phys. Rev. Lett. 102, 166803 (2009).

[34] V. Pardo and W. E. Pickett, Phys. Rev. B 81, 035111 (2010)

[35] Tsuneya Ando *et al.*, J. Phys. Soc. Jpn **71**, 1318 (2002).

[36] Iris Crassee *et al.*, Nature Physics **7**, 48 (2011).

[37] Philip B. Allen *et al.*, Phys. Rev. B **43**, 7482 (1991).

[38] N. P. Ong, Phys. Rev. B **37**, 193 (1987).

[39] M. I. Katsnelson *et al.*, Nature **384**, 620 (2006).

[40] Hidetoshi Fukuyama , Progress of Theoretical Physics **45**, 3 (1971).

[41] S. Das Sarma *et al.*, Phys. Rev. Lett. **102**, 206412 (2009).

[42] S. Banerjee *et al.*, Phys. Rev. Lett. **103**, 016402 (2009).

[43] Walter Greiner,Ludwig Neise and Horst St¨cker *Thermodynamics and Statistical mechanics* (Springer-Verlag, 1995), p. 196.

[44] Neil W. Ashcroft,N. David Mermin *Solid State Physics* (Brooks/Cole, 1976), p. 47.

[45] R. Balian *et al.*, Annals of Physics: 60, 401-447 (1970)

[46] R. Balian *et al.*, Annals of Physics: 64, 271-307 (1971)

[47] D. L. Kaufman, I. Kosztin, K. Schulten, Am. J. Phys., Vol. 67, No. 2, February 1999

[48] N. Dombey *et al.*, Physics Reports 315 (1999) 41-58

[49] O. Klein, Z. Phys. 53 (1929) 157.

[50] P. Dietl, F. Piéchon, and G. Montambaux, Phys. Rev. Lett. **100**, 236405 (2008).

[51] G. Montambaux, F. Biéchon, J. N. Fuchs, and M. O. Goerbig, Phys. Rev. B **80**, 153412 (2009).

[52] J.N. Fuchs, F. Piechon, M. O. Goerbig, and G. Montambaux, Eur. Phys. J. B (2010) DOI: 10.1140/epjb/e2010-00259-2

[53] R.P Feynman, A. R. Hibbs, Quantum Mechanics and Path Integrals, Dover Publications, Inc., Mineola, New York

[54] E. Wigner, Ann. of Math., 62, 548-564.

[55] E. Wigner, Ann. of Math., 67, 325-327.

[56] M. L. Mehta, Random Matrices, 2nd ed., (Academic Press, 1991).

[57] M. V. Berry, Physica Scripta. Vol. 40, 335-336, 1989

[58] M. V. Berry, Proceedings of the Royal Society of London. Series A, Mathematical and PhysicalSciences, Vol. 392, No. 1802 (Mar. 8, 1984), pp. 45-57

[59] D. L. Kaufman, I. Kostztin, K. Schulten, Am. J. Phys., Vol. 67, No. 2, February 1999

[60] R. W. Robinet, Am. J. Phys. 64, 440446 1996.

[61] M. V. Berry, Eur. J. Phys. 2, 91102 1981.

[62] I. Kosztin and K. Schulten, Int. J. Mod. Phys. C 8, 293325 1997.

[63] F. A. Buot, Phys. Rep. 234, 73174 1993.

[64] E. R. Mucciolo, R. B. Capaz, B. L. Altshuler, and J. D. Joannnopoulos, Phys. Rev. B, 50(12), 8245(7)

[65] B. D. Simons, A. Szafer, and B. L. Altshuler, Pis'ma Zh. Eksp. Teor. Fiz. 57,5, 268-272 1993

[66] S. Banerjee and W. E. Pickett, Low energy behavior of the semi-Dirac dispersion, To be published in P.R.B

[67] Chaos in Dynamical Systems, by Edward Ott, Cambridge University Press.

[68] I. Kosztin and K. Schulten, Int. J. Mod. Phys. C 8, 293325 (1997).

[69] Sam T Carr, Quantum Field Theory II An introduction to Feynman diagrams, A course for MPAGS, February, 2009